Numerical Methods for Optimal Trade Execution

by

Shu Tong Tse

A thesis
presented to the University of Waterloo
in fulfillment of the
thesis requirement for the degree of
Doctor of Philosophy
in
Computer Science

Waterloo, Ontario, Canada, 2012

I hereby declare that I am the sole author of this thesis. This is a true copy of the thesis, including any required final revisions, as accepted by my examiners.

I understand that my thesis may be made electronically available to the public.

Abstract

Optimal trade execution aims at balancing price impact and timing risk. With respect to the mathematical formulation of the optimization problem, we primarily focus on Mean Variance (MV) optimization, in which the two conflicting objectives are maximizing expected revenue (the flip side of trading impact) and minimizing variance of revenue (a measure of timing risk). We also consider the use of expected quadratic variation of the portfolio value process as an alternative measure of timing risk, which leads to Mean Quadratic Variation (MQV) optimization.

We demonstrate that MV-optimal strategies are quite different from MQV-optimal strategies in many aspects. These differences are in stark contrast to the common belief that MQV-optimal strategies are similar to, or even the same as, MV-optimal strategies. These differences should be of interest to practitioners since we prove that the classic Almgren-Chriss strategies (industry standard) are MQV-optimal, in contrary to the common belief that they are MV-optimal.

From a computational point of view, we extend theoretical results in the literature to prove that the mean variance efficient frontier computed using our method is indeed the complete Pareto-efficient frontier. First, we generalize the result in Li (2000) on the embedding technique and develop a post-processing algorithm that guarantees Pareto-optimality of numerically computed efficient frontier. Second, we extend the convergence result in Barles (1990) to viscosity solution of a system of nonlinear Hamilton Jacobi Bellman partial differential equations (HJB PDEs).

On the numerical aspect, we combine the techniques of similarity reduction, non-standard interpolation, and careful grid construction to significantly improve the efficiency of our numerical methods for solving nonlinear HJB PDEs.

Acknowledgements

First, I would like to thank Professor Peter Forsyth who supervised this thesis. At each struggling point in my research, I benefited tremendously from discussing with Peter in frequent unscheduled meetings, without which work that took weeks to finish could have taken months. I look forward to exiting his infinite loop of "How's your progress" cries that have made my thesis work converged at a higher rate.

I am grateful to my co-supervisor Justin Wan, who introduced me to Peter, convinced me to switch from mathematics to computer science, and guided me in other research work. A casual first meeting with Justin in my third year as an undergraduate has had the butterfly effect of changing my entire career.

I thank my committee members, Yuying Li, George Labahn and Ken Vetzal, for taking the time to review the thesis and give me valuable comments. Yuying and George also helped me on technical aspects in the thesis.

I would like to thank my external examiner, Robert Almgren, whose seminal work in optimal trade execution is intimately related to this thesis.

I also thank Heath Windcliff and Shannon Kennedy for collaboration and sharing their work at Morgan Stanley, which provides me with financial support.

I also benefit a lot from academic discussions with fellow schoolmates. Particular mention must be made of Ma Kai, Cui Zhenyu, Amir, Titian, Parsiad and Ad. Friendships from other SciCom members, especially Yoyo, Wang Bo and Han Dong, have given me many memorable moments in my first two years in Waterloo.

Thanks must also be made to my family for giving me the freedom to pursue my goals. Last but not least, I thank my long-distance girlfriend for her love and trust.

Contents

List of Tables

List of Figures

Chapter 1

Introduction

1.1 Algorithmic Trade Execution

Algorithmic trade execution has become a standard technique for institutional market players in recent years, particularly in the equity market where electronic trading is most prevalent. A trade execution algorithm typically seeks to execute a trade decision optimally upon receiving inputs from a human trader. For concreteness and exposition purposes, this thesis will discuss trade execution in the context of share liquidation.

At the relatively macro level, the execution decisions consist of the timing and quantity of sell order submissions. Mathematically, a macro-level liquidation policy can be modeled by an optimal selling velocity function $v^*(X(t), t; p)$, where $X(t)$ is the state vector at time t and p is the parameter vector. We work at this macro-level, using a continuous time model.

Given the macro-level decision, numerous micro-structural aspects of order submission decisions remain to be made, which include order types, order prices, execution venues, among others. We will not further discuss these micro-structural aspects of trade execution.

In practice, execution algorithms can be roughly classified [42] into the following overlapping types: (i) schedule-based type, which uses time or volume schedules to track selected benchmarks; (ii) liquidity seeking type, which sources liquidity in both dark and lit venues; and (iii) implementation shortfall type, which strikes a balance between the conflicting goals of minimizing both market impact and timing risk. In this thesis we focus on implementation shortfall type algorithms, which account for a significant portion of the methods used in practice [29].

1.2 Models for Implementation Shortfall Algorithms

Implementation shortfall [55] is defined as the difference between the mean execution price and the arrival price when trading starts. Implementation shortfall can be broken

down into permanent price impact, temporary price impact and timing risk. *Permanent price impact* comes from other trading parties adjusting their trades upon observing our trades [46], e.g. when other traders know about a large buyer in the market, they will tend to buy more, moving prices against the larger buyer. *Temporary price* impact comes from temporary imbalance of supply and demand, and is best illustrated by a large buy market order matching with sell orders of successively higher limit prices. *Timing risk* comes from potentially adverse random price changes.

There are two fundamental modeling aspects in any optimal execution model. The first aspect is the modeling of asset price dynamics in the presence of price impacts. In this aspect, our approach is similar to that of the pioneering works [18] and [9, 8]. In our models, price impacts are specified exogenously as functional forms that appear in the stochastic differential equations governing the state dynamics. In addition, temporary price impact is assumed to be instantaneous and affects only the executing trade. Another common approach in the literature generates price impacts endogenously via a limit order book model [53, 2, 1, 57], which gives rise to temporary price impacts that are transient [3, 33, 35].

The second aspect concerns the choice of what objective function to optimize. We primarily focus on Mean Variance (MV) optimization, in which the two conflicting objectives are maximizing expected revenue (the flip side of trading impact) and minimizing variance of revenue (a measure of timing risk). We also consider the use of expected quadratic variation of the portfolio value process as an alternative measure of timing risk, which leads to Mean Quadratic Variation (MQV) optimization.

A similar multi-objective optimization approach is used in [34], except that it uses time-averaged value-at-risk as the risk measure. Another common approach is to maximize the expectation of a utility function of revenue, see for example [59, 60, 52, 43].

1.3 Overview and Contributions

The Mean Variance objective is intuitive, well-known and aligns with performance measurement in optimal trade execution. For these reasons we focus on efficient computational methods for determining MV-optimal strategies. We consider the Mean Quadratic Variation objective to demonstrate that MV-optimal strategies are quite different from MQV-optimal strategies in many aspects. These differences are in stark contrast to the common belief that MQV-optimal strategies [9] (which are standard [44, 42, 40] in the optimal trade execution industry) are similar to, or even the same as, MV-optimal strategies.

The main contributions of this thesis with regard to computational methods are as follows.

- We extend the result in [47] on the embedding technique to tackle non-convex multi-period MV optimization problems. For non-convex problems, the embedding technique may produce Pareto-inefficient points. We prove a number of results that guarantee Pareto-optimality of the computed frontier.

- We extend the convergence result in [16] to the system of nonlinear HJB PDEs that arises under our regime switching trade execution model. First, we prove that our discretization of the system of nonlinear HJB PDEs is monotone, consistent and infinity-norm stable. Second, we prove in detail that these properties guarantee the convergence of numerical solutions to the viscosity solution, provided that a strong comparison principle holds.

- We combine the techniques of similarity reduction, non-standard interpolation, and careful grid construction to significantly improve the efficiency of our numerical methods for solving nonlinear HJB PDEs.

The main contributions of this thesis with regard to MV-optimal and MQV-optimal strategies are as follows.

- We show that it is important to adapt MV-optimal strategies to random changes in temporary price impact. When the real dynamics is rapidly switching between two regimes of differing price impacts, mis-specifying the dynamics as the non-switching mixture results in significant sub-optimality.

- We show that MQV-optimal strategies are poor approximations to MV-optimal strategies in many aspects. In particular, for the same variance, an MQV-optimal strategy can have significantly smaller expected revenue compared to an MV-optimal strategy.

- We prove that the classic strategies in [9, 8] are MQV-optimal, in contrary to the common belief that they are MV-optimal.

1.4 Outline

Chapters 2 to 5 study the Mean Variance optimization problem. Chapter 2 introduces our optimal trade execution models. Chapter 3 discusses computational methods. Chapter 4 details the proof of convergence to viscosity solution for a system of nonlinear HJB PDEs. Chapter 5 presents numerical results.

Chapter 6 studies the Mean Quadratic Variation optimization problem. Chapter 7 compares Mean Variance-optimal strategies with Mean Quadratic Variation-optimal strategies. Chapter 8 concludes.

Chapter 2

Optimal Trade Execution : Mean Variance Optimization Approach

This chapter introduces our optimal trade execution models in the context of Mean Variance optimization. We start by describing our trade execution models in Section 2.1, and then discuss Mean Variance optimization in Section 2.2.

2.1 Trade Execution Model

In this section, we first introduce our basic Geometric Brownian Motion (GBM) trade execution model and then extend it with a finite-state Markov chain to a Regime Switching model.

For generality, we will discuss Mean Variance optimization in the context of the Regime Switching model. Nevertheless, the basic GBM model will be used in most of our computational results.

2.1.1 Basic Model: Geometric Brownian Motion

Let

$$\begin{aligned} S &= \text{Price of the underlying risky asset,} \\ B &= \text{Balance of risk free bank account,} \\ A &= \text{Number of shares of underlying asset.} \\ P &= B + AS = \text{Portfolio Value.} \end{aligned}$$

The optimal execution problem over $t \in [0, T]$ has the initial condition

$$S(0) = s_{init},\ B(0) = 0,\ A(0) = \alpha_{init}. \tag{2.1.1}$$

If $\alpha_{init} > 0$, the trader is liquidating a long position (selling). If $\alpha_{init} < 0$, the trader is liquidating a short position (buying). In this thesis, for definiteness, we consider the selling case.

At terminal time $t = T$,

$$S = S(T),\ B = B(T),\ A = A(T) = 0,$$

where $B(T)$ is the cash generated by selling shares and investing in the risk free bank account B, with a final liquidation at $t = T^-$ to ensure that $A(T) = 0$.

In our research work, we consider Markovian trading strategies $v(\cdot)$ that specify a trading rate $v \in [v_{min}, 0]$ as a function of the current state, i.e. $v(\cdot) : (S(t), B(t), A(t), t) \mapsto v = v(S(t), B(t), A(t), t)$. Note that in using the shorthand notations $v(\cdot)$ for the mapping, and v for the value $v = v(S(t), B(t), A(t), t)$, the dependence of v on the current state is implicit.

By definition,

$$dA(t) = v\ dt. \tag{2.1.2}$$

As in [13], we assume that due to temporary price impact, selling shares at the rate v at the market price $S(t)$ gives an execution price $S_{exec}(v, t) \leq S(t)$. It follows that

$$dB(t) \quad = \quad \big(rB(t) - vS_{exec}(v, t)\big)dt, \tag{2.1.3}$$

where r is the risk free rate. Note that since $v \leq 0$ for selling, the term $(-vS_{exec}(v, t))$ represents the rate of cash obtained by selling shares at price $S_{exec}(v, t)$ at a rate v.

In the basic model, we suppose that the market price of the risky asset S follows a Geometric Brownian Motion, where the drift term is modified due to the permanent price impact of trading, i.e. we assume the dynamics

$$dS(t) \quad = \quad (\eta + g(v))S(t)\ dt + \sigma S(t)\ d\mathbb{W}(t), \tag{2.1.4}$$

where η is the drift rate, $g(v)$ is the permanent price impact function, σ is the volatility, and $\mathbb{W}(t)$ is a Wiener process under the real world measure.

In the basic model, we assume the temporary price impact scales linearly with the asset price, i.e.

$$S_{exec}(v, t) = f(v)S(t), \tag{2.1.5}$$

with

$$f(v) \quad = \quad (1 + \kappa_s \operatorname{sgn}(v)) \exp[\kappa_t \operatorname{sgn}(v)|v|^\beta], \tag{2.1.6}$$

where κ_s is the bid-ask spread parameter, κ_t is the temporary price impact factor, and β is the price impact exponent. The form (2.1.6) is suggested by empirical statistical analysis of order book dynamics [13, 6, 49, 56]. We also refer the interested reader to [4] for more discussion about price impact functions and a more general functional form.

Note that we assume $\kappa_s < 1$, so that $S_{exec}(v,t) \geq 0$, regardless of the magnitude of v.

The permanent price impact function $g(v)$ is assumed to be of the form

$$g(v) \;=\; \kappa_p v, \tag{2.1.7}$$

where κ_p is the permanent price impact factor. This linear form of permanent price impact function eliminates the possibilities of round-trip price manipulation [13, 38]; see also Appendix C.

Given the state $(S(T^-), B(T^-), A(T^-))$ at the instant $t = T^-$ before the end of the trading horizon, we have one final liquidation (if necessary) so that the number of shares owned at $t = T$ is $A(T) = 0$. The liquidation value, denoted by $B(T)$, after this final trade is defined as follows:[1]

$$\begin{aligned} B(T) &= B(T^-) + \lim_{v\to-\infty} A(T^-) S_{exec}(v, T^-) \\ &= \int_0^{T^-} e^{r(T-t')} \big(- v S_{exec}(v,t') \big)\, dt' + \lim_{v\to-\infty} A(T^-) S_{exec}(v, T^-). \end{aligned} \tag{2.1.8}$$

2.1.2 Extension to Regime Switching

Let $L(t)$ be a continuous-time stationary Markov chain taking values in $\mathcal{M} = \{1, \cdots, M\}$ such that $L(t)$ is independent of $\mathbb{W}(t)$ in (2.1.4). Let $\lambda_{lm} \geq 0$ denote the switching intensity from regime l to regime m, i.e.

$$P(L(t+dt) = m | L(t) = l) = \lambda_{lm}\, dt, \qquad \text{for } l \neq m. \tag{2.1.9}$$

In our regime switching model, the drift rate η, the volatility σ, the permanent price impact function $g(v)$ and the temporary price impact function $f(v)$ are regime-dependent; we use the notations

$$\eta^l = \eta(l), \quad \sigma^l = \sigma(l), \quad g^l(v) = g(v,l), \quad f^l(v) = f(v,l), \tag{2.1.10}$$

where $l = L(t)$ denotes the regime state at time t.

We also extend the trading strategy $v(\cdot)$ to be regime-dependent, i.e

$$v(\cdot) : (S(t), B(t), A(t), L(t), t) \mapsto v = v(S(t), B(t), A(t), L(t), t). \tag{2.1.11}$$

The dynamics of our regime switching trade execution model are specified by the Markov chain $L(t)$ and the equations

$$dA(t) = v\, dt, \tag{2.1.12}$$

[1] In actual implementation, we would replace $\lim_{v\to-\infty}$ by a finite $v_{\min} \ll 0$. Also, in the case of liquidating a short position (buying), which is not considered in this thesis, equation (2.1.8) would be defined as $B(T) = B(T^-) + \lim_{v\to\infty} A(T^-) S_{exec}(v, T^-)$, and we would replace $\lim_{v\to\infty}$ by a finite $v_{\max} \gg 0$ in implementation.

$$dB(t) = rB(t)dt - vf^l(v)S(t)dt, \tag{2.1.13}$$

$$dS(t) = \Big(\eta^l + g^l(v) - \sum_{\substack{m=1\\m\neq l}}^{M} \lambda^{lm}(\zeta^{lm} - 1)\Big)S(t)\ dt + \sigma^l S(t)\ d\mathbb{W}(t) + \sum_{\substack{m=1\\m\neq l}}^{M} (\zeta^{lm} - 1)S(t)\, dL(t), \tag{2.1.14}$$

where $\zeta^{lm} \geq 0$ is the stock price jump factor when switching from regime l to m, i.e. $S(t^+) = S(t^-)\zeta^{lm}$; and

$$dL(t) = \begin{cases} 1 \text{ with probability } \lambda^{lm}\, dt \\ 0 \text{ with probability } 1 - \lambda^{lm}\, dt \end{cases}. \tag{2.1.15}$$

Note that λ^{lm} and ζ^{lm} are defined only for $l \neq m$.

Assumption 2.1. We assume

$$f^l(0) = 1,\ g^l(0) = 0\ ;\ f^l(v) \in [0,1] \text{ and } g^l(v) \leq 0 \text{ for } v \leq 0. \tag{2.1.16}$$

for obvious financial reasons. We also assume that $f^l(v)$ and $g^l(v)$ are Lipschitz continuous in v, for technical reasons that will become apparent in the convergence proof in Chapter 4.

We remark that Assumption 2.1 is satisfied by (2.1.6) and (2.1.7), where there are no regime-dependence.

2.2 Mean Variance Optimization

This section introduces our Mean Variance (MV) optimization approach that aligns well with how performance is measured in the optimal trade execution industry. More specifically, suppose that a trade execution engine carries out many thousands of trades and uses the post-trade data to determine the realized mean return and the standard deviation. Assuming that the modeled dynamics very closely match the dynamics in the real world, an MV-optimal strategy in our framework would result in the largest realized mean return, for a given standard deviation, compared to any other possible strategy.

There are two variants of continuous time (multi-period) Mean Variance optimization, namely the pre-commitment version [17] and the time-consistent version [63]. The pre-commitment version of Mean Variance optimization aligns with performance measurement in practice as discussed above. We use the pre-commitment version throughout the thesis.

2.2.1 Mean Variance Optimality in the Pareto Sense

To simplify notations, we use $X(t) = (S(t), B(t), A(t), L(t))$ to denote the multi-dimensional space-state process and $x = (s, b, \alpha, l)$ to denote a space-state. We will also use the notation $X(t) = x$ in our context as a shorthand for $(S(t) = s, B(t) = b, A(t) = \alpha, L(t) = l)$.

Let $E^{x,t}_{v(\cdot)}[B(T)]$ be the expectation of $B(T)$ conditional on the initial state (x,t) and the control $v(\cdot):(x,t)\mapsto v=v(x,t)$. More specifically, define

$$\begin{aligned} E[\cdot] &: \text{ Expectation operator,} \\ E^{x,t}[\cdot] &: E[\cdot|X(t)=x] \text{ when observed at time } t, \\ E^{x,t}_{v(\cdot)}[\cdot] &: E^{x,t}[\cdot] \text{ with } v(\cdot) \text{ being the strategy that controls} \\ &\quad \text{the stochastic process } X(t) \text{ given by (2.1.9-2.1.15).} \end{aligned}$$

Similarly we define $Var^{x,t}_{v(\cdot)}[B(T)]$ as the variance of $B(T)$ conditional on the initial state (x,t) and the control $v(\cdot)$.

All optimizations will be over the set of admissible strategies defined as follows.

Definition 2.2. A strategy $v(\cdot):(x,t)\mapsto v=v(x,t)$ is said to be admissible if $v(x,t)\in[v_{min},0]$, where $v_{min}\leq 0$, and $v(x,t)=0$ when $A(t)=0$

Definition 2.3. An admissible strategy $v^*(\cdot)$ is defined to be Mean Variance optimal in the Pareto sense if there exists no admissible strategy $v(\cdot)$ such that

1. $E^{x,t}_{v(\cdot)}[B(T)]\geq E^{x,t}_{v^*(\cdot)}[B(T)], \quad Var^{x,t}_{v(\cdot)}[B(T)]\leq Var^{x,t}_{v^*(\cdot)}[B(T)]$.
2. At least one inequality in the above is strict.

Essentially, the mean-variance tradeoff of a Pareto-optimal strategy cannot be strictly dominated by any other strategy.

2.2.2 Scalarization

Although Pareto-optimality as defined in Section 2.2.1 is economically intuitive, it is mathematically inconvenient because there are two conflicting criteria to optimize. A standard scalarization reformulation [30] combines the two criteria into a single objective (the subtleties of the scalarization reformulation will be discussed in Chapter 3). More specifically, consider the following family of objective functionals parametrized by $\lambda>0$

$$\mathcal{F}_\lambda=\left\{J^{x,t}_\lambda\big(v(\cdot)\big):v(\cdot)\mapsto E^{x,t}_{v(\cdot)}\big[B(T)\big]-\lambda Var^{x,t}_{v(\cdot)}\big[B(T)\big]\right\}. \tag{2.2.1}$$

In the notation of (2.2.1), the members (functionals) in the family $\mathcal{F}_\lambda$ have different initial states (x,t) but the same λ. Given (x,t) and λ, we use $v^*_{x,t,\lambda}(\cdot)$ to denote an optimal policy that maximizes the corresponding functional, i.e. $J^{x,t}_\lambda\big(v(\cdot)\big)$.

2.2.3 Precommitment

According to previous discussion about performance measurement, optimal trade execution is concerned about determining $v^*_{x_0,0,\lambda_0}(\cdot)$, where $(x_0,0)=(X(t=0),t=0)$

denotes the initial state at the beginning of trade execution and λ_0 denotes the risk aversion level chosen. To maximize the performance metric in practice, i.e. $J_{\lambda_0}^{x_0,0}\big(v(\cdot)\big)$, the same strategy $v^*_{x_0,0,\lambda_0}(\cdot)$ should be used throughout the trading horizon $t \in [0,T]$, i.e. as time proceeds and the state changes to $(x',t') = (X(t'),t)$, the optimal trading rate is $v^*_{x_0,0,\lambda_0}(x',t')$, as opposed to $v^*_{x',t',\lambda_0}(x',t')$. In other words, the trader pre-commits to the strategy $v^*_{x_0,0,\lambda_0}(\cdot)$ and does not recompute $v^*(\cdot)$ as time proceeds.

2.2.4 Time Inconsistency of Optimal Strategies

As far as trade execution performance is concerned, it is sufficient to determine $v^*_{x,t,\lambda}(\cdot)$ for only $t = 0$. Nevertheless, it is interesting, from computational and economics points of view, to consider the relationship among optimal strategies $v^*_{x,t,\lambda}(\cdot)$ for $t \in [0,T]$.

Optimal strategies in our Mean Variance optimization framework are time-inconsistent in the following sense. Let (x_1,t_1) be some state at time t_1 and $v^*_{x_1,t_1,\lambda}(\cdot)$ be a corresponding optimal strategy that maximizes $J_\lambda^{x_1,t_1}\big(v(\cdot)\big)$. Let (x_2,t_2) be some other state at time $t_2 > t_1$ and $v^*_{x_2,t_2,\lambda}(\cdot)$ be a corresponding optimal strategy that maximizes $J_\lambda^{x_2,t_2}\big(v(\cdot)\big)$. The optimal strategies are time-inconsistent in the sense that, for $t' \geq t_2$,

$$v^*_{x_1,t_1,\lambda}(x',t') \;\; = \;\; v^*_{x_2,t_2,\lambda}(x',t') \;\; \text{does not always hold.} \tag{2.2.2}$$

Although time-inconsistency (2.2.2) is considered as unnatural by some authors in the context of long-term asset allocation [17] and creates computational difficulties, time-inconsistency often arises naturally in reasonably formulated problems in financial economics; see [20] for examples.

As discussed in [17], there is no dynamic programming principle for determining $v^*_{x,t,\lambda}(\cdot)$ for all $t \in [0,T]$ due to the time-inconsistency (2.2.2). Fortunately, it is sufficient for our purpose to determine $v^*_{x,t,\lambda}(\cdot)$ for only $t = 0$. The computational methods for determining $v^*_{x,0,\lambda}(\cdot)$ will be detailed in Chapter 3.

Chapter 3

Mean Variance Strategy: Numerical Method

We begin this chapter by explaining that it is necessary to transform the mean variance objective (2.2.1) for computation using dynamic programming, and the subtleties therein. Next, HJB PDEs are derived from the reformulation. Finally, the numerical issues of localization, boundary conditions and discretization are discussed in detail.

3.1 Embedding Technique for Mean Variance Optimization

The dynamic programming principle cannot be directly applied to solve the pre-commitment mean variance problem formulated as (2.2.1). This is because dynamic programming is applicable only for the expectation term but not the variance term in (2.2.1). For the expectation term in (2.2.1), dynamic programming is applicable due to the "smoothing-property" of conditional expectation, i.e. $E[B(T)|I_1] = E[E[B(T)|I_2]|I_1]$, where $I_1 \subseteq I_2$ are information sets. However, no analogous relation is available for the variance term in (2.2.1). More specifically, in general $(E[B(T)|I_1])^2 \neq E[(E[B(T)|I_2])^2|I_1]$, where the terms $(E[B(T)|I_i])^2$ arise from the variance term in (2.2.1).

In order to apply the dynamic programming principle to derive an HJB PDE for the MV problem, we will use the embedding technique introduced in [65, 47]. Instead of performing the scalarization (2.2.1), which is linear in $E^{x,t}_{v(\cdot)}[B(T)]$ and $Var^{x,t}_{v(\cdot)}[B(T)]$, the embedding technique performs a scalarization that is a quadratic function of $E^{x,t}_{v(\cdot)}[B(T)]$ and $Var^{x,t}_{v(\cdot)}[B(T)]$. This is called the embedding technique since every optimal control for the original linear scalarization problem (2.2.1) is an optimal control for the quadratic scalarization problem (but not vice versa in general). The quadratic scalarization problem can be solved using dynamic programming.

The embedding technique for multi-period mean variance optimization was originally developed in the context of asset allocation problems, in which the terminal bank account

value is typically a linear function of the control variable [47, 65, 48, 19], giving rise to convex problems. Applying the quadratic scalarization formulation to convex problems is relatively straightforward by the virtue of duality results [48]. In contrast, $B(T)$ is a nonlinear function of v in our optimal trade execution problem, and therefore the problem is in general non-convex. This potential non-convexity gives rise to a number of subtle issues in applying the embedding technique. In this section we prove a number of results to tackle these subtleties. In summary:

- The embedding technique generates a superset of the Pareto-optimal points. We develop a post-processing algorithm which can be used to eliminate the spurious points.
- We prove that all Pareto optimal points obtainable from the linear scalarization problem (2.2.1) can be obtained by solving the quadratic scalarization problem, even though only one out of possibly many optimal controls of the quadratic scalarization problem is computed.

The above results are quite general (not specific to our optimal trade execution problem) and can be applied to solving any multi-period mean variance optimization problem using the dynamic programming principle.

3.1.1 Scalarization

The following definition slightly extends the notion of Pareto optimality first introduced in Definition 2.3.

Definition 3.1. Let $(x_0, 0) = (X(t = 0), t = 0)$ denote the initial state. Let

$$\mathcal{Y} = \{(V, E) = (Var_{v(\cdot)}^{x_0,0}[B(T)], E_{v(\cdot)}^{x_0,0}[B(T)]) : v(\cdot) \text{ admissible } \} \tag{3.1.1}$$

denote the feasible objective space and $\bar{\mathcal{Y}}$ denote its closure. A point $(V_*, E_*) \in \bar{\mathcal{Y}}$ is called a Pareto (optimal) point if there exists no admissible strategy $v(\cdot)$ such that

$$\begin{aligned} E_{v(\cdot)}^{x_0,0}[B(T)] &\geq E_* \\ Var_{v(\cdot)}^{x_0,0}[B(T)] &\leq V_* \ , \end{aligned} \tag{3.1.2}$$

and at least one of the inequalities in equation (3.1.2) is strict. Essentially, the mean-variance tradeoff of a Pareto point cannot be strictly dominated by that of any admissible strategy. We denote the set of Pareto points by $\mathcal{P} \subseteq \bar{\mathcal{Y}}$.

The linear scalarization (2.2.1) can then be generalized as determining for each $\mu > 0$

$$\mathcal{Y}_{P(\mu)} = \big\{(V_0, E_0) \in \bar{\mathcal{Y}} : (V_0, E_0) = \inf_{(V,E)\in\mathcal{Y}} \mu V - E\big\}. \tag{3.1.3}$$

Remark 3.2. *It is well known that if the feasible objective space $\mathcal{Y}$ is convex, then every point in $\mathcal{P}$ is in some $\mathcal{Y}_{P(\mu)}$. In general, every point in $\mathcal{Y}_{P(\mu)}$ is in $\mathcal{P}$ but the converse may not hold. This thesis is concerned with determining $\bigcup_{\mu>0}\mathcal{Y}_{P(\mu)}$, which will turn out to be equal to $\mathcal{P}$ in our computational examples. The more difficult problem of determining the entire set $\mathcal{P}$, in the most general case, is an unsolved problem.*

Instead of computing the whole feasible objective space $\mathcal{Y}$ (which would be very computationally inefficient), we would like to use dynamic programming to solve for $\mathcal{Y}_{P(\mu)}$ via the value functions

$$P(x,t;\mu) = \inf_{v(\cdot)}\left\{\mu Var^{x,t}_{v(\cdot)}[B(T)] - E^{x,t}_{v(\cdot)}[B(T)]\right\}. \tag{3.1.4}$$

However, as pointed out in [65, 47], the value function $P(x,t;\mu)$ is not amenable to solution by means of dynamic programming due to the variance term. To overcome this difficulty, we use the embedding technique of [47, 65] to embed the objective in (3.1.4) into the value functions (parameterized by $\gamma > 0$)

$$Q(x,t;\gamma) = \inf_{v(\cdot)}\left\{E^{x,t}_{v(\cdot)}[(B(T)-\gamma/2)^2]\right\}, \tag{3.1.5}$$

which can be solved by dynamic programming.

Remark 3.3. *We remark that the quadratic objective can be considered as a target-based approach with a quadratic loss function [62]: by regarding $\gamma/2 > 0$ as a target (recall that $B(0) = 0$), we see that an optimal strategy should stop selling[1] when $B(t) = \gamma/2$, since more selling will increase $B(T)$ beyond $\gamma/2$, which is penalized in the quadratic objective.*

3.1.2 Previous Results

In this section, we review the embedding technique in [65, 47] using a more general notation. This generalization will help us derive some new results which are important for numerical algorithms.

The following property of the feasible objective space $\mathcal{Y}$ is essential in our new results on the embedding technique.

Proposition 3.4 (Bounded Properties of $\mathcal{Y}$)**.** *The feasible objective space $\mathcal{Y}$ is a non-empty subset of $\{(V,E) \in \mathbf{R}^2 : V \geq 0,\ 0 \leq E \leq C_E\}$ for some positive constant C_E.*

Proof. Since V represents variance, $V \geq 0$ is obvious. To prove the boundedness of E, we can assume without loss of generality that the interest rate r is zero. Hence,

$$\begin{aligned} dB(t) &= -vf^l(v)S(t)dt \\ &\leq -vS(t)dt \quad (\text{since } v \leq 0,\ f^l(v) \leq 1 \text{ by Assumption 2.1.16 and } S(t) \geq 0) \\ &\leq |v_{min}|S(t)dt, \end{aligned}$$

[1] Assuming zero interest rate. The case for non-zero interest rate is analogous.

which implies

$$E[B(T)] \leq B(0) + |v_{min}| E\left[\int_0^T S(t)dt\right],$$

where $E[\cdot]$ denotes $E^{x_0,0}_{v(\cdot)}[\cdot]$. By applying the result in [25] (for details see Appendix G), we can show that $\sup_{t\in[0,T]} E[S(t)]$ is bounded by a constant C_S, hence

$$E[B(T)] \leq B(0) + |v_{min}| C_S T, \tag{3.1.6}$$

which completes the proof. □

The authors of [65, 47] work directly with optimal controls (for the value functions $P(x,t;\mu)$ and $Q(x,t;\gamma)$), which may not exist if $\mathcal{Y}$ is not a closed set. To generalize their results, we work with the following point sets.

For the reader's convenience, the definition below restates (3.1.3).

Definition 3.5. For $\mu > 0$, define

$$\mathcal{Y}_{P(\mu)} = \{(V_0, E_0) \in \bar{\mathcal{Y}} : \mu V_0 - E_0 = \inf_{(V,E)\in\mathcal{Y}} \mu V - E\}\ , \tag{3.1.7}$$

and

$$\mathcal{Y}_P = \bigcup_{\mu>0} \mathcal{Y}_{P(\mu)}. \tag{3.1.8}$$

Definition 3.6. For $\gamma > 0$, define

$$\mathcal{Y}_{Q(\gamma)} = \{(V_*, E_*) \in \bar{\mathcal{Y}} : V_* + E_*^2 - \gamma E_* = \inf_{(V,E)\in\mathcal{Y}} V + E^2 - \gamma E\}. \tag{3.1.9}$$

and

$$\mathcal{Y}_Q = \bigcup_{\gamma>0} \mathcal{Y}_{Q(\gamma)}.$$

Note that since

$$\begin{aligned}
&Var^{x,t}_{v(\cdot)}[B(T)] + (E^{x,t}_{v(\cdot)}[B(T)])^2 - \gamma E^{x,t}_{v(\cdot)}[B(T)] \\
=&E^{x,t}_{v(\cdot)}[B(T)^2] - (E^{x,t}_{v(\cdot)}[B(T)])^2 + (E^{x,t}_{v(\cdot)}[B(T)])^2 - \gamma E^{x,t}_{v(\cdot)}[B(T)] \\
=&E^{x,t}_{v(\cdot)}[B(T)^2 - \gamma B(T)] \\
=&E^{x,t}_{v(\cdot)}[(B(T) - \gamma/2)^2] - \gamma^2/4,
\end{aligned}$$

the objective in (3.1.9) is essentially the same as that in (3.1.5), since including the constant term $-\gamma^2/4$ in (3.1.9) does not change $\mathcal{Y}_{Q(\gamma)}$. It is clear that dynamic programming can be used to determine optimal strategies of (3.1.5).

By Proposition 3.4, we have the following obvious results.

Lemma 3.7. *For any $\mu > 0$, $\mathcal{Y}_{P(\mu)}$ is non-empty, i.e. there exists $(V_0, E_0) \in \mathcal{Y}_{P(\mu)} \subseteq \bar{\mathcal{Y}}$ such that*

$$\mu V_0 - E_0 = \inf_{(V,E)\in\mathcal{Y}} \mu V - E.$$

Similarly, for any $\gamma > 0$, $\mathcal{Y}_{Q(\gamma)}$ is non-empty, i.e. there exists $(V_*, E_*) \in \mathcal{Y}_{Q(\gamma)} \subseteq \bar{\mathcal{Y}}$ such that

$$V_* + E_*^2 - \gamma E_* = \inf_{(V,E)\in\mathcal{Y}} V + E^2 - \gamma E.$$

Proof. Construct convergent sub-sequences using the boundedness result. □

Lemma 3.8. *If $(V', E') \in \bar{\mathcal{Y}}$, then*

$$\mu V' - E' \geq \inf_{(V,E)\in\mathcal{Y}} \mu V - E.$$

Similarly,

$$V' + E'^2 - \gamma E' \geq \inf_{(V,E)\in\mathcal{Y}} V + E^2 - \gamma E.$$

Proof. The objective functions are continuous. □

The following result is a slight generalization of the main result on the embedding technique in [65, 47].

Theorem 3.9. *Let $(V_0, E_0) \in \bar{\mathcal{Y}}$ and $\mu > 0$ be such that*

$$\mu V_0 - E_0 = \inf_{(V,E)\in\mathcal{Y}} \mu V - E, \quad \textit{i.e. } (V_0, E_0) \in \mathcal{Y}_{P(\mu)}. \tag{3.1.10}$$

Then

$$V_0 + E_0^2 - \gamma E_0 = \inf_{(V,E)\in\mathcal{Y}} V + E^2 - \gamma E, \quad \textit{i.e. } (V_0, E_0) \in \mathcal{Y}_{Q(\gamma)}. \tag{3.1.11}$$

where

$$\gamma = \frac{1}{\mu} + 2E_0 > 0. \tag{3.1.12}$$

Proof. Assume to the contrary that (3.1.11) does not hold. Then, by Lemma 3.8,

$$\inf_{(V,E)\in\mathcal{Y}} V + E^2 - \gamma E < V_0 + E_0^2 - \gamma E_0. \tag{3.1.13}$$

By Lemma 3.7, there exists $(V_*, E_*) \in \bar{\mathcal{Y}}$ such that

$$V_* + E_*^2 - \gamma E_* = \inf_{(V,E)\in\mathcal{Y}} V + E^2 - \gamma E. \tag{3.1.14}$$

Combining (3.1.13) and (3.1.14) gives

$$V_* + E_*^2 - \gamma E_* < V_0 + E_0^2 - \gamma E_0.$$

Rearranging and multiplying by $\mu > 0$ gives

$$\mu\big(V_* + E_*^2 - (V_0 + E_0^2)\big) - \gamma\mu(E_* - E_0) < 0. \tag{3.1.15}$$

Define the function

$$\pi^\mu(v, e) = \mu v - \mu e^2 - e.$$

Note that

$$\pi^\mu(v + e^2, e) = \mu v + \mu e^2 - \mu e^2 - e = \mu v - e. \tag{3.1.16}$$

It is easy to see that $\pi^\mu(v, e)$ is concave quadratic in (v, e). Consequently,

$$\begin{aligned} \pi^\mu(v + \triangle v, e + \triangle e) &\leq \pi^\mu(v, e) + \frac{\partial \pi^\mu(v, e)}{\partial v}\triangle v + \frac{\partial \pi^\mu(v, e)}{\partial e}\triangle e \\ &= \pi^\mu(v, e) + \mu\triangle v - (1 + 2\mu e)\triangle e. \end{aligned} \tag{3.1.17}$$

A direct application of (3.1.17) gives

$$\begin{aligned} \pi^\mu(V_* + E_*^2, E_*) &\leq \pi^\mu(V_0 + E_0^2, E_0) + \mu\big(V_* + E_*^2 - (V_0 + E_0^2)\big) - (1 + 2\mu E_0)(E_* - E_0) \\ &= \pi^\mu(V_0 + E_0^2, E_0) + \mu\big(V_* + E_*^2 - (V_0 + E_0^2)\big) - \gamma\mu(E_* - E_0) \\ &< \pi^\mu(V_0 + E_0^2, E_0), \end{aligned} \tag{3.1.18}$$

where we have used (3.1.12) in the equality and (3.1.15) in the last inequality.

By (3.1.16), the strict inequality (3.1.18) means that

$$\mu V_* - E_* < \mu V_0 - E_0,$$

which contradicts equation (3.1.10). □

It is immediate that the following holds, which explains the embedding terminology.

Corollary 3.10. *Every element in $\mathcal{Y}_P$ is in $\mathcal{Y}_Q$, i.e. $\mathcal{Y}_P \subseteq \mathcal{Y}_Q$.*

Remark 3.11 (Time-inconsistency)**.** *When solving for the value function $Q(x, t; \gamma)$* (3.1.5)*, γ is treated as a constant. However, when we consider the relationship between optimal controls of the transformed problem* (3.1.5) *and that of the original problem* (3.1.4)*, equation* (3.1.12) *in Theorem 3.9 shows that γ depends on the initial state, i.e. $\gamma = \gamma(x, t; \mu)$. Hence optimal strategies are time-inconsistent [20].*

3.1.3 Using the Embedding Technique in a Numerical Algorithm

We pointed out previously that the linear scalarization problem (Definition 3.5) involves the variance directly and does not allow the use of dynamic programming to compute

optimal strategies. Theorem 3.9 showed that optimal strategies can be found from the quadratic scalarization formulation (Definition 3.6).

We should be aware that for our optimal trade execution problem, the set of controls which generate a given Pareto point may not be unique (see Chapter 5 for more discussion). As a trivial example, consider the case of the point $(V, E) = (0, 0)$. This point can be clearly generated by selling all shares at an infinite rate at $t = 0$ since the price impact will cause the execution price to be zero. Alternatively, the trader could wait any time $t > 0$, and then sell all shares at an infinite rate, and achieve the same result.

In a typical numerical algorithm, when there are multiple optimal strategies that produce the same minimum value of the objective function, only one strategy will be selected. Therefore, we have to be cognizant of possible non-uniqueness of optimal strategies when dealing with the transformed problem.

The following summarizes the challenges and our main results on using the embedding technique in the context of a numerical algorithm.

- Since $\mathcal{Y}_P \subseteq \mathcal{Y}_Q$, the embedding technique may generate points in $\mathcal{Y}_Q$ which are not Pareto optimal points. We develop a post-processing algorithm which can be used to eliminate the spurious points.
- We prove that all Pareto optimal points obtainable from the linear scalarization problem (3.5) can be obtained by solving the quadratic scalarization problem (3.6), even though only one out of possibly many optimal controls of the quadratic scalarization problem is computed.

3.1.4 New Results

This section collects our new results on using the embedding technique in the context of a numerical algorithm.

The following definition of scalarization optimal point (SOP) will prove useful.

Definition 3.12. Let $\mathcal{X}$ be a non-empty subset of $\bar{\mathcal{Y}}$, i.e. the closure of the feasible objective space. We define

$$\mathcal{S}_\mu(\mathcal{X}) = \{(V_0, E_0) \in \bar{\mathcal{X}} : \mu V_0 - E_0 = \inf_{(V,E)\in\mathcal{X}} \mu V - E\}.$$

We call an element of $\mathcal{S}_\mu(\mathcal{X})$ a scalarization optimal point (SOP) w.r.t. $(\mathcal{X}, \mu)$.

We also define

$$\mathcal{S}(\mathcal{X}) = \{(V_0, E_0) : (V_0, E_0) \text{ is an SOP w.r.t. } (\mathcal{X}, \mu) \text{ for some } \mu > 0\}.$$

We call an element of $\mathcal{S}(\mathcal{X})$ a SOP w.r.t. $\mathcal{X}$.

Remark 3.13. *Note that Definition 3.12 generalizes Definition 3.5 in the sense that* $\mathcal{S}_\mu(\mathcal{Y}) = \mathcal{Y}_{P(\mu)}$ *and* $\mathcal{S}(\mathcal{Y}) = \mathcal{Y}_P$.

Remark 3.14. *For any $\mu > 0$, $\mathcal{S}_\mu(\mathcal{X})$ is non-empty by a trivial generalization of Lemma 3.7.*

Remark 3.15. *A point in $(V_0, E_0) \in \mathcal{S}_\mu(\mathcal{X})$ has the geometric interpretation that (V_0, E_0) lies on a supporting hyperplane [21] (in our case a supporting line with slope μ) of $\mathcal{X}$.*

Lemma 3.16. *For any $\mu > 0$,*

$$\inf_{(V,E)\in\mathcal{Y}} \mu V - E = \inf_{(V',E')\in\mathcal{Y}_Q} \mu V' - E'.$$

Proof. Let (V_0, E_0) be a SOP w.r.t. $(\mathcal{Y}, \mu)$. By Corollary 3.10, $\mathcal{Y}_P \subseteq \mathcal{Y}_Q$, hence $(V_0, E_0) \in \mathcal{Y}_Q$. Consequently,

$$\mu V_0 - E_0 = \inf_{(V,E)\in\mathcal{Y}} \mu V - E \geq \inf_{(V',E')\in\mathcal{Y}_Q} \mu V' - E'.$$

Equality follows since the reverse inequality

$$\inf_{(V,E)\in\mathcal{Y}} \mu V - E \leq \inf_{(V',E')\in\mathcal{Y}_Q} \mu V' - E'$$

holds by $\mathcal{Y}_Q \subseteq \bar{\mathcal{Y}}$. □

Theorem 3.17. *The SOPs of $\mathcal{Y}_Q$ are the same as the SOPs of $\mathcal{Y}$, i.e.*

$$\mathcal{S}(\mathcal{Y}_Q) = \mathcal{Y}_P = \mathcal{S}(\mathcal{Y}).$$

Proof. From Corollary 3.10, we have that $\mathcal{Y}_P \subseteq \mathcal{Y}_Q$. By definition, $\mathcal{Y}_Q \subseteq \bar{\mathcal{Y}}$. Suppose $(V_0, E_0) \in \mathcal{S}(\mathcal{Y}_Q)$. Hence there exists $\mu > 0$ such that

$$\mu V_0 - E_0 = \inf_{(V,E)\in\mathcal{Y}_Q} \mu V - E \ .$$

Since $(V_0, E_0) \in \bar{\mathcal{Y}}$, then from Lemma 3.16,

$$\mu V_0 - E_0 = \inf_{(V,E)\in\mathcal{Y}} \mu V - E \ ,$$

and $(V_0, E_0) \in \mathcal{S}(\mathcal{Y})$. Suppose $(V_0, E_0) \in \mathcal{S}(\mathcal{Y})$, then

$$\mu V_0 - E_0 = \inf_{(V,E)\in\mathcal{Y}} \mu V - E \ ,$$

and since $\mathcal{Y}_P \subseteq \mathcal{Y}_Q$, then $(V_0, E_0) \in \mathcal{Y}_Q$, and then from Lemma 3.16,

$$\mu V_0 - E_0 = \inf_{(V,E)\in\mathcal{Y}_Q} \mu V - E \ ,$$

hence $(V_0, E_0) \in \mathcal{S}(\mathcal{Y}_Q)$. □

The following theorem will prove useful when we construct a subset of $\mathcal{Y}_Q$ using a numerical algorithm.

Theorem 3.18 (Uniqueness of SOP points)**.** *If (V, E) is a SOP w.r.t. $\mathcal{Y}_Q$, then there exists a γ such that $(V, E) \in \mathcal{Y}_{Q(\gamma)}$ and $\mathcal{Y}_{Q(\gamma)}$ is a singleton.*

Proof. Let (V_*, E_*) be a SOP w.r.t. $(\mathcal{Y}_Q, \mu^*)$. By Lemma 3.16, $(V_*, E_*) \in \mathcal{Y}_{P(\mu^*)}$. Hence, by Theorem 3.9, there exists γ^* such that

$$(V_*, E_*) \in \mathcal{Y}_{Q(\gamma^*)}, \text{ where } \gamma^* = \frac{1}{\mu^*} + 2E_*. \tag{3.1.19}$$

Suppose there is another element of $\mathcal{Y}_{Q(\gamma^*)}$, which we label (V_0, E_0). Since both elements are in $\mathcal{Y}_{Q(\gamma^*)}$ we have that

$$V_* + E_*^2 - \gamma^* E_* = V_0 + E_0^2 - \gamma^* E_0 \quad = \quad \inf_{(V,E)\in\mathcal{Y}} V + E^2 - \gamma^* E \ ,$$

so that

$$V_0 + E_0^2 - (V_* + E_*^2) - \gamma^*(E_0 - E_*) = 0 \ . \tag{3.1.20}$$

Consider the function $\pi^{\mu^*}(v, e) = \mu^* v - \mu^* e^2 - e$ as in Proposition 3.9. Following similar steps as in the proof of Proposition 3.9, we obtain (using equations (3.1.19) and (3.1.20))

$$\begin{aligned} \pi^{\mu^*}(V_0 + E_0^2, E_0) &\leq \pi^{\mu^*}(V_* + E_*^2, E_*) + \mu^*(V_0 + E_0^2 - (V_* + E_*^2)) - (1 + 2\mu^* E_*)(E_0 - E_*) \\ &= \pi^{\mu^*}(V_* + E_*^2, E_*) + \mu^*(V_0 + E_0^2 - (V_* + E_*^2) - \gamma^*(E_0 - E_*)) \\ &= \pi^{\mu^*}(V_* + E_*^2, E_*) \ . \end{aligned} \tag{3.1.21}$$

Recalling that $\pi^{\mu^*}(v + e^2, e) = \mu^* v - e$, thus equation (3.1.21) yields

$$\mu^* V_0 - E_0 \ \leq \ \mu^* V_* - E_*.$$

Since $(V_*, E_*) \in \mathcal{Y}_{P(\mu^*)}$ and $(V_0, E_0) \in \bar{\mathcal{Y}}$,

$$\mu^* V_* - E_* = \inf_{(V,E)\in\mathcal{Y}} \mu^* V - E \leq \mu^* V_0 - E_0.$$

Hence

$$\mu^* V_0 - E_0 = \mu^* V_* - E_* \ . \tag{3.1.22}$$

Rewrite equations (3.1.20) and (3.1.22) as

$$\mu^*(V_* - V_0) - (E_* - E_0) \ = \ 0 \tag{3.1.23}$$

$$(V_* - V_0) + (E_* - E_0)(E_* + E_0 - \gamma^*) \ = \ 0 \ . \tag{3.1.24}$$

Noting equation (3.1.19), equation (3.1.24) becomes

$$(V_* - V_0) + (E_* - E_0)(E_0 - E_* - 1/\mu^*) \ = 0 \ . \tag{3.1.25}$$

Solving equations (3.1.23) and (3.1.25) for $(E_* - E_0)$ gives the unique solution $E_* = E_0$ and $V_* = V_0$. □

We immediately have the following result for elements of $\mathcal{Y}_{Q(\gamma)}$.

Corollary 3.19 (Properties of $\mathcal{Y}_{Q(\gamma)}$)**.** *For a fixed $\gamma > 0$, $\mathcal{Y}_{Q(\gamma)}$ is either*

- *A singleton containing a SOP w.r.t. $\mathcal{Y}_Q$.*
- *A non-empty set that does not contain any SOP w.r.t $\mathcal{Y}_Q$.*

Since only one out of possibly many optimal controls (which all minimize $V + E^2 - \gamma E$) is selected, a typical numerical algorithm will generate a subset of $\mathcal{Y}_Q$, which we denote by $\mathcal{Y}_Q^{num}$. We define the following in view of Corollary 3.19.

Definition 3.20 (Numerical $\mathcal{Y}_Q$)**.** Let $\mathcal{Y}_{Q(\gamma)}^{num}$ be a singleton subset of $\mathcal{Y}_{Q(\gamma)}$, defined as follows. $\mathcal{Y}_{Q(\gamma)}^{num}$ contains either

- The unique single point which is SOP w.r.t. $\mathcal{Y}_Q$ if $\mathcal{Y}_{Q(\gamma)}$ is the singleton set containing a point SOP w.r.t. $\mathcal{Y}_Q$.
- A single point if $\mathcal{Y}_{Q(\gamma)}$ does not contain any points SOP w.r.t. $\mathcal{Y}_Q$. The single point is selected arbitrarily.

Let

$$\mathcal{Y}_Q^{num} = \bigcup_{\gamma > 0} \mathcal{Y}_{Q(\gamma)}^{num}.$$

Lemma 3.21. *If (V_0, E_0) is a SOP w.r.t. $\mathcal{Y}_Q$, then $(V_0, E_0) \in \mathcal{Y}_Q^{num}$, i.e. $\mathcal{S}(\mathcal{Y}_Q) \subseteq \mathcal{Y}_Q^{num}$*

Proof. By Theorem 3.18, there exists $\gamma > 0$, such that $(V_0, E_0) \in \mathcal{Y}_{Q(\gamma)}$ and $\mathcal{Y}_{Q(\gamma)}$ is a singleton. Hence $(V_0, E_0) \in \mathcal{Y}_Q^{num}$ by Assumption 3.20. □

Lemma 3.22. *For any $\mu > 0$,*

$$\inf_{(V,E) \in \mathcal{Y}_Q} \mu V - E = \inf_{(V',E') \in \mathcal{Y}_Q^{num}} \mu V' - E'.$$

Proof. Let $(V_0, E_0) \in \bar{\mathcal{Y}}_Q$ be SOP w.r.t. $(\mathcal{Y}_Q, \mu)$. It follows from Lemma 3.21 that $(V_0, E_0) \in \mathcal{Y}_Q^{num}$. Hence

$$\mu V_0 - E_0 = \inf_{(V,E) \in \mathcal{Y}_Q} \mu V - E \geq \inf_{(V',E') \in \mathcal{Y}_Q^{num}} \mu V' - E'.$$

The reverse inequality holds since $\mathcal{Y}_Q^{num} \subseteq \mathcal{Y}_Q$. □

Our main result is proving the correctness of the following simple post-processing algorithm that recovers $\mathcal{Y}_P$ from $\mathcal{Y}_Q^{num}$.

Theorem 3.23. *The set $\mathcal{S}(\mathcal{Y}_Q^{num})$ is identical to the set of Pareto points $\mathcal{Y}_P$, i.e.*

$$\mathcal{S}(\mathcal{Y}_Q^{num}) = \mathcal{Y}_P = \mathcal{S}(\mathcal{Y}) \ .$$

Proof. By Theorem 3.17, we know that $\mathcal{S}(\mathcal{Y}_Q) = \mathcal{Y}_P$. Hence we need only show that $\mathcal{S}(\mathcal{Y}_Q^{num}) = \mathcal{S}(\mathcal{Y}_Q)$.

Suppose $(V_0, E_0) \in \mathcal{S}(\mathcal{Y}_Q)$. Hence there exists $\mu > 0$ such that

$$\mu V_0 - E_0 = \inf_{(V,E)\in\mathcal{Y}_Q} \mu V - E \ .$$

From Lemma 3.21, $\mathcal{S}(\mathcal{Y}_Q) \subseteq \mathcal{Y}_Q^{num}$, hence $(V_0, E_0) \in \mathcal{Y}_Q^{num}$. From Lemma 3.22,

$$\mu V_0 - E_0 = \inf_{(V,E)\in\mathcal{Y}_Q^{num}} \mu V - E \ ,$$

and $(V_0, E_0) \in \mathcal{S}(\mathcal{Y}_Q^{num})$. Suppose $(V_0, E_0) \in \mathcal{S}(\mathcal{Y}_Q^{num})$, then

$$\mu V_0 - E_0 = \inf_{(V,E)\in\mathcal{Y}_Q^{num}} \mu V - E \ ,$$

and from Assumption 3.20, $(V_0, E_0) \in \bar{\mathcal{Y}}_Q$. From Lemma 3.22,

$$\mu V_0 - E_0 = \inf_{(V,E)\in\mathcal{Y}_Q} \mu V - E \ ,$$

hence $(V_0, E_0) \in \mathcal{S}(\mathcal{Y}_Q)$. □

3.1.5 Numerical Estimates of $\mathcal{Y}_Q^{num}$

In general, $\mathcal{Y}_Q^{num}$ needs to be approximated in two aspects:

1. $\mathcal{Y}_{Q(\gamma)}^{num}$ can be computed for only finitely many $\gamma > 0$, giving rise to *finite set error*.
2. $\mathcal{Y}_{Q(\gamma)}^{num}$ needs to be approximated by a sequence of points converging to $\mathcal{Y}_{Q(\gamma)}^{num}$, e.g. due to PDE discretization error/Monte Carlo sampling error (examples in Section 5.2).

We denote by $(\mathcal{Y}_Q^{num})^k$ a sequence of approximations that contain the above errors, where $(\mathcal{Y}_Q^{num})^{k+1}$ uses finer meshes and more Monte Carlo simulations than $(\mathcal{Y}_Q^{num})^k$.

Theoretically, these additional approximations give rise to subtleties in applying our new results on the embedding technique, i.e. whether $\mathcal{S}((\mathcal{Y}_Q^{num})^k)$ converge smoothly to $\mathcal{S}(\mathcal{Y}_Q^{num})$. Fortunately, the sequence of approximations $\mathcal{S}((\mathcal{Y}_Q^{num})^k)$ can be plotted/tabulated and thus smooth convergence can be (heuristically) confirmed, in which case the theoretical subtleties should not be a concern.

3.1.6 Implementing the $\mathcal{S}$ operator

In this section we discuss an approach for implementing the $\mathcal{S}$ operator for a finite set $\mathcal{A} = \{(V_k, E_k)\}$, where $k = 1, \cdots, K$. Essentially, we show that $\mathcal{S}(\mathcal{A})$ can be obtained from the upper-left convex hull of $\mathcal{A}$.

Standard algorithms exist for generating the (vertices of the) convex hull of a finite set of points [14]. The upper-left convex hull is defined as the part of the convex hull which starts with the left-most vertex and ends with the top-most vertex by going clockwise. (If there are multiple left-most/top-most vertices, the upper-left convex hull starts with the top-most left-most vertex and ends with the left-most top-most vertex).

Theorem 3.24. *$\mathcal{S}(\mathcal{A})$ can be obtained from a convex hull algorithm by*

$$\mathcal{S}(\mathcal{A}) = \mathcal{C}_{ul}(\mathcal{A}) \cap \mathcal{A},$$

where $\mathcal{C}_{ul}(\mathcal{A})$ denotes the upper-left convex hull of $\mathcal{A}$.

Proof. Let us order (in clockwise order) the vertices in the upper-left convex hull by $\mathbb{P}_l = (\mathbb{V}_l, \mathbb{E}_l)$, where $l = 1, \cdots, L$.

Let $(\mathbb{V}_l, \mathbb{E}_l) \in \mathcal{C}_{ul}(\mathcal{A}) \cap \mathcal{A}$. Since $(\mathbb{V}_l, \mathbb{E}_l)$ is a vertex on the upper-left convex hull, there exists a positive-sloping supporting hyperplane (in our case a line) of $\mathcal{A}$ that goes through $(\mathbb{V}_l, \mathbb{E}_l)$. Hence $(\mathbb{V}_l, \mathbb{E}_l) \in \mathcal{S}(\mathcal{A})$ by Remark 3.15.

Let $(V, E) \in \mathcal{S}(\mathcal{A})$. Since $\mathcal{S}(\mathcal{A}) \subseteq \mathcal{A}$ for the finite set $\mathcal{A}$, $(V, E) = (V_k, E_k) \in \mathcal{A}$. Since a supporting hyperplane of $\mathcal{A}$ always intersects the boundary of the convex hull of $\mathcal{A}$, (V_k, E_k) must be a vertex in the convex hull. $(V_k, E_k) \in \mathcal{C}_{ul}(\mathcal{A})$ then follows since there exists a supporting hyperplane through (V_k, E_K) that (i) has positive slope; and (ii) have $\mathcal{A}$ on its right. □

3.2 HJB PDE Formulation

In this section, we develop an HJB PDE formulation to solve the Mean Variance optimization problem under the regime switching model.

3.2.1 Value Functions

In the embedding technique we solve for the value function (3.1.5), i.e.

$$Q(x, t; \gamma) = \inf_{v(\cdot)} \Big\{ E^{x,t}_{v(\cdot)} \Big[\big(B(T) - \frac{\gamma}{2} \big)^2 \Big] \Big\}, \tag{3.2.1}$$

for initial states (x, t), where $x = (s, b, \alpha, l)$.

To avoid the need to compute separate value functions for different values of γ, we change variables. Recall that, from (2.1.1) and (2.1.13), the process $B(t)$ follows the dynamics

$$dB(t) = \big(rB(t) - vf^l(v)S(t)\big)dt.$$

We define the new process

$$\mathcal{B}(t) = e^{r(T-t)}B(t) - \frac{\gamma}{2}, \tag{3.2.2}$$

which satisfies

$$d\mathcal{B}(t) = -re^{r(T-t)}B(t)dt + e^{r(T-t)}dB(t) = -e^{r(T-t)}vf^l(v)S(t)dt,$$

and

$$\mathcal{B}(T) = B(T) - \frac{\gamma}{2}.$$

Hence

$$\inf_{v(\cdot)}\Big\{E^{s,b=0,\alpha,l,t=0}_{v(\cdot)}\Big[\big(B(T) - \frac{\gamma}{2}\big)^2\Big]\Big\} = \inf_{v(\cdot)}\Big\{E^{s,\mathfrak{b},\alpha,l,t=0}_{v(\cdot)}\Big[\mathcal{B}(T)^2\Big]\Big\},$$

where $\mathfrak{b} = \mathcal{B}(0) = -\gamma/2$.

Let $\tau = T - t$ be the backward time. We define value functions V^l by

$$V^l = V^l(s, \mathfrak{b}, \alpha, \tau) = \inf_{v(\cdot)}\Big\{E^{s,\mathfrak{b},\alpha,l,t=T-\tau}_{v(\cdot)}\Big[\mathcal{B}(T)^2\Big]\Big\}, \tag{3.2.3}$$

where we have used the notation $\mathfrak{b}$ for a state of the process $\mathcal{B}(t)$.

We also define the value functions

$$U^l = U^l(s, \mathfrak{b}, \alpha, \tau) = E^{s,\mathfrak{b},\alpha,l,t=T-\tau}_{v^*(\cdot)}[\mathcal{B}(T)], \tag{3.2.4}$$

where $v^*(\cdot)$ is an optimal control[2] in (3.2.3). The value functions U^l will be required to compute the mean variance efficient frontier, as discussed in Section 3.6. It will be clear in Section 3.6 that mean and variance for various risk aversion levels γ can be determined from the same value functions V^l and U^l; this is the reason we change variables from $B(t)$ to $\mathcal{B}(t)$.

3.2.2 Systems of HJB PDEs

Before deriving the systems of HJB PDEs for solving V^l and U^l, we first define some shorthand for ease of exposition. The reader is suggested to review the notation in Section

[2]If optimal controls are not unique, the value of $E^{s,\mathfrak{b},\alpha,l,t=T-\tau}_{v^*(\cdot)}[\mathcal{B}(T)]$ in general depends on the choice of optimal control. This is one of the subtleties that was discussed in Section 3.1. By Theorem 3.23, this non-uniqueness is not a practical concern since using the post-processing algorithm will guarantee the Pareto-optimality of the computed frontier.

2.1.2. Define

$$\lambda^l = \sum_{\substack{m=1 \\ m\neq l}}^{M} \lambda^{lm} \quad , \quad \rho^l = \sum_{\substack{m=1 \\ m\neq l}}^{M} \lambda^{lm}(\zeta^{lm} - 1), \tag{3.2.5}$$

the differential operator $\mathcal{L}^l$ by

$$\mathcal{L}^l V^l = \frac{(\sigma^l s)^2}{2} V^l_{ss} + (\eta^l - \rho^l) s V^l_s - \lambda^l V^l,$$

and the operator $\mathcal{J}^l$ by

$$\mathcal{J}^l V = \sum_{\substack{m=1 \\ m\neq l}}^{M} \lambda^{lm} V^m(\zeta^{lm} s, \mathfrak{b}, \alpha, \tau).$$

We also define the Lagrangian differential operator $\frac{D^l}{D\tau}(v)$ by

$$\frac{D^l V^l}{D\tau}(v) = V^l_\tau - g^l(v) s V^l_s + e^{r\tau} v f^l(v) s V^l_{\mathfrak{b}} - v V^l_\alpha,$$

which is the rate of change of V^l along the characteristics $s = s(\tau')$, $\mathfrak{b} = \mathfrak{b}(\tau')$, $\alpha = \alpha(\tau')$ defined by the trading velocity v through

$$\frac{ds}{d\tau'} = -g^l(v)s, \quad \frac{d\mathfrak{b}}{d\tau'} = e^{r\tau} v f^l(v) s, \quad \frac{d\alpha}{d\tau'} = -v. \tag{3.2.6}$$

By standard dynamic programming arguments (see Appendix A for details), the value functions V^l solve the system of nonlinear HJB PDEs

$$-\mathcal{L}^l V^l - \mathcal{J}^l V + \max_{v\in[v_{min},0]} \frac{D^l V^l}{D\tau}(v) = 0; \quad l = 1, \ldots, M, \tag{3.2.7}$$

in the domain $\Omega = \{s \geq 0, \mathfrak{b} \leq 0, \alpha \geq 0, \tau > 0\}$, with initial condition at $\tau = 0$ given by

$$V^l(s, \mathfrak{b}, \alpha, \tau = 0) = (\mathfrak{b} + as \lim_{v\to-\infty} f^l(v))^2. \tag{3.2.8}$$

After the optimal trading velocities v^* have been obtained from solving the system of nonlinear HJB PDEs (3.2.7), we can then determine the expected values by solving the system of linear PDEs

$$-\mathcal{L}^l U^l - \mathcal{J}^l U + \frac{D^l U^l}{D\tau}(v^*) = 0; \quad l = 1, \ldots, M, \tag{3.2.9}$$

in the domain Ω, with initial condition at $\tau = 0$ given by

$$U^l(s, \mathfrak{b}, \alpha, \tau = 0) = \mathfrak{b} + as \lim_{v\to-\infty} f^l(v). \tag{3.2.10}$$

Since v^* has been determined, the PDEs in the system (3.2.9) are linear and inexpensive to solve.

3.3 Localization and Boundary Conditions

For computational purposes, we localize the domain Ω to $\Omega_L = \{s \in [0, s_{max}], \mathscr{b} \in [\mathscr{b}_{min}, 0], \alpha \in [0,1], \tau \in [0,T]\}$. The following remark explains why it suffices to consider only non-positive $\mathscr{b}$.

Remark 3.25. *Recall from (3.2.2) that $\mathcal{B}(0) < 0$. Intuitively, in view of definition (3.2.3), when $\mathscr{b} < 0$ an optimal strategy should increase $\mathcal{B}(t)$ towards zero by selling stocks. When $\mathscr{b} = 0$, any selling can only increase $\mathcal{B}(T)$ and therefore an optimal strategy should not sell until the final liquidation, which essentially discards the remaining stock holding. Therefore, $\mathcal{B}(t)$ should stay at zero after it has reached zero from below. In fact, this observation that $\mathcal{B}(t)$ should not exceed the target of zero has already been seen in Remark 3.3 in terms of the original variable $B(t)$.*

Let us now consider how to localize the system of PDEs (3.2.7) for V^l and impose boundary conditions.

For the localized problem, we define $\mathcal{J}^l$ by

$$\mathcal{J}^l V = \sum_{\substack{m=1 \\ m \neq l}}^{M} \lambda^{lm} V^m(\min\{\zeta^{lm} s, s_{max}\}, \mathscr{b}, \alpha, \tau),$$

to ensure that V^m is evaluated within Ω_L.

No boundary conditions are required at $s = 0$ because all V_s and V_{ss} terms vanish in (3.2.7).

No boundary condition is required at $\alpha = 1$ since $-v \geq 0$ and thus the characteristics are outgoing there.

No boundary condition is required at $\mathscr{b} = \mathscr{b}_{min} < 0$ since $e^{r\tau} v f^l(v) s \leq 0$ and thus the characteristics are outgoing there.

At $s = s_{max}$, we use the boundary conditions $V^l_s = 0$ and $V^l_{ss} = 0$.

The rationale for imposing $V^l_s = V^l_{ss} = 0$ at $s = s_{max}$ is that $V^l \to \textit{constant}$ as $s \to \infty$ when other variables are held constant. Note that this is obvious when $\alpha = 0$; otherwise, consider separately the cases where $\mathscr{b} < 0$ and $\mathscr{b} = 0$. Intuitively, in view of definition (3.2.3), when $\mathscr{b} < 0$ an optimal strategy should increase $\mathcal{B}(t)$ towards zero by selling stocks. As $s \to \infty$ and $\alpha s \gg |\mathscr{b}|$, an optimal strategy will force $\mathcal{B}(T) \to 0$ (and $V^l \to 0$). When $\mathscr{b} = 0$, any selling can only increase $\mathcal{B}(T)$ and therefore an optimal strategy should not sell until the final liquidation which will essentially discard the remaining stock holding, and consequently V^l will be independent of s.

The boundary conditions $V^l_s = 0$ and $V^l_{ss} = 0$ at $s = s_{max}$ are clearly approximations for a finite s_{max}. We shall verify that if s_{max} is sufficiently large then this does not cause any appreciable error in the region of interest.

At $\mathfrak{b} = 0$ and $\alpha = 0$, we impose $v = 0$ so that $(s, \mathfrak{b}, \alpha, \tau)$ stays in Ω_L. These are legitimate since $\mathfrak{b}$ should not become positive (see Remark 3.25) and α should not become negative (i.e. a short position).

The localized problem for U^l is extremely similar to that for V^l. To avoid repeating ourselves, henceforth our discussion on numerical methods will be detailed for only V^l.

3.4 Formal Formulation of Localized Problem

We now formalize the localized problem with boundary conditions discussed in the previous section. We will use the notation[3] $x = (s, \mathfrak{b}, \alpha, \tau)$ to denote a point in $\Omega_L = \{s \in [0, s_{max}], \mathfrak{b} \in [\mathfrak{b}_{min}, 0], \alpha \in [0, 1], \tau \in [0, T]\}$. Note that since different values of l correspond to different PDEs in the system, l does not appear in this notation which concerns the domain of a single PDE.

Definition 3.26. The following domains partition Ω_L.

$$\begin{aligned}
\Omega_{in} &= \{s < s_{max}, \mathfrak{b} \in [\mathfrak{b}_{min}, 0), \alpha > 0, \tau > 0\} \\
\Omega_{s_{max}} &= \{s = s_{max}, \mathfrak{b} \in [\mathfrak{b}_{min}, 0), \alpha > 0, \tau > 0\} \\
\Omega_{v=0} &= \{s < s_{max}, \mathfrak{b} \in [\mathfrak{b}_{min}, 0), \alpha = 0, \tau > 0\} \cup \{s < s_{max}, \mathfrak{b} = 0, \tau > 0\} \\
\Omega_{s_{max}, v=0} &= \{s = s_{max}, \mathfrak{b} \in [\mathfrak{b}_{min}, 0), \alpha = 0, \tau > 0\} \cup \{s = s_{max}, \mathfrak{b} = 0, \tau > 0\} \\
\Omega_{\tau_0} &= \{\tau = 0\}
\end{aligned}$$

Definition 3.27. The following definition of the Lagrangian differential operator $\frac{D^l}{D\tau}(x, v)$ encompasses various boundary conditions.

$$\frac{D^l V^l}{D\tau}(x, v) = \begin{cases} V^l_\tau(x) - g^l(v) s V^l_s(x) + e^{r\tau} v f^l(v) s V^l_{\mathfrak{b}}(x) - v V^l_\alpha(x) & x \in \Omega_{in} \\ V^l_\tau(x) + e^{r\tau} v f^l(v) s V^l_{\mathfrak{b}}(x) - v V^l_\alpha(x) & x \in \Omega_{s_{max}} \\ V^l_\tau(x) & x \in \Omega_{v=0} \cup \Omega_{s_{max}, v=0} \end{cases} \tag{3.4.1}$$

[3]Note that the same notation x was previously used to mean a state $x = (s, b, \alpha, l)$ of the process $X(t) = (S(t), B(t), A(t), L(t))$. The meaning of the notation x should be clear from the context and no confusion should arise.

Definition 3.28. Using the notations

$$\begin{aligned}
DV^l(x) &= (V_s^l(x), V_\mathscr{b}^l(x), V_\alpha^l(x), V_\tau^l(x)),\\
D^2V^l(x) &= V_{ss}^l(x),\\
\mathcal{L}^lV^l(x) &= \frac{(\sigma^l s)^2}{2}V_{ss}^l(x) + (\eta^l - \rho^l)sV_s^l(x) - \lambda^l V^l(x),\\
\mathcal{J}_L^lV(x) &= \sum_{\substack{m=1\\ m\neq l}}^{M} \lambda^{lm}V^m(\min\{\zeta^{lm}s, s_{max}\}, \mathscr{b}, \alpha, \tau),
\end{aligned}$$

the system of HJB PDEs (3.2.7) can be formally written as

$$F^l(x, V^l(x), \{V^m(\min\{\zeta^{lm}s, s_{max}\}, \mathscr{b}, \alpha, \tau)\}^{m\neq l}, DV^l(x), D^2V^l(x)) = 0 \quad \text{for } l = 1, \cdots, M, \tag{3.4.2}$$

where

$$F^l(x, V^l(x), \{V^m(\min\{\zeta^{lm}s, s_{max}\}, \mathscr{b}, \alpha, \tau)\}^{m\neq l}, DV^l(x), D^2V^l(x))$$
$$= \begin{cases}
F_{in}^l(\cdots) = -\mathcal{L}^lV^l(x) - \mathcal{J}_L^lV(x) + \lambda^lV^l(x) + \max_{v\in[v_{min},0]}\frac{D^lV^l}{D\tau}(x,v) & x \in \Omega_{in}\\
F_{s_{max}}^l(\cdots) = -\mathcal{J}_L^lV(x) + \lambda^lV^l(x) + \max_{v\in[v_{min},0]}\frac{D^lV^l}{D\tau}(x,v) & x \in \Omega_{s_{max}}\\
F_{v=0}^l(\cdots) = -\mathcal{L}^lV^l(x) - \mathcal{J}_L^lV(x) + \lambda^lV^l(x) + \frac{D^lV^l}{D\tau}(x,v) & x \in \Omega_{v=0}\\
F_{s_{max},v=0}^l(\cdots) = -\mathcal{J}_L^lV(x) + \lambda^lV^l(x) + \frac{D^lV^l}{D\tau}(x,v) & x \in \Omega_{s_{max},v=0}\\
F_{\tau=0}^l(\cdots) = V^l(x) - \mathscr{b}^2 & x \in \Omega_{\tau=0}
\end{cases}$$

3.5 Discretization

For easy reference, notations in this and subsequent sections are defined/summarized in Table 3.1.

3.5.1 Computational Grid

Define a set of nodes $\{s_i\}$, $\{\mathscr{b}_j\}$, $\{\alpha_k\}$ and $\{\tau_n\}$, where $0 \le i \le i_{max}$, $0 \le j \le j_{max}$, $0 \le k \le k_{max}$, and $0 \le n \le n_{max}$. We order the nodes in ascending order and make $\tau_n = n\triangle\tau$, where $\triangle\tau = T/n_{max}$.

3.5.2 Discretizing $\mathcal{L}^lV^l$

We use standard finite difference methods to discretize $\mathcal{L}^lV^l(x_{i,j,k,n+1})$. Let $(\mathcal{L}_h^l\, V_h^l)_{i,j,k,n+1}$ denote the discretized version of $\mathcal{L}^lV^l(x_{i,j,k,n+1})$. $\mathcal{L}^lV^l(x_{i,j,k,n+1})$ is discretized using cen-

Notations	Descriptions
$x = (s, \mathscr{b}, \alpha, \tau)$	a point in Ω_L
Ω_h	grid; spacing between neighboring nodes is $O(h)$
$x_{i,j,k,n}$	grid node $(s_i, \mathscr{b}_j, \alpha_k, \tau_n)$ in Ω_h
x_h	shorthand notation for $x_{i,j,k,n+1}$
$V_h = (V_h^1, \cdots, V_h^M)$	$\mathbf{R}^M$-valued discrete function defined on Ω_h
V_h^l	l-th component of V_h; real-valued
$V_{i,j,k,n}^l$	value of V_h^l at $x_{i,j,k,n}$
$\hat{x}_{i,j,k,n}(v) = (s_{\hat{i}}, \mathscr{b}_{\hat{j}}, \alpha_{\hat{k}}, \tau_n)$	foot of Lagrangian characteristics; not on grid in general
$\tilde{x}^{l\to m}$	shorthand for $(\min\{\zeta^{lm}s, s_{max}\}, \mathscr{b}, \alpha, \tau)$.
$\tilde{x}_{i,j,k,n+1}^{l\to m}$	shorthand for $(\min\{\zeta^{lm}s_i, s_{max}\}, \mathscr{b}_j, \alpha_k, \tau_{n+1})$.
$V_{interp}^l(\hat{x}_{i,j,k,n}(v))$	linear interpolated value of V_h^l
$V_{interp}^m(\tilde{x}_{i,j,k,n+1}^{l\to m})$	linear interpolated value of V_h^m
$\{V_{i',j,k,n+1}^l\}_{i'\neq i}$	values $V_{i',j,k,n+1}^l$ defining $(\mathcal{L}_h^l V_h^l)_{i,j,k,n+1}$, where $i' \neq i$
$\{V_{i',j',k',n}^l\}$	values $V_{i',j',k',n}^l$ defining $V_{interp}^l(\hat{x}_{i,j,k,n}(v))$
$\{V_{i',j',k',n+1}^m\}^{m\neq l}$	values $V_{i',j',k',n+1}^m$ defining $V_{interp}^m(\tilde{x}_{i,j,k,n+1}^{l\to m})$

TABLE 3.1: *Summary of notations for discretizing the system of HJB PDEs (3.2.7) for the Mean Variance problem.*

tral, forward, or backward differencing in the s direction to give

$$(\mathcal{L}_h^l V_h^l)_{i,j,k,n+1} = a_i^l\big(V_{i-1,j,k,n+1}^l\big) - \big(a_i^l + b_i^l + \lambda^l\big)\big(V_{i,j,k,n+1}^l\big) + b_i^l\big(V_{i+1,j,k,n+1}^l\big)$$
$$\text{for all } i \text{ except } i = 0, i_{max},$$

where the positive coefficient condition

$$a_i^l \geq 0 \text{ and } b_i^l \geq 0 \tag{3.5.1}$$

is guaranteed by the algorithm [28]. The boundary conditions at $s = 0$ and $s = s_{max}$ are taken into account by setting

$$a_0^l = b_0^l = a_{i_{max}}^l = b_{i_{max}}^l = 0.$$

3.5.3 Discretizing the Lagrangian Derivative Terms

The discretized version of the Lagrangian derivative $\frac{D^l V^l}{D\tau}(x_h, v)$ is given by

$$\frac{D^l V^l}{D\tau}(x_{i,j,k,n+1}, v) = \frac{1}{\triangle\tau}\Big(V_{i,j,k,n+1}^l - V_{interp}^l(\hat{x}_{i,j,k,n}(v))\Big), \tag{3.5.2}$$

where $\hat{x}_{i,j,k,n}(v) = (s_{\hat{i}}, \mathscr{b}_{\hat{j}}, \alpha_{\hat{k}}, \tau_n)$ is the foot of the characteristics when we solve the ODEs (3.2.6) initially at $x_{i,j,k,n+1}$, from τ_{n+1} to τ_n, and $V_{interp}^l(\hat{x}_{i,j,k,n}(v))$ denotes a linear inter-

polated value.

The foot of the Lagrangian characteristics can be written as a function of the destination point x_h and the trading velocity v as

$$(s_{\hat{i}}, \mathfrak{b}_{\hat{j}}, \alpha_{\hat{k}}, \tau_n) = \mathcal{I}^l(x_{i,j,k,n+1}, v, \triangle\tau), \tag{3.5.3}$$

where $\mathcal{I}^l = (\mathcal{I}^l_1, \mathcal{I}^l_2, \mathcal{I}^l_3, \mathcal{I}^l_4)$ is defined for $x \in \Omega_L$ and $v \in [v_{min}, 0]$ by

$$\mathcal{I}^l_1(x, v, \triangle\tau) = \begin{cases} s\exp(g^l(v)\triangle\tau) & s \neq s_{max} \\ s & s = s_{max} \end{cases}, \tag{3.5.4}$$

$$\mathcal{I}^l_2(x, v, \triangle\tau) = \mathfrak{b} - e^{r\tau} v s f^l(v)\Big(\frac{e^{g^l(v)\triangle\tau} - 1}{g^l(v)}\Big), \tag{3.5.5}$$

$$\mathcal{I}^l_3(x, v, \triangle\tau) = \alpha + v\triangle\tau, \tag{3.5.6}$$

$$\mathcal{I}^l_4(x, v, \triangle\tau) = \tau - \triangle\tau. \tag{3.5.7}$$

Remark 3.29. *Note that $s = s_{max}$ has to be treated separately in (3.5.4) because of the boundary condition $V_s = V_{ss} = 0$ at $s = s_{max}$.*

For theoretical purposes, we can approximate (3.5.3) - (3.5.7) by

$$s_{\hat{i}} = \begin{cases} s_i + s_i g^l(v)\triangle\tau + O((\triangle\tau)^2) & i < i_{max} \\ s_i & i = i_{max} \end{cases}, \tag{3.5.8}$$

$$\mathfrak{b}_{\hat{j}} = \mathfrak{b}_j - e^{r\tau_{n+1}} v s_i f^l(v)\triangle\tau + O((\triangle\tau)^2), \tag{3.5.9}$$

$$\alpha_{\hat{k}} = \alpha_k + v\triangle\tau, \tag{3.5.10}$$

$$\tau_n = \tau_{n+1} - \triangle\tau. \tag{3.5.11}$$

3.5.4 Discretizing $\max_{v\in[v_{min},0]} \frac{D^l V^l}{D\tau}(x, v)$

In order to motivate our discretization technique, we will first explain why the following straightforward discretization has conceptual difficulties:

$$\max_{v\in[v_{min},0]} \frac{D^l V^l}{D\tau}(x_{i,j,k,n+1}, v) \approx \frac{1}{\triangle\tau}\Big(V^l_{i,j,k,n+1} - \min_{v\in[v_{min},0]} V^l_{interp}(\hat{x}_{i,j,k,n}(v))\Big). \tag{3.5.12}$$

The problem with the discretization (3.5.12) is that the point at which we interpolate V^l_h, i.e. the point $\hat{x}_{i,j,k,n}(v) = \mathcal{I}^l(x_h, v, \triangle\tau)$, may go out of Ω_L for some $v \in [v_{min}, 0]$.

3.5.4.1 Restriction of admissible velocities

We now proceed more formally and set up notations that will be useful later in proving consistency of our numerical scheme.

According to Definition 3.27, restricting admissible velocities is relevant only when a grid node $x_h \in \Omega_{in} \cup \Omega_{s_{max}}$. For such x_h in a grid Ω_h with time spacing $\triangle\tau$, we define

$$\Omega_{\mathbf{V}^l_{h,res}} = \Big\{ x_h \in \Omega_{in} \cup \Omega_{s_{max}} \text{ s.t. } \exists v \in [v_{min}, 0] \text{ s.t. } \mathcal{I}^l(x_h, v, \triangle\tau) \notin \Omega_L \Big\} \tag{3.5.13}$$

to be the places where the set of admissible velocities needs to be restricted so that $\mathcal{I}^l(x_h, v, \triangle\tau)$ stays in Ω_L.

For $x_h \in \Omega_{in} \cup \Omega_{s_{max}} \cup \Omega_{v=0} \cup \Omega_{s_{max},v=0}$, we define $\mathbf{V}^l_{h,res}(x_h)$ to be the set of restricted admissible velocities, i.e.

$$\mathbf{V}^l_{h,res}(x_h) = \begin{cases} \{v \in [v_{min}, 0] \text{ s.t. } \mathcal{I}^l(x_h, v, \triangle\tau) \in \Omega_L\}, & x_h \in \Omega_{in} \cup \Omega_{s_{max}} \\ \{0\}, & x_h \in \Omega_{v=0} \cup \Omega_{s_{max},v=0} \end{cases}$$

Note that $\mathbf{V}^l_{h,res}(x_h)$ is guaranteed to be non-empty since $\mathcal{I}^l(x_{i,j,k,n+1}, v = 0, \triangle\tau) = (s_i, \text{ß}_j, \alpha_k, \tau_n) \in \Omega_L$.

3.5.4.2 Discretizing the control space

For a grid node $x_{i,j,k,n+1}$, we discretize the set[4] of restricted admissible velocities $\mathbf{V}^l_{h,res}(x_{i,j,k,n+1})$ into a discrete set $\hat{\mathbf{V}}^l_{h,res}(x_{i,j,k,n+1})$ in the usual way such that the maximum spacing between neighboring nodes goes to zero at a rate of $O(h)$.

Our discretization can now be stated as

$$\max_{v \in [v_{min}, 0]} \frac{D^l V^l}{D\tau}(x_{i,j,k,n+1}, v) \approx \frac{1}{\triangle\tau} \Big(V^l_{i,j,k,n+1} - \min_{v \in \hat{\mathbf{V}}^l_{h,res}(x_{i,j,k,n+1})} V^l_{interp}(\hat{x}_{i,j,k,n}(v)) \Big).$$

Since V^l_h may not be convex, we use a linear search as the minimization algorithm to guarantee global optimality.

3.5.5 Discretizing $\mathcal{J}^l V$

The discretized version of $\mathcal{J}^l V$ at node $x_{i,j,k,n+1}$ is given by

$$(\mathcal{J}^l_h V_h)_{i,j,k,n+1} = \sum_{\substack{m=1 \\ m \neq l}}^{M} \lambda^{lm} V^m_{interp}(\tilde{x}^{l \to m}_{i,j,k,n+1}),$$

where the notation $\tilde{x}^{l \to m}_{i,j,k,n+1}$ is defined in Table 3.1 and $V^m_{interp}(\tilde{x}^{l \to m}_{i,j,k,n+1})$ is a linear interpolated value.

[4]We note that $\mathbf{V}^l_{h,res}(x_h)$ is a closed and bounded interval of the form $[v^l_{h,res}(x_h), 0]$ by continuity arguments.

3.5.6 Complete Discretization Scheme

For the $\mathbf{R}^M$-valued discrete function V_h defined on grid Ω_h, let

$$\begin{aligned}
&\mathcal{H}^l_{i,j,k,n+1}\Big(h, V^l_{i,j,k,n+1}, \{V^l_{i',j,k,n+1}\}_{i'\neq i}, \{V^l_{i',j',k',n}\}, \{V^m_{i',j',k',n+1}\}^{m\neq l}\Big) \\
&= -\sum_{\substack{m=1\\ m\neq l}}^{M} \lambda^{lm}\, V^m_{interp}(\tilde{x}^{l\to m}_{i,j,k,n+1}) \\
&\quad + \frac{1}{\triangle\tau}\Big(V^l_{i,j,k,n+1} - \min_{v\in\hat{\mathbf{V}}^l_{h,res}(x_{i,j,k,n+1})} V^l_{interp}(\hat{x}_{i,j,k,n}(v))\Big) - (\mathcal{L}^l_h\, V^l_h)_{i,j,k,n+1}, \qquad (3.5.14)
\end{aligned}$$

where

$$\begin{aligned}
\{V^l_{i',j,k,n+1}\}_{i'\neq i} &= \{\text{values } V^l_{i',j,k,n+1} \text{ defining } (\mathcal{L}^l_h\, V^l_h)_{i,j,k,n+1},\ \text{where } i'\neq i\} \\
\{V^l_{i',j',k',n}\} &= \{\text{values } V^l_{i',j',k',n} \text{ defining } V^l_{interp}(\hat{x}_{i,j,k,n}(v)),\ \text{where } i',j',k' \text{ are arbitrary}\} \\
\{V^m_{i',j',k',n+1}\}^{m\neq l} &= \{\text{values } V^m_{i',j',k',n+1} \text{ defining } V^m_{interp}(\tilde{x}^{l\to m}_{i,j,k,n+1}),\ \text{where } i',j',k' \text{ are arbitrary}\}
\end{aligned}$$

The complete discretization scheme can be given as

$$\mathcal{G}^l_{i,j,k,n+1}\Big(h, V^l_{i,j,k,n+1}, \{V^l_{i',j,k,n+1}\}_{i'\neq i}, \{V^l_{i',j',k',n}\}, \{V^m_{i',j',k',n+1}\}^{m\neq l}\Big) = 0 \text{ for } l = 1,\cdots,M, \qquad (3.5.15)$$

where

$$\mathcal{G}^l_{i,j,k,n+1} = \begin{cases} V^l_{i,j,k,n+1} - \mathcal{b}^2_j & \tau_{n+1} = 0 \\ \mathcal{H}^l_{i,j,k,n+1} & \tau_{n+1} > 0 \end{cases} \qquad (3.5.16)$$

The linear discretized equations (3.5.15) are solved at each time step as follows: the optimal control is first determined by linear interpolation, then the equations are solved using a fixed point iteration scheme [36, 37].[5]

Note that solution of the system of discrete equations (3.5.15) is an $\mathbf{R}^M$-valued discrete function V defined on the grid Ω_h. We will prove that the discrete solutions converge to the viscosity solution in Chapter 4.

3.6 Computing Results of Practical Interest

In this section, we discuss two methods for computing results of practical interest for Mean Variance optimal strategies. The PDE method is more elegant whereas the Hybrid (PDE-Monte Carlo) method is more versatile.

[5] In the papers [36, 37], the scheme is called a fixed point policy iteration method since it can also be used to determine the optimal control in other discretizations; in our case, the optimal control is already determined based on time n information from the semi-Lagrangian discretization.

3.6.1 The PDE Method

The PDE method can be used to obtain the mean variance efficient frontier[6] by straightforward evaluation of value functions. The PDE method requires solving the system of linear PDEs (3.2.9) in addition to solving (3.2.7).

In the PDE method, the mean variance efficient frontier is obtained directly from the value functions (3.2.7) and (3.2.9). For each value of γ, the corresponding point on the frontier $\mathcal{Y}_Q$ (for initial regime $L(0) = l$) can be shown to be given by the expressions

$$E^{s,\mathfrak{b},\alpha,l,t=0}_{v^*(\cdot)}[B(T)] = U^l_0(\mathfrak{b}) + \frac{\gamma}{2}, \tag{3.6.1}$$

$$Var^{s,\mathfrak{b},\alpha,l,t=0}_{v^*(\cdot)}[B(T)] = V^l_0(\mathfrak{b}) - (U^l_0(\mathfrak{b}))^2, \tag{3.6.2}$$

where $\mathfrak{b} = \mathcal{B}(0) = -\gamma/2$ by equation (3.2.2), and $U^l_0(\mathfrak{b})$ and $V^l_0(\mathfrak{b})$ are shorthand notations for

$$V^l_0(\mathfrak{b}) \equiv V^l(s, \mathfrak{b}, \alpha, \tau = T) = E^{s,\mathfrak{b},\alpha,l,t=0}_{v^*(\cdot)}[\mathcal{B}(T)^2],$$
$$U^l_0(\mathfrak{b}) \equiv U^l(s, \mathfrak{b}, \alpha, \tau = T) = E^{s,\mathfrak{b},\alpha,l,t=0}_{v^*(\cdot)}[\mathcal{B}(T)].$$

The formula (3.6.1) and (3.6.2) are obtained by solving for $E^{s,\mathfrak{b},\alpha,l,t=0}_{v^*(\cdot)}[B(T)]$ and $E^{s,\mathfrak{b},\alpha,l,t=0}_{v^*(\cdot)}[B(T)^2]$ from the linear system

$$E^{s,\mathfrak{b},\alpha,l,t=0}_{v^*(\cdot)}[B(T)^2] - \gamma E^{s,\mathfrak{b},\alpha,l,t=0}_{v^*(\cdot)}[B(T)] + \frac{\gamma^2}{4} = E^{s,\mathfrak{b},\alpha,l,t=0}_{v^*(\cdot)}[\mathcal{B}(T)^2]$$
$$E^{s,\mathfrak{b},\alpha,l,t=0}_{v^*(\cdot)}[B(T)] - \frac{\gamma}{2} = E^{s,\mathfrak{b},\alpha,l,t=0}_{v^*(\cdot)}[\mathcal{B}(T)]$$

Remark 3.30. *Note that mean and variance for various risk aversion levels γ can be determined from the same value functions V^l and U^l using different values of $\mathfrak{b}$. This means that the entire efficient frontier can be obtained with a single PDE solve.*

This was the reason we changed variables from $B(t)$ to $\mathcal{B}(t)$; if we were to work with $Q(x, t; \gamma)$ in (3.2.1)*, we would need to compute separate value functions for each value of γ.*

3.6.2 The Hybrid (PDE-Monte Carlo) Method

In the Hybrid method, the optimal control $v^*(\cdot)$ is first obtained by solving the system of HJB PDEs (3.2.7). Monte Carlo simulations are then carried out (see Appendix E for details) to estimate quantities of interest, using the optimal control $v^*(\cdot)$. An advantage of the Hybrid method is that we can estimate interesting statistics (e.g. liquidation progress) that are difficult to obtain directly from the value functions.

[6]Technically, this means $\mathcal{Y}_Q$ as defined in Definition 3.6. This terminology will be used in the rest of this section.

3.7 Improving Efficiency

In this section we explain how we combine the techniques of similarity reduction, non-standard interpolation and grid scaling to significantly improve the efficiency of our numerical methods for solving the system of HJB PDEs (3.2.7). These techniques are important in overcoming the challenges in solving (3.2.7). Without these techniques, solving (3.2.7) to satisfactory precision would be computationally expensive.

For readers who need to solve HJB PDEs that pose similar challenges, the techniques discussed here will be of interest. On the other hand, readers who are not interested in these techniques can safely skip this section, which is largely independent of the rest of the thesis.

We also note that our convergence proof in Chapter 4 is for the discretization scheme (3.5.15) that uses none of the techniques in this section. It is straightforward, but algebraically tedious, to prove convergence for the case of using similarity reduction; we refer interested readers to [31] for such a proof in the single regime case.

We will discuss the techniques using V^l (3.2.3) as an example. The same techniques can be applied to U^l (3.2.4).

In this section we explain the techniques by analyzing the HJB PDE. Section 5.2.7 will illustrate the improvements by numerical results.

3.7.1 Similarity Reduction

It can be verified that the form of the system of PDEs (3.2.7) and the initial condition (3.2.8) imply the homogeneity properties (for positive scalar ξ)

$$V^l(\xi s, \xi \mathcal{b}, \alpha, \tau) = \xi^2 V^l(s, \mathcal{b}, \alpha, \tau), \tag{3.7.1}$$

$$v^*(\xi s, \xi \mathcal{b}, \alpha, \tau, l) = v^*(s, \mathcal{b}, \alpha, \tau, l), \tag{3.7.2}$$

which suggests the use of similarity reduction as follows. By the homogeneity property (3.7.1),

$$V^l(s, \mathcal{b}, \alpha, \tau) = (\frac{\mathcal{b}}{\mathcal{b}^*})^2 V^l(\frac{s\mathcal{b}^*}{\mathcal{b}}, \mathcal{b}^*, \alpha, \tau). \tag{3.7.3}$$

Therefore we only need a single grid node $\mathcal{b}^* < 0$ in the $\mathcal{b}$ direction, which saves significant computational cost. For $\mathcal{b} = 0$, (3.7.1) implies the boundary condition $V^l = 0$. In using similarity reduction, the calculation of $V^l_{interp}(\hat{x}_{i,j,k,n}(v))$ needs to be adapted by using a discrete version of (3.7.3), i.e.

$$V^l_{interp}(\hat{x}_{i,j,k,n}(v)) = \big(\frac{\mathcal{b}_{\hat{j}}}{\mathcal{b}^*}\big)^2 V^l_{interp}(\frac{s_{\hat{i}}\mathcal{b}^*}{\mathcal{b}_{\hat{j}}}, \mathcal{b}^*, \alpha_{\hat{k}}, \tau_n).$$

3.7.2 Parametric Curve Interpolation Method

Recall that in our semi-Lagrangian discretization, we need to interpolate the discrete value function V^l at the foot of the Lagrangian characteristics, i.e. the term $V^l_{interp}(\hat{x}_{i,j,k,n}(v))$ in (3.5.2). It turns out that standard linear interpolation, which interpolates along the axes directions, has poor accuracy in approximating V^l. To obtain accurate interpolation results, we develop a parametric curve interpolation method, which is essentially linear interpolation along a carefully chosen direction.

We explain the parametric curve interpolation method by considering a limiting case with extreme parameter values $\sigma = \kappa_t = 0$, and typical parameter values $r = \kappa_p = \kappa_s = \eta = 0$ (single regime). Since the asset price is constant, problem (3.2.3) degenerates to the deterministic control problem of minimizing $\mathcal{B}(T)^2$. Moreover, since there is no pricing impact, $\mathcal{B}(T) = \alpha s + \mathscr{b}$ with certainty[7]. Consequently, the value function V is [8]

$$V(s, \mathscr{b}, \alpha, \tau) = \inf_{v(\cdot)} E^{s,\mathscr{b},\alpha,T-\tau}_{v(\cdot)}[\mathcal{B}(T)^2] = \mathcal{B}(T)^2 = (\alpha s + \mathscr{b})^2, \tag{3.7.4}$$

which can also be verified by direct substitution into the HJB equation (3.2.7), (3.2.8) as follows. First, note that the initial condition (3.2.8) is satisfied because $f(v) \equiv 1$. To verify (3.2.7), note that the parameter values yield the simplifications

$$\mathcal{L}V = 0, \quad \frac{DV}{D\tau}(v) = V_\tau + vsV_{\mathscr{b}} - vV_\alpha. \tag{3.7.5}$$

Substituting (3.7.4) into (3.7.5) gives

$$V_\tau = 0, V_{\mathscr{b}} = 2(\alpha s + \mathscr{b}), V_\alpha = 2s(\alpha s + \mathscr{b}) \implies \frac{DV}{D\tau}(v) \equiv 0 \text{ for all } v. \tag{3.7.6}$$

Since any admissible trading velocity v is optimal in this case, the problem of determining the optimal control v is completely ill-posed.

The above limiting case motivates the definition of the parametric curve interpolation method. In the limiting case, the method is defined as replacing linear interpolation along the α-axis direction by linear interpolation along the parametric curve L defined by

$$\begin{aligned} L &= (s_{\hat{i}}, \mathscr{b}_{\hat{j}}, \alpha_{\hat{k}}) + \zeta(\frac{ds}{d\zeta}, \frac{d\mathscr{b}}{d\zeta}, \frac{d\alpha}{d\zeta}), \\ \frac{ds}{d\zeta} = 0, \quad \frac{d\mathscr{b}}{d\zeta} &= vs_{\hat{i}}, \quad \frac{d\alpha}{d\zeta} = -v. \end{aligned} \tag{3.7.7}$$

Note that different parametric curves L are used for different trading velocities v (the candidate control). In the limiting case, linear interpolation along the parametric curve L is exact, since (3.7.7) defines a curve of constant wealth $\{\alpha s + \mathscr{b} = \text{ constant}\}$. The differ-

[7] Our definition of the liquidation value in (2.1.8) is designed to handle this case so that $\lim_{v\to-\infty} A(T^-)S_{exec}(v, T^-) = A(T^-)S(t^-)$ when $\kappa_t = 0$

[8] We drop the superscript l since there is only one regime.

ence between standard axis-aligned interpolation and the parametric curve interpolation method is illustrated in Figure 3.1.

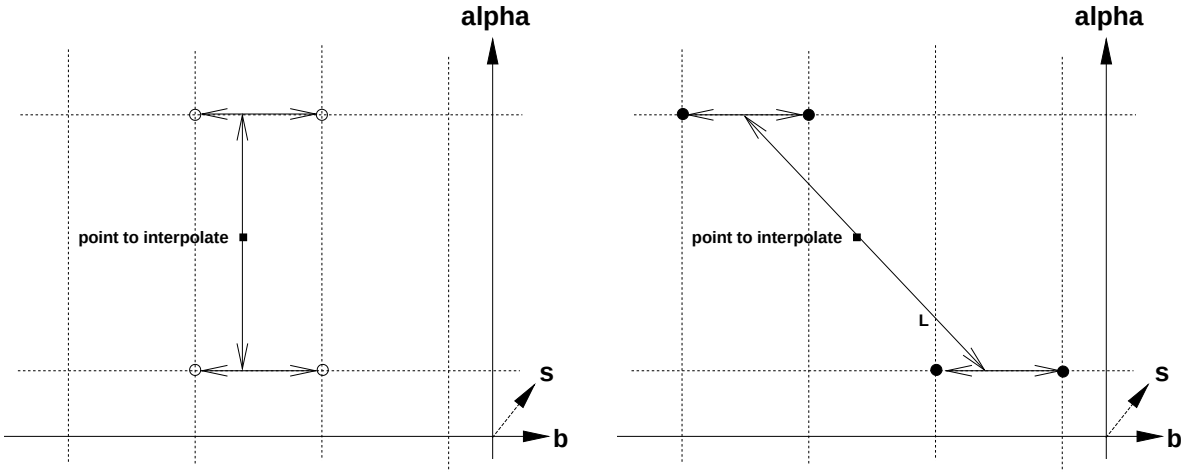

(a) The standard method linearly interpolates along the axes directions.

(b) In the parametric curve method, linear interpolation along the α-axis direction is replaced by linear interpolation along L.

FIGURE 3.1: *Comparing the two methods of interpolation at the foot of characteristics, shown as "point to interpolate" in the diagram. The dashed lines correspond to the computational grid and the dots are interpolation nodes.*

For general parameter values, the definition of the parametric curve L is generalized to

$$\begin{aligned} L &= (s_{\hat{i}}, \mathbf{b}_{\hat{j}}, \alpha_{\hat{k}}) + \zeta(\frac{ds}{d\zeta}, \frac{d\mathbf{b}}{d\zeta}, \frac{d\alpha}{d\zeta}), \\ \frac{ds}{d\zeta} = -g(v)s_{\hat{i}}, \quad \frac{d\mathbf{b}}{d\zeta} &= e^{r\tau_{n+1}} v f(v) s_{\hat{i}}, \quad \frac{d\alpha}{d\zeta} = -v. \end{aligned} \tag{3.7.8}$$

To conclude our discussion about the parametric curve interpolation method, we note the following.

- Since equations (3.7.8) express how changes in α lead to changes in s and $\mathbf{b}$ through both trading revenue ($\frac{d\mathbf{b}}{d\zeta} = v s_{\hat{i}}$) and pricing impact (the terms $g(v)$ and $f(v)$), interpolating along L can be seen as an extension to interpolation along L defined in (3.7.7), which takes into account trading revenue but not pricing impact.
- It turns out that the parametric curve interpolation method illustrated in Figure 3.1(b) is very accurate along the α direction. Consequently, our computational grid will use much fewer nodes in the α direction than in the s direction; see Chapter 5 for details.

3.7.3 Scaled Grid

Consider again the analytical solution (3.7.4) for the limiting case. Recall that V changes slowly along curves of constant wealth $\{(\alpha s + \beta) = const\}$. This property of V suggests a computational grid with constant curves of wealth built into it as follows, which is illustrated in Figure 3.2.

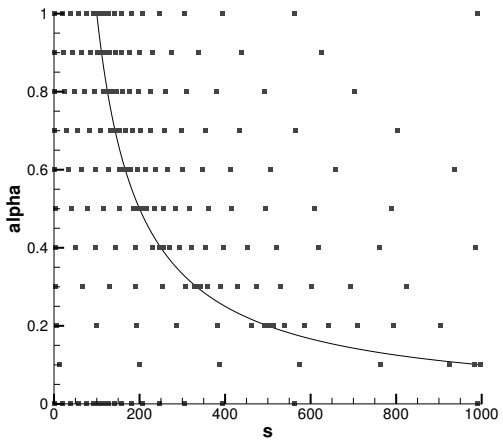

FIGURE 3.2: *The scaled computational grid.*

- For $\alpha > 0$, scale the s grid by $\{s_i\} \to \{s_i\}/\alpha$.
- For $\alpha = 0$, no scaling is performed, i.e. the original s grid $\{s_i\}$ is used.

3.8 Summary

The main results in this chapter are the followings.

- We extend the result in [47] on the embedding technique to tackle non-convex multi-period MV optimization problems. For non-convex problems, the embedding technique may produce Pareto-inefficient points. We prove a number of results that guarantee Pareto-optimality of the computed frontier.
- We combine the techniques of similarity reduction, non-standard interpolation, and careful grid construction to significantly improve the efficiency of our numerical methods for solving nonlinear HJB PDEs.

Chapter 4

Proof of Convergence to Viscosity Solution for System of PDEs

In this chapter, we extend the convergence result in [16] to a quasi-monotone [39] system of nonlinear PDEs.

It was proved in [16] that for a nonlinear second-order PDE, any monotone, consistent and infinity-norm stable discretization scheme converges to the viscosity solution, provided that there exists a strong comparison principle for the PDE. We extend this result for a nonlinear PDE to the quasi-monotone system of nonlinear HJB PDEs (3.4.2) that arises under our regime switching trade execution model. Although our proof (Proposition 4.17) is given in this concrete context, it can be easily adapted to similar systems of nonlinear PDEs.

We choose to prove convergence for the discretization scheme (3.5.15), which does not use similarity reduction and other techniques for improving efficiency. This allows us to concentrate on the new results regarding a system of PDEs (from a regime switching model) without further algebraic complication. For readers interested in proof of convergence in the case of using similarity reduction, [31] provides a proof in the single regime case.

This chapter is organized as follows. Section 4.1 defines the viscosity solution for the system (3.4.2). Sections 4.2 to 4.4 show that our discretization (3.5.15) of the system (3.4.2) is monotone, consistent, and infinity-norm stable. Finally, Section 4.5 proves the main convergence result, i.e. these properties of the discretization scheme guarantee the convergence of numerical solutions to the viscosity solution.

For easy reference, notations in this chapter are defined/summarized in Table 4.1.

4.1 Viscosity Solution Formulation

To define viscosity solution, we need to introduce the notions of upper and lower semi-continuous envelope. For a real-valued function $\omega : C \mapsto \mathbf{R}$ defined on the closed set C,

Notations	Descriptions
ϕ^l	$\phi^l : \Omega_L \mapsto \mathbf{R}$ has continuous derivatives of all orders
$\{\Omega_{h_q}\}_{q\in\mathbf{N}} \to \Omega_L$	a sequence of grids with spacing $O(h_q)$, where $h_q \to 0$ as $q \to \infty$
$x_{i_q,j_q,k_q,n_q} = (s_{i_q}, \boldsymbol{\iota}_{j_q}, \alpha_{k_q}, \tau_{n_q})$	a grid node in Ω_{h_q}.
x_{h_q}	shorthand for x_{i_q,j_q,k_q,n_q+1}.
$V_{h_q} = (V_{h_q}^1, \cdots, V_{h_q}^M)$	$\mathbf{R}^M$-valued discrete function defined on Ω_{h_q}
$V_{h_q}^l$	l-th component of V_{h_q}; real-valued
$\{x_{h_q}\}_{q\in\mathbf{N}} \to x$	a sequence of grid nodes converging to $x \in \Omega_L$.
$\phi^l_{i,j,k,n}$	value of ϕ^l evaluated at grid node $x_{i,j,k,n}$ in Ω_h
$\phi^l_{i_q,j_q,k_q,n_q}$	value of ϕ^l evaluated at grid node x_{i_q,j_q,k_q,n_q} in Ω_{h_q}

TABLE 4.1: *Summary of notations for Chapter 4.*

the upper semi-continuous envelope ω^* and lower semi-continuous envelope ω_* are defined as

$$\omega^*(x) = \limsup_{\epsilon\to 0}\{\omega(y) \text{ s.t. } |x-y| < \epsilon, y \in C\},$$
$$\omega_*(x) = \liminf_{\epsilon\to 0}\{\omega(y) \text{ s.t. } |x-y| < \epsilon, y \in C\}.$$

Definition 4.1 (Definition of viscosity solution of the system of PDEs (3.4.2))**.** An $\mathbf{R}^M$-valued function $u = (u^1, \cdots, u^M)$, where each $u^l : \Omega_L \mapsto \mathbf{R}$ is locally bounded, is called a viscosity sub-solution (respectively super-solution) [39, 23, 15, 61] of the system of PDEs (3.4.2), if for all (real-valued) test functions $\phi^l \in C^\infty(\Omega_L)$ and all $x \in \Omega_L$ such that $u^{l*} - \phi^l$ (respectively $u^l_* - \phi^l$) has a strict local maximum (respectively minimum) of zero at $x = (s, \boldsymbol{\iota}, \alpha, \tau) \in \Omega_L$, we have

$$F^l_*(x, u^{l*}(x), \{u^{m*}(\tilde{x}^{l\to m})\}^{m\neq l}, D\phi^l(x), D^2\phi^l(x)) \le 0,$$

(respectively

$$F^{l*}(x, u^l_*(x), \{u^m_*(\tilde{x}^{l\to m})\}^{m\neq l}, D\phi^l(x), D^2\phi^l(x)) \ge 0.)$$

Since there is no coupling of derivative terms among individual PDEs in the system (3.4.2), the test function for the l-th equation should be scalar-valued and replaces only the l-th component of the solution u, as in the above definition of viscosity solution. Consequently, there is no information regarding how the m-th component of the solution u compares with the test function ϕ^l. Recall that a key step in the convergence proof of [16] consists of (i) comparing the numerical solution with the test function; and (ii) using monotonicity of the numerical scheme to obtain inequality in the right direction. In using the above definition, only the l-th component of the numerical solution can be replaced by test function ϕ^l, the m-th component must be handled separately. It is in this sense that we extend the convergence result of [16] to systems of PDEs that arise under a regime switching model; see the proof of Proposition 4.17 for the details. A related recent work

that also generalizes the result of [16] to systems of PDEs is [23].

We note that this technicality is overlooked in [54], which compares a vector-valued numerical solution with a test function in its convergence proof.[1]

Remark 4.2. *The above definition, which assumes $\phi^l \in C^\infty(\Omega_L)$, is equivalent to the more common definition which assumes $\phi^l \in C^2(\Omega_L)$. This equivalence is discussed in [15] and [61].*

4.2 Monotonicity

The notion of monotonicity in [16] needs to be extended for discretization of a system. To motivate the extended definition, let us first show that the system of PDEs (3.4.2) has the quasi-monotone property, which is an important assumption in the theory of viscosity solution for systems of PDEs [39].

Proposition 4.3. *Let $w_1, w_2 \in \mathbf{R}^M$ and $l \in \{1, \cdots, M\}$. We use the notation $w_1 \geq_l w_2$ to mean that $w_1 \geq w_2$ component-wise and $w_1^l = w_2^l$. The system of PDEs (3.4.2) is called quasi-monotone [39] if whenever $w_1 \geq_l w_2$, then*

$$F^l(x, w_1^l, \{w_1^m\}^{m\neq l}, D\phi^l(x), D^2\phi^l(x)) \leq F^l(x, w_2^l, \{w_2^m\}^{m\neq l}, D\phi^l(x), D^2\phi^l(x))$$

for all $x \in \Omega_L$ and $\phi^l \in C^\infty(\Omega_L)$.

Proof. This follows from straightforward calculation by noting that the switching intensities λ^{lm} are by definition nonnegative. □

We now prove that our discretization scheme is monotone. Note that the definition of monotonicity with respect to the last argument of $\mathcal{G}^l_{i,j,k,n+1}$ in (4.2.1) below is a discrete version of the quasi-monotone property (Proposition 4.3).

Proposition 4.4. *The numerical scheme (3.5.15) is monotone in the following sense. For any two $\mathbf{R}^M$-valued discrete functions W_h and U_h defined on Ω_h such that $W_h \geq U_h$ and $W^l_{i,j,k,n+1} = U^l_{i,j,k,n+1}$,*

$$\begin{aligned}
&\mathcal{G}^l_{i,j,k,n+1}\Big(h, W^l_{i,j,k,n+1}, \{W^l_{i',j,k,n+1}\}_{i'\neq i}, \{W^l_{i',j',k',n}\}, \{W^m_{i',j',k',n+1}\}^{m\neq l}\Big) \\
\leq &\mathcal{G}^l_{i,j,k,n+1}\Big(h, U^l_{i,j,k,n+1}, \{U^l_{i',j,k,n+1}\}_{i'\neq i}, \{U^l_{i',j',k',n}\}, \{U^m_{i',j',k',n+1}\}^{m\neq l}\Big)
\end{aligned} \tag{4.2.1}$$

Proof. The following proof consists of simple positive coefficient condition analysis.

Note that from the definition of $\mathcal{G}^l_{i,j,k,n+1}$ in (3.5.16), we only need to focus on the case when $\mathcal{G}^l_{i,j,k,n+1} = \mathcal{H}^l_{i,j,k,n+1}$; the other case is trivial.

[1] See equation (30) in the proof of Theorem 4.8 in [54].

Linear interpolation guarantees that the term $V^l_{interp}(\hat{x}_{i,j,k,n}(v))$ can be written as

$$\begin{aligned} &V^l_{interp}(\hat{x}_{i,j,k,n}(v)) \\ &= \sum_{\substack{0\le i'\le i_{max}\\ 0\le j'\le j_{max}\\ 0\le k'\le k_{max}}} \hat{w}_{i',j',k'}(v)\, V^l_{i',j',k',n}, \text{ where } \hat{w}_{i',j',k'}(v)\in[0,1], \sum_{\substack{0\le i'\le i_{max}\\ 0\le j'\le j_{max}\\ 0\le k'\le k_{max}}} \hat{w}_{i',j',k'}(v) = 1. \end{aligned} \tag{4.2.2}$$

and the term $V^m_{interp}(\tilde{x}^{l\to m}_{i,j,k,n+1})$ can be written as

$$V^m_{interp}(\tilde{x}^{l\to m}_{i,j,k,n+1}) = \sum_{0\le i'\le i_{max}} \tilde{w}_{i'}\, V^m_{i',j,k,n+1}, \text{ where } \tilde{w}_{i'}\in[0,1], \sum_{0\le i'\le i_{max}} \tilde{w}_{i'} = 1. \tag{4.2.3}$$

The positive coefficient discretization (3.5.1) guarantees that

$$\begin{aligned} &(\mathcal{L}^l_h\, V^l_h)_{i,j,k,n+1} \\ &= a^l_i\big(V^l_{i-1,j,k,n+1}\big) - \big(a^l_i + b^l_i + \lambda^l\big)\big(V^l_{i,j,k,n+1}\big) + b^l_i\big(V^l_{i+1,j,k,n+1}\big), \text{ where } a^l_i, b^l_i, \lambda^l \ge 0 \end{aligned} \tag{4.2.4}$$

The monotonicity (4.2.1) directly follows by subtracting the right hand side of (4.2.1) from the left hand side, using the positive coefficient conditions (4.2.2)-(4.2.4), and noting that

$$\begin{aligned} &-\min_{v\in\hat{\mathbf{V}}^l_{h,res}(x_{i,j,k,n+1})} \big\{W^l_{interp}(\hat{x}_{i,j,k,n}(v))\big\} - \Big(-\min_{v\in\hat{\mathbf{V}}^l_{h,res}(x_{i,j,k,n+1})} \big\{U^l_{interp}(\hat{x}_{i,j,k,n}(v))\big\}\Big) \\ &\le \max_{v\in\hat{\mathbf{V}}^l_{h,res}(x_{i,j,k,n+1})} \big\{\hat{w}_{i',j',k'}(v)\, U^l_{i',j',k',n} - \hat{w}_{i',j',k'}(v)\, W^l_{i',j',k',n}\big\} \\ &\le 0. \end{aligned}$$

□

4.3 Consistency

This section proves that the numerical scheme (3.5.15) is a consistent approximation to the system (3.4.2) in the viscosity solution sense. Before stating our definition of consistency, we introduce the following notation.

Definition 4.5. Let $\{d^m\}^{m\neq l}$ be a set of real values d^m. We use the notation

$$\mathcal{G}^l_{i,j,k,n+1}\Big(h, W^l_{i,j,k,n+1}, \{W^l_{i',j,k,n+1}\}_{i'\neq i}, \{W^l_{i',j',k',n}\}, \{d^m\}^{m\neq l}\Big)$$

to mean

$$\mathcal{G}^l_{i,j,k,n+1}\Big(h, W^l_{i,j,k,n+1}, \{W^l_{i',j,k,n+1}\}_{i'\neq i}, \{W^l_{i',j',k',n}\}, \{W^m_{i',j',k',n+1} = d^m\}^{m\neq l}\Big),$$

i.e. for a fixed m, $W^m_{i',j',k',n+1}$ all have the same value d^m.

Definition 4.6. The numerical scheme (3.5.15) is said to be consistent with the HJB PDE (3.4.2) if for a sequence of grids $\{\Omega_{h_q}\}_{q\in\mathbf{N}} \to \Omega_L$ and sequences of points

$$\{x_{h_q} = x_{i_q,j_q,k_q,n_q+1}\}_{q\in\mathbf{N}} \to x = (s, \mathfrak{b}, \alpha, \tau) \in \Omega_L, \quad \{\xi_q\}_{q\in\mathbf{N}} \to 0, \quad \{d_q^m\}_{q\in\mathbf{N}}^{m\neq l} \to d^m, \tag{4.3.1}$$

we have

$$\begin{aligned}
&\liminf_{q\to\infty} \mathcal{G}^l_{i_q,j_q,k_q,n_q+1}\Big(h_q, \phi^l_{i_q,j_q,k_q,n_q} + \xi_q, \{\phi^l_{i',j_q,k_q,n_q+1}\}_{i'\neq i_q} + \xi_q, \{\phi^l_{i',j',k',n_q}\} + \xi_q, \{d_q^m\}^{m\neq l}\Big) \\
\geq& F^l_*(x, \phi^l(x), \{d^m\}^{m\neq l}, D\phi^l(x), D^2\phi^l(x))
\end{aligned} \tag{4.3.2}$$

and

$$\begin{aligned}
&\limsup_{q\to\infty} \mathcal{G}^l_{i_q,j_q,k_q,n_q+1}\Big(h_q, \phi^l_{i_q,j_q,k_q,n_q} + \xi_q, \{\phi^l_{i',j_q,k_q,n_q+1}\}_{i'\neq i_q} + \xi_q, \{\phi^l_{i',j',k',n_q}\} + \xi_q, \{d_q^m\}^{m\neq l}\Big) \\
\leq& F^{l*}(x, \phi^l(x), \{d^m\}^{m\neq l}, D\phi^l(x), D^2\phi^l(x))
\end{aligned} \tag{4.3.3}$$

Before going into the details, it is helpful to review the discretization scheme to have an overall idea of what needs to be shown. For the reader's convenience, we reproduce the discretization (3.5.14) below. For $\tau_{n+1} > 0$,

$$\begin{aligned}
&\mathcal{G}^l_{i,j,k,n+1}\Big(h, V^l_{i,j,k,n+1}, \{V^l_{i',j,k,n+1}\}_{i'\neq i}, \{V^l_{i',j',k',n}\}, \{V^m_{i',j',k',n+1}\}^{m\neq l}\Big) \\
=& -\sum_{\substack{m=1\\ m\neq l}}^{M} \lambda^{lm}\, V^m_{interp}(\tilde{x}^{l\to m}_{i,j,k,n+1}) \\
&+ \frac{1}{\triangle\tau}\Big[V^l_{i,j,k,n+1} - \min_{v\in\hat{\mathbf{V}}^l_{h,res}(x_{i,j,k,n+1})} \big\{V^l_{interp}(\hat{x}_{i,j,k,n}(v))\big\}\Big] - (\mathcal{L}^l_h\, V^l_h)_{i,j,k,n+1}.
\end{aligned}$$

Our proof of consistency will proceed as follows. Section 4.3.1 shows that the semi-Lagrangian term $V^l_{interp}(\hat{x}_{i,j,k,n}(v))$ is a consistent discretization. Section 4.3.2 performs a classical error analysis of the discretization scheme for infinitely differentiable test functions, temporarily ignoring the errors due to restricting the set of admissible velocities to $\mathbf{V}^l_{h,res}(x)$. Section 4.3.3 treats the technical issues that arise from restricting the set of admissible velocities to $\mathbf{V}^l_{h,res}(x)$. Section 4.3.4 proves the main consistency result.

Remark 4.7 (Technical comment on definition of consistency)**.** *In Definition 4.6, the last argument of $\mathcal{G}^l_{i_q,j_q,k_q,n_q+1}$ is $\{d_q^m\}^{m\neq l}$, instead of the more typical $\{\psi^m_{i',j',k',n_q+1}\}^{m\neq l}$, i.e. values of locally bounded functions $\psi^m : \Omega_L \mapsto \mathbf{R}$ at grid nodes in Ω_{h_q}. The rationale of using $\{d_q^m\}^{m\neq l}$ will become apparent in our main convergence proof (Proposition 4.17).*

4.3.1 Semi-Lagrangian Interpolation

Lemma 4.8. *Let $x_h = x_{i,j,k,n+1} = (s_i, \ell_j, \alpha_k, \tau_{n+1}) \in \Omega_h$ and $v \in \mathbf{V}^l_{h,res}(x_h)$, we have*

$$\frac{1}{\triangle\tau}\Big[\phi^l(x_h) - \phi^l_{interp}(\hat{x}_{i,j,k,n}(v))\Big] = \frac{D^l\phi^l}{D\tau}(x_h, v) + O(\triangle\tau),$$

where $\phi^l_{interp}(\hat{x}_{i,j,k,n}(v))$ is a linearly interpolated value.

Proof. Recall the definition of $\frac{D^l\phi^l}{D\tau}(x,v)$ in (3.4.1) for three different cases. In each case, the proof follows from straightforward Taylor's expansion around $x_{i,j,k,n+1}$ using (3.5.8 - 3.5.11), similar to that in [26]. We note that the boundary conditions are correctly handled at $s = s_{max}$. Since $s_{\hat{i}} = s_{max}$ by construction (3.5.8), there is no ϕ_s term in the Taylor's expansion of ϕ^l_{interp} when $s = s_{max}$, which agrees with the definition of $\frac{D^l\phi^l}{D\tau}(x,v)$ in (3.4.1) . □

4.3.2 Truncation Error Analysis : Smooth Test Functions

In this section, we perform a truncation error analysis on our numerical scheme (3.5.15-3.5.16). For ease of exposition in proving consistency with regard to restricting the set of admissible velocities, we define the following terms.

Definition 4.9. Using the notation of Section 3.4, define

$$\begin{aligned}
&\mathcal{F}^l_{\mathbf{V}^l_{h,res}\cap in}(x, \phi^l(x), \{d^m\}^{m\neq l}, D\phi^l(x), D^2\phi^l(x)) \\
=& -\mathcal{L}^l\phi^l(x) - \sum_{\substack{m=1\\ m\neq l}}^{M} \lambda^{lm} d^m + \lambda^l\phi^l(x) + \max_{v\in\mathbf{V}^l_{h,res}(x)} \frac{D^l\phi^l}{D\tau}(x,v)
\end{aligned}$$

and

$$\begin{aligned}
&\mathcal{F}^l_{\mathbf{V}^l_{h,res}\cap s_{max}}(x, \phi^l(x), \{d^m\}^{m\neq l}, D\phi^l(x), D^2\phi^l(x)) \\
=& -\sum_{\substack{m=1\\ m\neq l}}^{M} \lambda^{lm} d^m + \lambda^l\phi^l(x) + \max_{v\in\mathbf{V}^l_{h,res}(x)} \frac{D^l\phi^l}{D\tau}(x,v)
\end{aligned}$$

Lemma 4.10. *We have for all grid nodes $x_h = x_{i,j,k,n+1} \in \Omega_h$*

$$\mathcal{G}^l_{i,j,k,n+1}\Big(h, \phi^l_{i,j,k,n} + \xi, \{\phi^l_{i',j,k,n+1}\}_{i'\neq i} + \xi, \{\phi^l_{i',j',k',n}\} + \xi, \{d^m\}^{m\neq l}\Big)$$
$$= \begin{cases} F^l_{in}(x_h, \phi^l(x_h), \{d^m\}^{m\neq l}, D\phi^l(x_h), D^2\phi^l(x_h)) + O(h) + O(\xi) & \text{if } x_h \in \Omega_{in} \setminus \Omega_{\mathbf{V}^l_{h,res}} \\ F^l_{s_{max}}(x_h, \phi^l(x_h), \{d^m\}^{m\neq l}, D\phi^l(x_h), D^2\phi^l(x_h)) + O(h) + O(\xi) & \text{if } x_h \in \Omega_{s_{max}} \setminus \Omega_{\mathbf{V}^l_{h,res}} \\ \mathcal{F}^l_{\mathbf{V}^l_{h,res}\cap in}(x_h, \phi^l(x_h), \{d^m\}^{m\neq l}, D\phi^l(x_h), D^2\phi^l(x_h)) + O(h) + O(\xi) & \text{if } x_h \in \Omega_{\mathbf{V}^l_{h,res}} \cap \Omega_{in} \\ \mathcal{F}^l_{\mathbf{V}^l_{h,res}\cap s_{max}}(x_h, \phi^l(x_h), \{d^m\}^{m\neq l}, D\phi^l(x_h), D^2\phi^l(x_h)) + O(h) + O(\xi) & \text{if } x_h \in \Omega_{\mathbf{V}^l_{h,res}} \cap \Omega_{s_{max}} \\ F^l_{v=0}(x_h, \phi^l(x_h), \{d^m\}^{m\neq l}, D\phi^l(x_h), D^2\phi^l(x_h)) + O(h) + O(\xi) & \text{if } x_h \in \Omega_{v=0} \\ F^l_{s_{max},v=0}(x_h, \phi^l(x_h), \{d^m\}^{m\neq l}, D\phi^l(x_h), D^2\phi^l(x_h)) + O(h) + O(\xi) & \text{if } x_h \in \Omega_{s_{max},v=0} \\ F^l_{\tau=0}(x_h, \phi^l(x_h), \{d^m\}^{m\neq l}, D\phi^l(x_h), D^2\phi^l(x_h)) + O(\xi) & \text{if } x_h \in \Omega_{\tau=0} \end{cases}$$

Proof. Consider the case $x_h = x_{i,j,k,n+1} \in \Omega_{in} \setminus \Omega_{\mathbf{V}^l_{h,res}}$. By definition we have

$$\begin{aligned} &\mathcal{G}^l_{i,j,k,n+1}\Big(h, \phi^l_{i,j,k,n} + \xi, \{\phi^l_{i',j,k,n+1}\}_{i'\neq i} + \xi, \{\phi^l_{i',j',k',n}\} + \xi, \{d^m\}^{m\neq l}\Big) \\ &= -\sum_{\substack{m=1\\m\neq l}}^{M} \lambda^{lm}\, d^m + \frac{1}{\triangle\tau}\Big[\phi^l(x_h) + \xi - \min_{v\in\hat{\mathbf{V}}^l_{h,res}(x_{i,j,k,n+1})} \big\{\phi^l_{interp}(\hat{x}_{i,j,k,n}(v)) + \xi\big\}\Big] \\ &\quad - \Big(a^l_i\left(\phi^l(x_{i-1,j,k,n+1}) + \xi\right) - \left(a^l_i + b^l_i + \lambda^l\right)\left(\phi^l(x_{i,j,k,n+1}) + \xi\right) + b^l_i\left(\phi^l(x_{i+1,j,k,n+1}) + \xi\right)\Big) \\ &= -\sum_{\substack{m=1\\m\neq l}}^{M} \lambda^{lm}\, d^m + \frac{1}{\triangle\tau}\Big[\phi^l(x_h) - \min_{v\in\hat{\mathbf{V}}^l_{h,res}(x_{i,j,k,n+1})} \phi^l_{interp}(\hat{x}_{i,j,k,n}(v))\Big] - \Big((\mathcal{L}^l_h\phi^l)_{i,j,k,n+1} - \lambda^l\xi\Big) \end{aligned} \tag{4.3.4}$$

Note that the term d^m in (4.3.4) above is a result of linear interpolating (4.2.3) the constant grid values $\{d^m\}^{m\neq l}$ (see Remark 4.7).

By Taylor series expansion and the smoothness of ϕ^l,

$$(\mathcal{L}^l_h\phi^l)_{i,j,k,n+1} = (\mathcal{L}^l\phi^l)(x_{i,j,k,n+1}) + O(h). \tag{4.3.5}$$

By Lemma 4.8,

$$\frac{1}{\triangle\tau}\Big[\phi^l(x_h) - \phi^l_{interp}(\hat{x}_{i,j,k,n}(v))\Big] = \frac{D^l\phi^l}{D\tau}(x_h, v) + O(h). \tag{4.3.6}$$

Since the coefficients of the PDEs are Lipschitz continuous (see Assumption 2.1), discretizing the control space $\mathbf{V}^l_{h,res}(x_{i,j,k,n+1})$ as $\hat{\mathbf{V}}^l_{h,res}(x_{i,j,k,n+1})$ gives an $O(h)$ error, i.e.

$$\max_{v\in\hat{\mathbf{V}}^l_{h,res}(x_{i,j,k,n+1})} \frac{D^l\phi^l}{D\tau}(x_h, v) = \max_{v\in\mathbf{V}^l_{h,res}(x_{i,j,k,n+1})} \frac{D^l\phi^l}{D\tau}(x_h, v) + O(h). \tag{4.3.7}$$

Since $x_h = x_{i,j,k,n+1} \in \Omega_{in} \setminus \Omega_{\mathbf{V}^l_{h,res}}$,

$$\mathbf{V}^l_{h,res}(x_{i,j,k,n+1}) = [v_{min}, 0]. \tag{4.3.8}$$

Substituting (4.3.5) - (4.3.8) into (4.3.4) gives

$$\begin{aligned}
&\mathcal{G}^l_{i,j,k,n+1}\Big(h, \phi^l_{i,j,k,n} + \xi, \{\phi^l_{i',j,k,n+1}\}_{i'\neq i} + \xi, \{\phi^l_{i',j',k',n}\} + \xi, \{d^m\}^{m\neq l}\Big) \\
=& -\sum_{\substack{m=1\\ m\neq l}}^{M} \lambda^{lm}\, d^m + \max_{v\in[v_{min},0]} \frac{D^l\phi^l}{D\tau}(x_h, v) - (\mathcal{L}^l\phi^l)(x_{i,j,k,n+1}) + O(h) + O(\xi) \\
=& F^l_{in}(x_h, \phi^l(x_h), \{d^m\}^{m\neq l}, D\phi^l(x_h), D^2\phi^l(x_h)) + O(h) + O(\xi)
\end{aligned}$$

The rest of the lemma can be proved by similar direct calculations in (4.3.4) together with (4.3.6) - (4.3.8). □

4.3.3 Handling restricted set of admissible velocities

Note that Lemma 4.10 would be sufficient for proving consistency in the viscosity sense if $\mathcal{F}^l_{\mathbf{V}^l_{h,res}\cap in}$ and $\mathcal{F}^l_{\mathbf{V}^l_{h,res}\cap s_{max}}$ were F^l_{in} and $F^l_{s_{max}}$ respectively. Although it is possible to impose (ad-hoc) conditions on the grid so that $\Omega_{\mathbf{V}^l_{h,res}}$ becomes an empty set in the limit (in which case Lemma 4.10 would be sufficient for proving consistency), we opt for generality in the grid construction. The cost of this generality is the need to prove the following two technical lemmas.

Lemma 4.11 shows how to bound $\mathcal{F}^l_{\mathbf{V}^l_{h,res}\cap in}$ and $\mathcal{F}^l_{\mathbf{V}^l_{h,res}\cap s_{max}}$.

Lemma 4.11.

$$F^l_{v=0}(x_{h_q}, \cdots) \leq \mathcal{F}^l_{\mathbf{V}^l_{h_q,res}\cap in}(x_{h_q}, \cdots) \leq F^l_{in}(x_{h_q}, \cdots). \tag{4.3.9}$$

and

$$F^l_{s_{max},v=0}(x_{h_q}, \cdots) \leq \mathcal{F}^l_{\mathbf{V}^l_{h_q,res}\cap s_{max}}(x_{h_q}, \cdots) \leq F^l_{s_{max}}(x_{h_q}, \cdots), \tag{4.3.10}$$

where $(x_{h_q}, \cdots)$ *stands for* $(x_{h_q}, \phi^l(x_{h_q}), \{d^m_q\}^{m\neq l}, D\phi^l(x_{h_q}), D^2\phi^l(x_{h_q}))$.

Proof. Note that the definitions of $F^l_{in}(x_{h_q}, \cdots)$, $\mathcal{F}^l_{\mathbf{V}^l_{h_q,res}\cap in}(x_{h_q}, \cdots)$ and $F^l_{v=0}(x_{h_q}, \cdots)$ differ only in the sets of admissible velocities; for $F^l_{in}(x_{h_q}, \cdots)$ the set is $[v_{min}, 0]$, for $\mathcal{F}^l_{\mathbf{V}^l_{h_q,res}\cap in}(x_{h_q}, \cdots)$ the set is $\mathbf{V}^l_{h_q,res}(x_{h_q})$, for $F^l_{v=0}(x_{h_q}, \cdots)$ the set is $\{0\}$. Since we are maximizing over the sets of admissible velocities, and $\{0\} \subseteq \mathbf{V}^l_{h_q,res}(x_{h_q}) \subseteq [v_{min}, 0]$, this proves (4.3.9). The proof for (4.3.10) is very similar. □

Lemma 4.11 suggests that it is clearly consistent to bound $\mathcal{F}^l_{\mathbf{V}^l_{h,res}\cap in}$ (respectively $\mathcal{F}^l_{\mathbf{V}^l_{h,res}\cap s_{max}}$) from the above by F^l_{in} (respectively $F^l_{s_{max}}$). The next lemma shows that it

is also consistent to bound $\mathcal{F}^l_{\mathbf{V}^l_{h,res}\cap in}$ (respectively $\mathcal{F}^l_{\mathbf{V}^l_{h,res}\cap s_{max}}$) from the above by $F^l_{v=0}$ (respectively $F^l_{s_{max},v=0}$).

Lemma 4.12. *Let* $\{x_{h_q} = (s_{i_q}, \mathcal{b}_{j_q}, \alpha_{k_q}, \tau_{n_q+1}) \in \Omega_{h_q}\}_{q\in\mathbf{N}} \to x = (s, \mathcal{b}, \alpha, \tau) \in \Omega_L$. *Then the following implications hold.*

$$x_{h_q} \in \Omega_{\mathbf{V}^l_{h_q,res}} \cap \Omega_{in} \text{ for infinitely many } q \Longrightarrow x \in closure(\Omega_{v=0}). \tag{4.3.11}$$

$$x_{h_q} \in \Omega_{\mathbf{V}^l_{h_q,res}} \cap \Omega_{s_{max}} \text{ for infinitely many } q \Longrightarrow x \in closure(\Omega_{s_{max},v=0}). \tag{4.3.12}$$

Proof. We will prove (4.3.11) in some detail. The proof for (4.3.12) is similar.

First, note that by Definition 3.26,

$$closure(\Omega_{v=0}) = \{\mathcal{b} = 0 \text{ or } \alpha = 0\} \cap \Omega_L,$$

thus it remains to prove $\mathcal{b} = 0$ or $\alpha = 0$. We proceed using proof by contradiction. Assume to the contrary that $\mathcal{b} < 0$ and $\alpha > 0$, we will show that

$$(s_{\hat{i_q}}, \mathcal{b}_{\hat{j_q}}, \alpha_{\hat{k_q}}, \tau_{n_q}) = \mathcal{I}^l(x_{h_q}, v, \triangle\tau) \in \Omega_L \text{ for all } v \in [v_{min}, 0] \text{ for all } q \text{ sufficiently large,} \tag{4.3.13}$$

which would lead to a contradiction by definition (3.5.13).

Showing (4.3.13) is equivalent to showing that each of the followings holds for q sufficiently large: (i) $s_{\hat{i_q}} \in [0, s_{max}]$; (iia) $\mathcal{b}_{\hat{j_q}} \geq \mathcal{b}_{min}$; (iib)$\mathcal{b}_{\hat{j_q}} \leq 0$; (iiia)$\alpha_{\hat{k_q}} \geq 0$; and (iiib) $\alpha_{\hat{k_q}} \leq 1$.

The following is basically a straightforward analysis of the formula (3.5.4-3.5.7) together with the assumptions $f^l(v) \geq 0$, $g^l(v) \leq 0$ and $v \leq 0$; see (2.1.16).

By the assumptions on the signs of $f^l(v), g^l(v)$ and v, (i), (iia) and (iiib) hold trivially.

Finally, since $\triangle\tau \to 0$ as $q \to \infty$ and the admissible control set $[v_{min}, 0]$ is compact, by continuity we have

$$\lim_{q\to\infty} \mathcal{b}_{\hat{j_q}} = \lim_{q\to\infty} \mathcal{b}_{j_q} = \mathcal{b} < 0 \text{ and } \lim_{q\to\infty} \alpha_{\hat{k_q}} = \lim_{q\to\infty} \alpha_{k_q} = \alpha > 0,$$

which proves (iib) and (iiia). □

4.3.4 Proof of Consistency

We need one final easy lemma before proving the main consistency result.

Lemma 4.13. *Let* $\{\Omega_{h_q}\}_{q\in\mathbf{N}} \to \Omega_L$ *and* $\{x_{h_q}\}_{q\in\mathbf{N}} \to x \in \Omega_L$, *then for* $x \in closure(\Omega_{in})$ *(*x_{h_q} *not necessarily in* Ω_{in}*) and sequences* $\{d^m_q\}^{m\neq l}_{q\in\mathbf{N}} \to d^m$

$$\begin{aligned}&\liminf_{q\to\infty} F^l_{in}(x_{h_q}, \phi^l(x_{h_q}), \{d^m_q\}^{m\neq l}, D\phi^l(x_{h_q}), D^2\phi^l(x_{h_q}))\\ \geq& F^l_*(x, \phi^l(x), \{d^m\}^{m\neq l}, D\phi^l(x), D^2\phi^l(x)).\end{aligned} \tag{4.3.14}$$

Similarly,

$$\begin{aligned}&\limsup_{q\to\infty} F^l_{in}(x_{h_q},\phi^l(x_{h_q}),\{d^m_q\}^{m\neq l},D\phi^l(x_{h_q}),D^2\phi^l(x_{h_q}))\\ \leq& F^{l*}(x,\phi^l(x),\{d^m\}^{m\neq l},D\phi^l(x),D^2\phi^l(x)).\end{aligned}\tag{4.3.15}$$

By identical arguments, the above results hold when the pair (Ω_{in},F^l_{in}) is replaced by $(\Omega_{s_{max}},F^l_{s_{max}})$, $(\Omega_{v=0},F^l_{v=0})$, $(\Omega_{s_{max},v=0},F^l_{s_{max},v=0})$ or $(\Omega_{\tau=0},F^l_{\tau=0})$.

Proof. The result follows easily by the definition of lower-semicontinuous envelope F^l_*, the convergence of d^m_q to d^m, and the smoothness of ϕ^l. Similar steps can be used to show (4.3.15). □

Having proved Lemma 4.10-4.13, proving consistency in the viscosity sense will be straightforward.

Proposition 4.14. *The numerical scheme (3.5.15) is consistent with the HJB PDE (3.4.2) in the sense of Definition 4.6.*

Proof. We will prove only (4.3.2). The proof of (4.3.3) is more straightforward (does not require Lemma 4.12)

In applying Lemma 4.10, it is obvious that the only tricky case is when $x_{h_q}\in\Omega_{\mathbf{V}^l_{h_q,res}}$ for infinitely many q. Without loss of generality, we can assume $x_{h_q}\in\Omega_{\mathbf{V}^l_{h_q,res}}$ for all q.

Note that for each q, we may have

$$x_{h_q} \in \Omega_{\mathbf{V}^l_{h_q,res}}\cap\Omega_{in};\ \text{and/or}\tag{4.3.16}$$

$$x_{h_q} \in \Omega_{\mathbf{V}^l_{h_q,res}}\cap\Omega_{s_{max}}\tag{4.3.17}$$

For ease of exposition, we focus on the case when (4.3.16) holds for all q. The situation when either (4.3.16) or (4.3.17) can hold can be similarly handled.

Applying Lemma 4.10 (to each grid Ω_{h_q}) gives

$$\begin{aligned}&\liminf_{q\to\infty}\mathcal{G}^l_{i_q,j_q,k_q,n_q+1}(h_q,\phi^l_{i_q,j_q,k_q,n_q}+\xi_q,\{\phi^l_{i',j_q,k_q,n_q+1}\}_{i'\neq i_q}+\xi_q,\{\phi^l_{i',j',k',n_q}\}+\xi_q,\{d^m_q\}^{m\neq l})\\ =\ &\liminf_{q\to\infty}\mathcal{F}^l_{\mathbf{V}^l_{h_q,res}\cap in}(x_{h_q},\phi^l(x_{h_q}),\{d^m_q\}^{m\neq l},D\phi^l(x_{h_q}),D^2\phi^l(x_{h_q}))+O(h_q)+O(\xi_q)\\ =\ &\liminf_{q\to\infty}\mathcal{F}^l_{\mathbf{V}^l_{h_q,res}\cap in}(x_{h_q},\phi^l(x_{h_q}),\{d^m_q\}^{m\neq l},D\phi^l(x_{h_q}),D^2\phi^l(x_{h_q}))+\lim_{q\to\infty}O(h_q)+O(\xi_q)\\ =\ &\liminf_{q\to\infty}\mathcal{F}^l_{\mathbf{V}^l_{h_q,res}\cap in}(x_{h_q},\phi^l(x_{h_q}),\{d^m_q\}^{m\neq l},D\phi^l(x_{h_q}),D^2\phi^l(x_{h_q}))\\ \geq\ &\liminf_{q\to\infty}F^l_{v=0}(x_{h_q},\phi^l(x_{h_q}),\{d^m_q\}^{m\neq l},D\phi^l(x_{h_q}),D^2\phi^l(x_{h_q}))\qquad(4.3.18)\\ \geq\ &F^l_*(x,\phi^l(x),\{d^m\}^{m\neq l},D\phi^l(x),D^2\phi^l(x)),\qquad(4.3.19)\end{aligned}$$

where we have used Lemma 4.11 in (4.3.18) to lowerbound $\mathcal{F}^l_{\mathbf{V}^l_{h_q,res}\cap in}$ by $F^l_{v=0}$. Note that the application of Lemma 4.13 in (4.3.19) is legitimate since the closure condition is satisfied by using (4.3.11) in Lemma 4.12.

When either (4.3.16) or (4.3.17) can hold, we just need to (i) lower bound $\mathcal{F}^l_{\mathbf{V}^l_{h_q,res}\cap in}$ by $F^l_{v=0}$ if (4.3.16) holds; and (ii) lower bound $\mathcal{F}^l_{\mathbf{V}^l_{h_q,res}\cap s_{max}}$ by $F^l_{s_{max},v=0}$ if (4.3.17) holds. The application of Lemma 4.13 will be legitimate since the closure condition is satisfied by using (4.3.11) and (4.3.12) in Lemma 4.12. □

4.4 Stability

Proposition 4.15. *The numerical scheme (3.5.15) (for the localized problem* (3.4.2) *on* Ω_L*) is unconditionally stable in the infinity norm. More precisely,*

$$0 \le V^l_{i,j,k,n} \le K,$$

where $K = \mathcal{b}^2_{min}$ *is a constant independent of the grid* Ω_h*.*

Proof. We proceed by induction. The base case ($n = 0, \tau_n = 0$) is obvious from the initial condition $V^l_{i,j,k,n} = \mathcal{b}^2_j$.

For $\tau_{n+1} > 0$, $V^l_{i,j,k,n+1}$ is solved from $\mathcal{H}^l_{i,j,k,n+1} = 0$ (See (3.5.14)), which we rewrite as

$$\begin{aligned} & V^l_{i,j,k,n+1} - \triangle\tau(\mathcal{L}^l_h\, V^l_h)_{i,j,k,n+1} - \sum_{\substack{m=1\\ m\neq l}}^{M} \lambda^{lm} \triangle\tau\, V^m_{interp}(\tilde{x}^{l\to m}_{i,j,k,n+1}) \\ = & \min_{v\in\hat{\mathbf{V}}^l_{h,res}(x_{i,j,k,n+1})} V^l_{interp}(\hat{x}_{i,j,k,n}(v)) \end{aligned} \tag{4.4.1}$$

Note that the left hand side of (4.4.1) consists of nodes $V^{l'}_{i',j,k,n+1}$ with various values of i' and l', and the same values of j, k and $n+1$. Therefore (4.4.1) can be written as a matrix equation

$$(I - \triangle\tau L)V^{l'}_{i',j,k,n+1} = RHS$$

by considering all $i' = 0, \cdots, i_{max}$ and all $l' = 1, \cdots, M$ with fixed j, k and n. By (i) the positive coefficient condition $a^l_i, b^l_i, \lambda^l \ge 0$ (4.2.4); (ii) $\lambda_{lm} \ge 0$; (iii) $m \neq l$ in (4.4.1); and (iv) the use of linear interpolation, $(I - \triangle\tau L)$ is an M-matrix. Since RHS (which consists solely of nodes at time step n) is non-negative by the induction hypothesis and linear interpolation, we have proved that $V^l_{i,j,k,n+1} \ge 0$.

To prove the other inequality, rearranging the terms in (4.4.1) and applying the induction hypothesis gives

$$(1 + (a^l_i + b^l_i + \lambda^l)\triangle\tau)V^l_{i,j,k,n+1} \le K + \lambda^l\triangle\tau||V_{n+1}|| + \triangle\tau(a^l_i + b^l_i)||V_{n+1}||,$$

where $||V_{n+1}|| = \max_{i,j,k,l}\{V^l_{i,j,k,n+1}\}$. It then easily follows that

$$0 \le V^l_{i,j,k,n+1} \le ||V_{n+1}|| \le K.$$

□

4.5 Convergence

We prove convergence of the numerical scheme (3.5.15) under the following assumption on the PDE system (3.4.2).

Assumption 4.16. Strong Comparison Principle for (3.4.2)
If $\overline{V}^l$ is an upper semi-continuous subsolution of (3.4.2) and $\underline{V}^l$ is a lower semi-continuous supersolution of (3.4.2), then

$$\overline{V}^l \le \underline{V}^l \quad \text{in } \Omega_{int} \cup \partial\Omega_{reg},$$

where Ω_{int} stands for the interior of Ω_L and $\partial\Omega_{reg} \subseteq \partial\Omega_L$ stands for the regular part of the boundary $\partial\Omega_L$ (regular meaning that boundary conditions imposed on $\partial\Omega_{reg}$ influence the solution in the interior domain; see [41, 27] for more discussion).

We note that the strong comparison principle has recently been proved for a similar system of PDE from a regime switching model in [32].

Proposition 4.17. *Under Assumption 4.16, numerical solutions of (3.5.15) converge locally uniformly in $\Omega_{int} \cup \partial\Omega_{reg}$ to the unique continuous viscosity solution of (3.4.2).*

Proof. Define the upper semi-continuous function $\overline{V} : \Omega_L \to \mathbf{R}^M$ component-wise by

$$\overline{V}^l(x) = \limsup_{\substack{h\to 0 \\ x_h \to x}} V^l_h(x_h).$$

Note that $\overline{V}^l$ is bounded by Proposition 4.15.

For a fixed l, let $\phi^l \in C^\infty(\Omega_L)$ be a test function such that $\overline{V}^l - \phi^l$ has a strict local maximum of zero at $x \in \Omega_L$. By a classic argument in the theory of viscosity solution (see e.g. [27]), there exists sequence $\{\Omega_{h_q}\}_{q\in\mathbf{N}} \to \Omega_L$ and sequence[2] $\{x_{h_q} = x_{i_q,j_q,k_q,n_q+1}\}_{q\in\mathbf{N}} \to x \in \Omega_L$ such that $V^l_{h_q} - \phi^l$ has a global maximum at x_{h_q} and

$$V^l_{i_q,j_q,k_q,n_q+1} \to \overline{V}^l(x). \tag{4.5.1}$$

[2]Note that this x_{h_q} may not be the same as that in (4.3.1).

Let ξ_q be defined by[3]

$$V^l_{i_q,j_q,k_q,n_q+1} = \phi^l_{i_q,j_q,k_q,n_q+1} + \xi_q, \quad \text{where } \xi_q \to 0 \text{ by (4.5.1) and } \overline{V}^l(x) = \phi^l(x) \tag{4.5.2}$$

Since x_{h_q} is a global maximum of $V^l_{h_q} - \phi^l$, we have

$$V^l_{i_q,j_q,k_q,n_q+1} \le \phi^l_{i_q,j_q,k_q,n_q+1} + \xi_q, \quad \text{for } x_{i',j',k',n'} \in \Omega_{h_q} \tag{4.5.3}$$

Since $V^l_{h_q}$ is a numerical solution,

$$\mathcal{G}^l_{i_q,j_q,k_q,n_q+1}\Big(h_q, V^l_{i_q,j_q,k_q,n_q+1}, \{V^l_{i',j_q,k_q,n_q+1}\}_{i'\neq i_q}, \{V^l_{i',j',k',n_q}\}, \{V^m_{i',j',k',n_q+1}\}^{m\neq l}\Big) = 0 \tag{4.5.4}$$

By the monotonicity property (4.2.1) in Proposition 4.4, substituting (4.5.2) and (4.5.3) to (4.5.4) gives the inequality

$$0 \ge \mathcal{G}^l_{i_q,j_q,k_q,n_q+1}\Big(h_q, \phi^l_{i_q,j_q,k_q,n_q}+\xi_q, \{\phi^l_{i',j_q,k_q,n_q+1}\}_{i'\neq i_q}+\xi_q, \{\phi^l_{i',j',k',n_q}\}+\xi_q, \{V^m_{i',j',k',n_q+1}\}^{m\neq l}\Big) \tag{4.5.5}$$

To proceed, for each $m \neq l$, let $N^m_q = \{x^m_{h_q}\} \subseteq \{\Omega_{h_q}\}_{q\in\mathbf{N}}$ be the interpolation nodes such that the values $\{V^m_{h_q}(x^m_{h_q})\}$ (subset of $\{V^m_{i',j',k',n_q+1}\}$) are used for linear interpolating $V^m_{interp}(\tilde{x}^{l\to m}_{i_q,j_q,k_q,n_q})$, where $\tilde{x}^{l\to m}_{i_q,j_q,k_q,n_q} \to \tilde{x}^{l\to m}$. By virtue of linear interpolation, we know that for each $m \neq l$,

$$V^m_{interp}(\tilde{x}^{l\to m}_{i_q,j_q,k_q,n_q}) \le \max_{x^m_{h_q}\in N^m_q} \{V^m_{h_q}(x^m_{h_q})\}$$

and

$$\max_{x^m_{h_q}\in N^m_q} |x^m_{h_q} - \tilde{x}^{l\to m}| \to 0 \text{ as } q \to \infty.$$

Consequently,

$$\limsup_{q\to\infty} V^m_{interp}(\tilde{x}^{l\to m}_{i_q,j_q,k_q,n_q}) \le \limsup_{q\to\infty} \max_{x^m_{h_q}\in N^m_q} \{V^m_{h_q}(x^m_{h_q})\} \le \overline{V}^m(\tilde{x}^{l\to m})$$

Define sequences $\{d^m_q\}_{q\in\mathbf{N}}$ by

$$d^m_q = \max\big\{\overline{V}^m(\tilde{x}^{l\to m}), \sup_{q'\ge q} v_{q'}\big\}, \text{ where } v_q = \max_{x^m_{h_q}\in N^m_q} \{V^m_{h_q}(x^m_{h_q})\}$$

such that

$$d^m_q \ge \text{each } V^m_{h_q}(x^m_{h_q}) \text{ used in linear interpolation}, \quad d^m_q \to \overline{V}^m(\tilde{x}^{l\to m}) \text{ as } q \to \infty$$

By the monotonic property (4.2.1) of $\mathcal{G}^l_{i,j,k,n+1}$ in the last argument (discrete quasi-

[3]Note that for any finite grid size, the global maximum at x_{h_q} will not necessarily be zero, i.e. $\xi_q \neq 0$ in general.

monotonicity)

$$\liminf_{q\to\infty} \mathcal{G}^l_{i_q,j_q,k_q,n_q+1}\Big(h_q, \phi^l_{i_q,j_q,k_q,n_q} + \xi_q, \{\phi^l_{i',j_q,k_q,n_q+1}\}_{i'\neq i_q} + \xi_q, \{\phi^l_{i',j',k',n_q}\} + \xi_q, \{V^m_{i',j',k',n_q+1}\}^{m\neq l}\Big)$$
$$\geq \liminf_{q\to\infty} \mathcal{G}^l_{i_q,j_q,k_q,n_q+1}\Big(h_q, \phi^l_{i_q,j_q,k_q,n_q} + \xi_q, \{\phi^l_{i',j_q,k_q,n_q+1}\}_{i'\neq i_q} + \xi_q, \{\phi^l_{i',j',k',n_q}\} + \xi_q, \{d^m_q\}^{m\neq l}\Big) \tag{4.5.6}$$

By Proposition 4.14 and $d^m_q \to \overline{V}^m(\tilde{x}^{l\to m})$ as $q \to \infty$

$$\liminf_{q\to\infty} \mathcal{G}^l_{i_q,j_q,k_q,n_q+1}\Big(h_q, \phi^l_{i_q,j_q,k_q,n_q} + \xi_q, \{\phi^l_{i',j_q,k_q,n_q+1}\}_{i'\neq i_q} + \xi_q, \{\phi^l_{i',j',k',n_q}\} + \xi_q, \{d^m_q\}^{m\neq l}\Big)$$
$$\geq F^l_*(x, \phi^l(x), \{\overline{V}^m(\tilde{x}^{l\to m})\}^{m\neq l}, D\phi^l(x), D^2\phi^l(x)) \tag{4.5.7}$$

In summary, (4.5.5), (4.5.6) and (4.5.7) give

$$F^l_*(x, \phi^l(x), \{\overline{V}^m(\tilde{x}^{l\to m})\}^{m\neq l}, D\phi^l(x), D^2\phi^l(x)) \leq 0$$

By assumption, $\overline{V}^l(x) = \phi^l(x)$, therefore

$$F^l_*(x, \overline{V}^l(x), \{\overline{V}^m(\tilde{x}^{l\to m})\}^{m\neq l}, D\phi^l(x), D^2\phi^l(x)) \leq 0$$

Note that $\overline{V}^l$ and $\overline{V}^m$ are their own upper semi-continuous envelopes by construction, thus $\overline{V}^l$ is a sub-solution of (3.4.2).

Similarly, the lower semi-continuous function $\underline{V} : \Omega_L \to \mathbf{R}^M$ defined component-wise by

$$\underline{V}^l(x) = \liminf_{\substack{h\to 0\\ x_h\to x}} V^l_h(x_h)$$

is a super-solution of (3.4.2).

By Assumption 4.16, $\overline{V}^l \leq \underline{V}^l$ in $\Omega_{int} \cup \partial\Omega_{reg}$. On the other hand, $\overline{V}^l \geq \underline{V}^l$ by construction. Hence we have

$$\overline{V}^l = \underline{V}^l \quad \text{in } \Omega_{int} \cup \partial\Omega_{reg}.$$

This immediately implies point-wise convergence to the unique continuous viscosity solution of (3.4.2). Locally uniform convergence follows by a variation of Dini's theorem[4]. □

4.6 Summary

The main result in this chapter is the following.

[4]The classical Dini's theorem [58] states that if a monotonically increasing sequence of continuous real-valued functions on a compact topological space converges point-wise to a continuous function, then the convergence is uniform.

- We extend the convergence result in [16] to the system of nonlinear HJB PDEs that arises under our regime switching trade execution model. First, we prove that our discretization of the system of nonlinear HJB PDEs is monotone, consistent and infinity-norm stable. Second, we prove in detail that these properties guarantee the convergence of numerical solutions to the viscosity solution, provided that a strong comparison principle holds.

Chapter 5

Mean Variance Optimization: Numerical Results

This chapter presents numerical results for the Mean Variance optimization problem. We start by a brief discussion about parameter values in Section 5.1. Numerical results for the basic Geometric Brownian Motion model are then presented in Section 5.2. Finally, Section 5.3 presents numerical results for the Regime Switching model.

5.1 Trade Execution Model Parameters

The set of common parameter values shared by all computational examples in the thesis is summarized in Table 5.1. There are a number of points that are worth noting.

- Our numerical methods are designed to handle the quite general trade execution model in Section 2.1. The restriction to the parameter values in Table 5.1 is by no means necessary from a computational point of view.
- Since the drift rate is extremely hard to estimate in practice for a short trading horizon (e.g. one day), we set $\eta = 0$ (we refer reader to [11] for more discussion about drift rate in the context of optimal trade execution).
- Since interest rate has little effect over a short trading horizon, we set $r = 0$.
- Recall that we use a linear permanent price impact function (2.1.7) to eliminate the possibilities of round-trip price manipulation. As such, integrating (2.1.7) w.r.t.

η	r	κ_p	κ_s	s_{init}	α_{init}	β	T	v_{min}	Action
0.0	0.0	0.0	0.0	100	1.0	1.0	1/250	-1000/T	Sell

TABLE 5.1: *Parameter values shared by all computational examples in the thesis.*

Case	σ	κ_t	Percentage of Daily Volume
1	1.0	2×10^{-6}	16.7%
2	0.2	2.4×10^{-6}	20.0%
3	0.2	6×10^{-7}	5.0%
4	0.2	1.2×10^{-7}	1.0%
5	0.2	2.4×10^{-8}	0.2%

TABLE 5.2: *Computational cases for Section 5.2. The cases have different volatility and temporary impact factors. Other parameters are the same as that specified in Table 5.1.*

time would give total permanent price impact $= \kappa_p \alpha_{init}$, which is a constant that does not affect execution optimality in our model. Therefore, we set $\kappa_p = 0$.

- The cost from spread is in practice much smaller than that from temporary price impact, so we set $\kappa_s = 0$.
- We note that s_{init} and α_{init} can be normalized to 100.0 and 1.0 respectively without loss of generality.

5.2 Geometric Brownian Motion Model

In this section we report numerical results for the Mean Variance optimal trade execution problem under the basic Geometric Brownian Motion model of Section 2.1.1.

5.2.1 Computational Cases

The computational cases we consider have parameters as listed in Table 5.2. Case 1 corresponds to liquidating a high volatility stock with low liquidity. Case 2 to Case 5 correspond to liquidating a low volatility stock with various levels of liquidity.

Note that we simulate liquidating different percentages of the daily volume by using different values of κ_t while keeping the total liquidation volume unchanged. More specifically, we simulate liquidating $Y\%$ of the daily volume by using $\kappa_t = (1.2 \times 10^{-7})Y$ while keeping α_{init} unchanged at unity. The estimate that $\kappa_t = 1.2 \times 10^{-7}$ corresponds to liquidating 1% of the daily volume is explained in Appendix F.

5.2.2 Computational Information

In this section we provide brief information in using the PDE method and the Hybrid (PDE-Monte Carlo) method to compute results of interest. The reader can review the two methods in Section 3.6.

Refinement Level	Timesteps	s nodes	$\mathscr{b}$ node	α nodes	v nodes
0	200	369	1	11	8
1	400	737	1	21	15
2	800	1473	1	41	29
3	1600	2945	1	81	57

TABLE 5.3: *Computational grid for Section 5.2. The same grid is used for solving the HJB PDE (3.2.7) and in the Hybrid method.*

Table 5.3 shows the computational grid for solving the PDEs (3.2.7) and (3.2.9), and for the Hybrid method (for interpolating optimal selling velocities v^* during Monte Carlo simulations). We note the following points about the design of the computational grid. (Readers interested in this should review Section 3.7.)

- The v nodes are required to carry out a linear search to determine optimal controls. Note that we use quite few v nodes to save computational time. Numerical experiments show that using more v nodes gives little improvement in computing the value functions.
- There is only one node in the $\mathscr{b}$ direction (with value $\mathscr{b}^* = -100$) because of the use of similarity reduction; see Section 3.7.1 for details.
- The number of s nodes is significantly more than the number of α nodes. This is because our parametric curve interpolation scheme (Section 3.7.2) has small errors in interpolating along the α direction.

In using the Hybrid (PDE-Monte Carlo) method, we always use enough simulations to reduce sampling error to negligible levels in our reported results. For example, $400,000$ simulations are used for Case 1 where the volatility is large.

5.2.3 Numerical Convergence

Table 5.4 reports convergence information in solving the PDEs (3.2.7) and (3.2.9) for Case 1. We note that first order convergence rate is observed. The next section contains additional graphical illustrations of convergence.

Table 5.5 shows that s_{max} is sufficiently large so that the boundary conditions at $s = s_{max}$ introduce negligible errors.

5.2.4 Efficient Frontiers

The mean variance efficient frontier[1] can be computed using either the PDE method or the Hybrid method discussed in Section 3.6. Figure 5.1 plots the efficient frontiers computed

[1]Technically, this means $\mathcal{Y}_Q$ as defined in Definition 3.6. We will use the this terminology throughout this chapter since no confusion should arise. See also Section 5.2.5.

Refinement Level	V	U	Mean	Variance	Standard Deviation
0	4.1483	-1.7042	99.5458	1.2439	1.1153
1	4.0109	-1.6842	99.5658	1.1745	1.0838
2	3.9427	-1.6742	99.5758	1.1398	1.0676
3	3.9086	-1.6691	99.5808	1.1226	1.0595

TABLE 5.4: *Convergence table for solving the PDEs (3.2.7) and (3.2.9) for the value functions V and U, respectively. Mean and variance are calculated from the value functions as discussed in Section 3.6. Results are reported for Case 1 at the risk preference level $\gamma = 202.5$. First order convergence rate is observed for this case (and other cases not reported), as expected.*

Refinement Level	s_{max}	V	U	Mean	Variance	Standard Deviation
3	20,000	3.9086	-1.6691	99.5808	1.1226	1.0595
3	40,000	3.9086	-1.6692	99.5808	1.1223	1.0594

TABLE 5.5: *Convergence test to confirm s_{max} is sufficient large for the Mean Variance problem. Results for $s_{max} = 20,000$ are the same as that reported in Table 5.4. Results for $s_{max} = 40,000$ show that increasing s_{max} makes negligible difference.*

using the two methods for each of the computational case in Table 5.2. We plot standard deviation instead of variance so that the x-axis and the y-axis have the same unit (dollar).

We make the following comments on Figure 5.1 from a computational point of view.

- The same computational grid is used in both the PDE method and the Hybrid method (for interpolating optimal selling velocities v^* during Monte Carlo simulations) at each refinement level.
- The frontiers computed by both the PDE method and the Hybrid method converge to the same limit as the computational grid is refined.
- The frontiers computed by the Hybrid (PDE-Monte Carlo) method converge faster than those computed by the PDE methods. This may seem counter-intuitive as the Monte Carlo simulations use the optimal trading strategies determined by the PDE method. Nevertheless, it is plausible that Monte Carlo simulations produce better estimates of expected values and standard deviations, which is what our numerical results suggest.

5.2.5 Verifying Pareto Optimality

Recall the discussion in Section 3.1 about the subtleties in applying the embedding technique to numerically solve mean variance optimization problems. In this section we use Theorem 3.23 to verify the Pareto-optimality of the computed frontiers in Figure 5.1. For

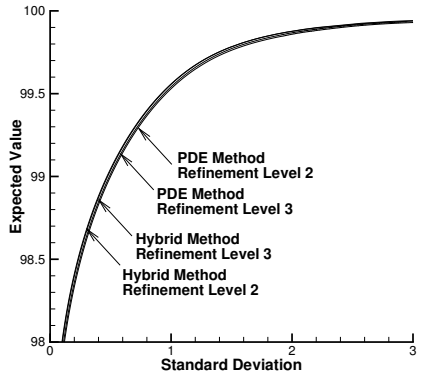

(a) σ=1.0, $\kappa_t = 2 \times 10^{-6}$

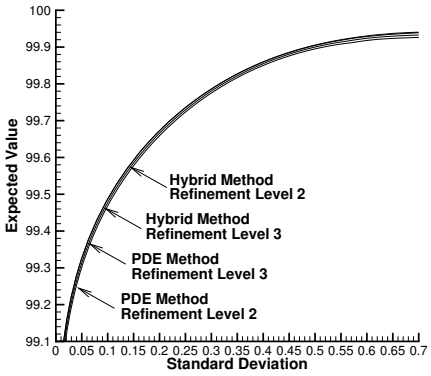

(b) σ=0.2, $\kappa_t = 2.4 \times 10^{-6}$

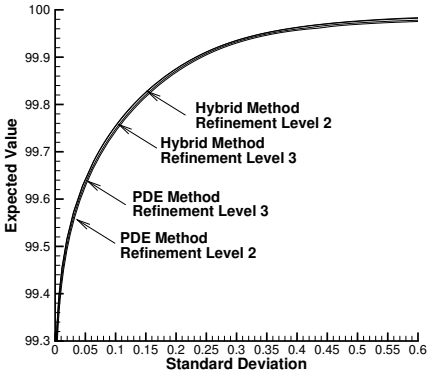

(c) σ=0.2, $\kappa_t = 6 \times 10^{-7}$

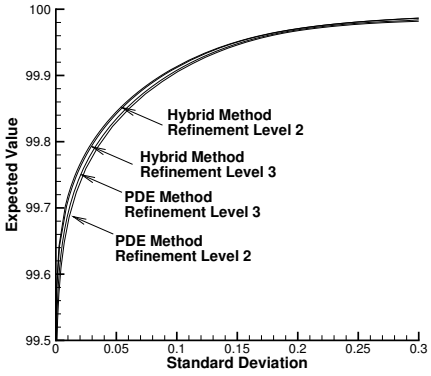

(d) σ=0.2, $\kappa_t = 1.2 \times 10^{-7}$

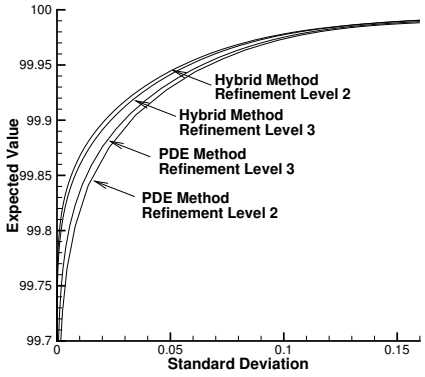

(e) σ=0.2, $\kappa_t = 2.4 \times 10^{-8}$

FIGURE 5.1: *Efficient frontiers of Mean Variance-optimal strategies. The frontiers labeled with PDE are obtained from the PDE value functions. The frontiers labeled with Hybrid are obtained from Monte Carlo simulations which use the optimal controls determined by solving the HJB PDE (3.2.7).*

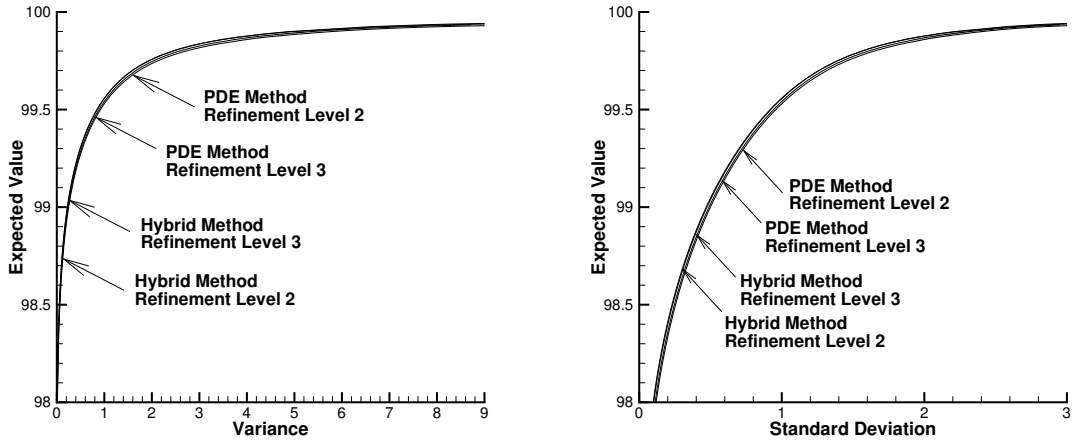

(a) Expected value against variance.

(b) Expected value against standard deviation.

FIGURE 5.2: *Plot of $\mathcal{Y}_Q^{num}$ for Case 1 in Table 5.2. Numerical solution has essentially converged at the higher grid refinement levels.*

illustration, we reproduce the result in Figure 5.1(a) in Figure 5.2(b); Figure 5.2(a) plots expected value against variance instead of standard deviation.

Using the terminology of Section 3.1, Figure 5.2(a) plots $\mathcal{Y}_Q^{num}$ for two grid refinement levels. It is clear that the numerical solution has essentially converged at the higher refinement level. From the plot, we see that every point of $\mathcal{Y}_Q^{num}$ lies on the upper-left convex hull of $\mathcal{Y}_Q^{num}$. Therefore, every point on $\mathcal{Y}_Q^{num}$ is Pareto-optimal by Theorem 3.23.

As discussed in Section 3.1.5, discretization of γ gives rise to theoretical subtleties in applying Theorem 3.23 to numerical solutions. For the example plotted above, we believe that these should not be a concern since

- Although we did not compute $\mathcal{Y}_{Q(\gamma)}^{num}$ for all $\gamma > 0$, we have used sufficiently many γ values to compute $\mathcal{Y}_Q^{num}$, i.e. computing $\mathcal{Y}_{Q(\gamma)}^{num}$ for more γ values results in a negligible change to the plotted $\mathcal{Y}_Q^{num}$. We also note that mean and variance increases monotonically with γ.
- The numerical convergence of $\mathcal{Y}_Q^{num}$ (or $\mathcal{S}(\mathcal{Y}_Q^{num})$) is smooth.
- We have used sufficiently many Monte Carlo simulations so that the standard error is negligible.

All mean variance efficient frontiers in the thesis can be verified to be Pareto optimal in the same way.

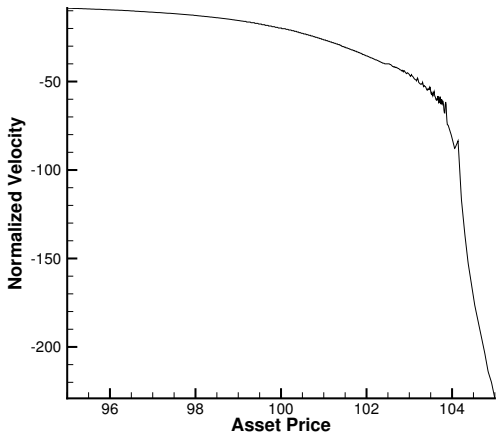

(a) This MV-optimal strategy has mean 99.29, standard deviation 0.68, and corresponds to $\gamma = 199.82$. The optimal normalized velocity at the beginning of the execution is approximately -20.0.

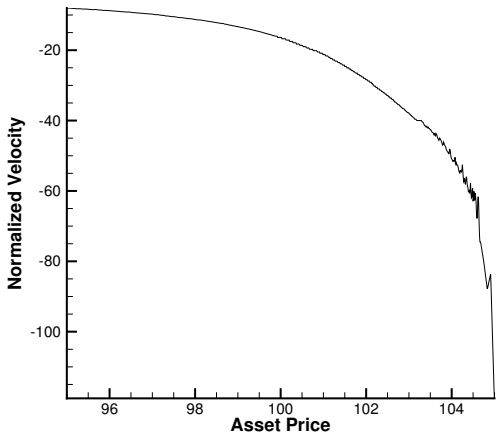

(b) This MV-optimal strategy has mean 99.50, standard deviation 0.90, and corresponds to $\gamma = 201.30$. The optimal normalized velocity at the beginning of the execution is approximately -16.4.

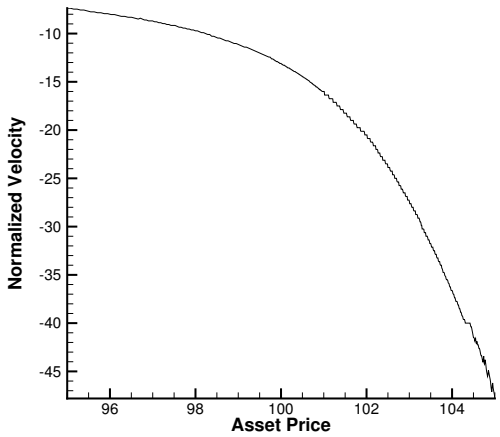

(c) This MV-optimal strategy has mean 99.65, standard deviation 1.13, and corresponds to $\gamma = 203.50$. The optimal normalized velocity at the beginning of the execution is approximately -13.1.

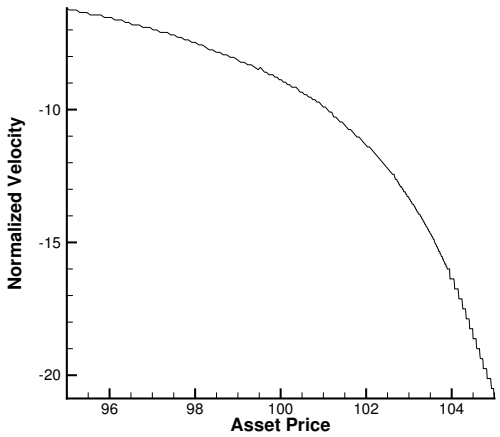

(d) This MV-optimal strategy has mean 99.78, standard deviation 1.46, and corresponds to $\gamma = 209.42$. The optimal normalized velocity at the beginning of the execution is approximately -8.8.

FIGURE 5.3: *MV-optimal strategies for the case σ=1.0, $\kappa_t = 2 \times 10^{-6}$ for different risk preference levels γ, plotted at $t = 0$ and $s = s_{init} = 100$. A normalized velocity of -1.0 corresponds to the constant liquidation rate $-\alpha_{init}/T$. Refinement level 3 is used to compute the results.*

5.2.6 MV-optimal Trading Strategies

Figure 5.3 plots the MV-optimal strategies in Case 1 for various risk preference levels. MV-optimal strategies for the other cases have similar properties. We make the following comments on Figure 5.3 about MV-optimal strategies.

- MV-optimal strategies sell much faster as the stock price increases (becomes more favorable for selling). We note that similar results have been reported in [51].
- As the risk preference level γ increases, it is optimal to sell slower. Consequently, the mean increases since trading impact is reduced, and the standard deviation increases since there is more timing risk.

We make the following comments on Figure 5.3 from a computational point of view.

- Comparing the four subfigures would reveal that the curves are the same curve scaled differently. This is because different risk preference levels γ correspond to different initial asset prices under similarity reduction.[2]
- The curves are not smooth when Normalized Velocity is between -40 and -100. These very fast initial selling rates correspond to small levels of mean and standard deviation that are not of practical interest. Moreover, Figure 5.1 shows that the efficient frontiers are smooth even though the optimal controls are not smooth.
- The non-smoothness observed above is an unavoidable consequence of numerically determining the optimal selling rate when the objective function is flat and close to zero. Reader interested in the detail can read Section 5.2.7 and look at the figures therein for illustrations.
- We have refined the v grid at $t = 0$ for plotting purposes. The original coarse v grid is sufficient for computing the value functions accurately.

5.2.7 Illustrations of Computational Techniques

Recall the efficiency-improving techniques discussed in Section 3.7. In this section we use numerical results to illustrate the improvement.

Figure 5.4 illustrates the value function V computed under a traditional Cartesian grid and that computed under the scaled grid illustrated schematically in Figure 3.2. Since the two value functions have very similar values, in the following we sometimes refer to them as "the value function".

We make the following comments about Figure 5.4.

[2]Using equations (3.2.2) and (3.7.2), the optimal velocity at risk preference level γ is $v^*(s_{init}, -\gamma/2, \alpha_{init}, T) = v^*(-2\mathcal{b}^* s_{init}/\gamma, \mathcal{b}^*, \alpha_{init}, T)$.

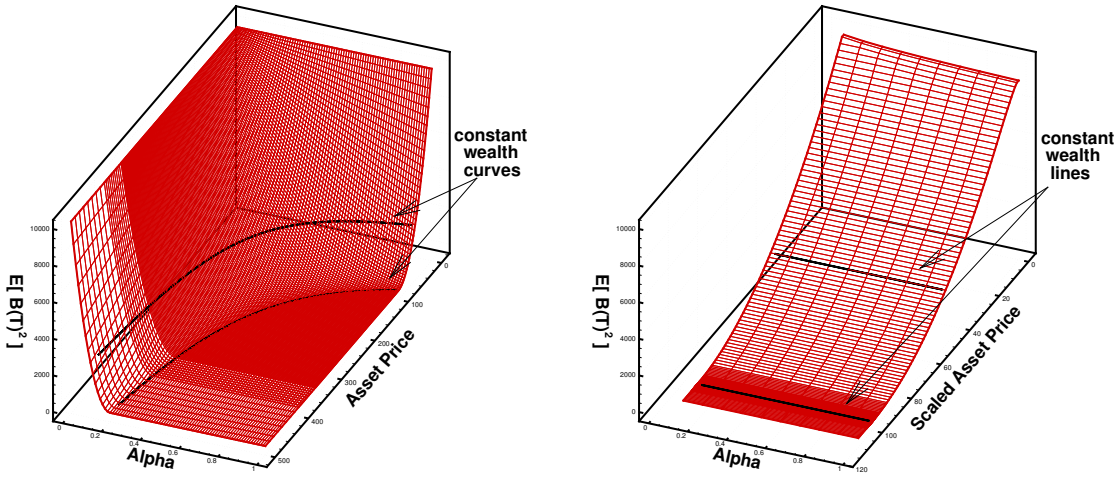

(a) Value function under Cartesian grid.

(b) Value function under the scaled grid.

FIGURE 5.4: *Illustrations of value function V for the case σ=1.0, $\kappa_t = 2 \times 10^{-6}$, plotted at $t = 0$. Note that there is no $\mathfrak{b}$ grid since similarity reduction is used with $\mathfrak{b}^* = -100$ (see Section 3.7.1).*

- Note that the value function at $t = 0$ is approximately $(\min\{\alpha s + \mathfrak{b}^*, 0\})^2$ (see the discussion in Section 3.7.2). When plotted under a traditional Cartesian grid in Figure 5.4(a), the value function has a more complicated shape than when plotted under the scaled grid Figure 5.4(b). In particular, curves of constant wealth, i.e. $\{\alpha s + \mathfrak{b} = const\}$, are straight lines under the scaled grid by construction.
- Table 5.4 shows that accuracy in the region where V is small is important since this region corresponds to the most curved part of the efficient frontier. The scaled grid has more nodes in the region where V is small.
- There is a large region where $V = V_s = V_{\mathfrak{b}} = V_\alpha = 0$. Optimal selling velocity v is not unique in this region (the value function V is unique though); see also Section 3.7.2.

Figure 5.5 illustrates the improvement made by the parametric curve interpolation method by comparing interpolated values on *exactly the same* discrete value function V^l (with values very similar to that in Figure 5.4).

We make the following comments on Figure 5.5.

- The parametric curve linear interpolation produces a smooth approximation of the local objective, whereas the standard linear interpolation method has large errors.
- Since the local objective is essentially a portion of the value function, the flatness of the local objective in Figure 5.5 is clearly a consequence of the flatness of the value function (see e.g. Figure 5.4(a))

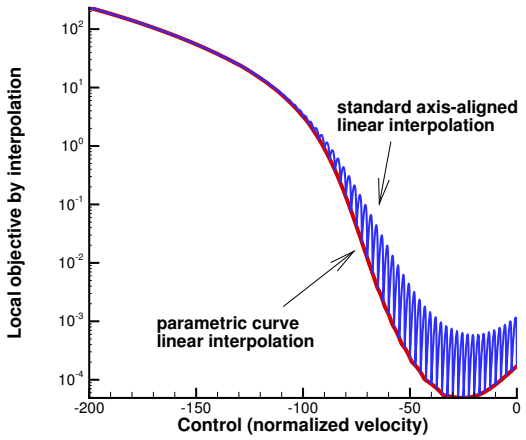

FIGURE 5.5: *Two methods for interpolating exactly the same discrete value function V^l at the foot of the Lagrangian characteristics, i.e. $V^l_{interp}(\hat{x}_{i,j,k,n}(v))$. The local objective $V^l_{interp}(\hat{x}_{i,j,k,n}(v))$ is plotted as function of the normalized velocity v/T. The parametric curve interpolation method is a significant improvement compared to the poor accuracy of standard linear interpolation.*

- Here we have used thousands of values of v (the control variable) for illustration purposes. When solving the HJB PDE, much fewer candidate controls are used (see Table 5.3). In that case, the standard interpolation method can produce large errors in estimating both the optimal control and the minimum objective value.

We also note that Figure 5.4 also explains the improvement made by the parametric curve interpolation method. Figure 5.4(a) shows that the value function changes rapidly and quadratically when s is fixed but α is changing, i.e. along $\{s = const\}$, causing large α-direction interpolation error for the standard axis-aligned interpolation method. In contrast, the parametric curve method interpolates (almost) along the curves of constant wealth, along which the value function changes slowly, as can be clearly seen in Figure 5.4(b). Recall that the curves of constant wealth are equivalent to $ScaledAssetPrice = const$ by construction.

5.3 Regime Switching Model

In this section we report numerical results for the Mean Variance optimal trade execution problem under the Regime Switching model of Section 2.1.2.

Regime	σ	κ_t	Percentage of Daily Volume	Description
A	0.2	2.4×10^{-6}	20.0%	largest impact
B	0.2	6×10^{-7}	5.0%	smallest impact
C	0.2	1.2×10^{-6}	10.0%	$2 \times$ smallest impact
D	0.2	1.5×10^{-6}	12.5%	Average of Regimes A and B

TABLE 5.6: *Underlying regimes for Section 5.3. The underlying regimes differ only in their temporary price impact factors. Other parameters are the same as that specified in Table 5.1.*

5.3.1 Computational Cases

Table 5.7 lists the Regime Switching computational cases, which are based on individual underlying regimes specified in Table 5.6.

Note that the underlying regimes in Table 5.6 differ only in their temporary price impact factors κ_t. We choose to focus on temporary price impact for the following reasons: (i) it directly affects execution cost and execution strategies; (ii) it is random and difficult to determine in practice [10]; (iii) as we will see, it is beneficial to adapt execution strategies to the level of temporary price impact. We refer interested readers to [7] for a more detailed discussion on the importance of considering stochastic liquidity.

In the context of liquidating large-cap stocks, the temporary impact factors κ_t considered in Table 5.6 are near the high end of those encountered in practice, e.g. liquidation of U.S. government's stock holdings acquired during the 2008 credit crisis [64]. In the context of liquidating small-cap stocks, which have much less liquidity on average, our temporary impact factors are more typical.

The computational cases in Table 5.7 are built on the underlying regimes in Table 5.6. Case AB-0, AB-4, AB-40 and AB-400 study regime switching between Regime A and Regime B. Case GREEDY is the same as AB-400, except that selling is allowed in only Regime B (the regime with smaller impact). Case GREEDY-PROXY, which is just the single Regime C with no switching, will be used as a proxy to Case GREEDY. In Case MISSPEC-AVERAGE the true dynamics is that of Case AB-400 and we investigate the (suboptimal) performance of the optimal strategy for Regime D.

5.3.2 Computational Grid

The computational grid is listed in Table 5.8, which is the same as Table 5.3 for the GBM model, except that the number of time steps is multiplied by ten. We note that many time steps are required to compute Case AB-400 and Case GREEDY since there are 400 switchings on average over the trading horizon.

Case	Initial Regimes	$\lambda^{12} = \lambda^{21}$	$\zeta^{12} = \zeta^{21}$	Description
AB-0	A or B	0	1	No Switching
AB-4	A or B	1000	1	4 Switchings/Day
AB-40	A or B	10000	1	40 Switchings/Day
AB-400	A or B	100000	1	400 Switchings/Day
GREEDY	A or B	100000	1	sell in only Regime B
GREEDY-PROXY	C	N/A	N/A	compare with GREEDY
MISSPEC-AVERAGE	D	N/A	N/A	true dynamics is AB-400

TABLE 5.7: *Computational cases for Section 5.3. The underlying regimes are specified in Table 5.6.*

Refinement Level	Timesteps	s nodes	$\mathscr{b}$ node	α nodes	v nodes
0	2000	369	1	11	8
1	4000	737	1	21	15
2	8000	1473	1	41	29

TABLE 5.8: *Computational grid for Section 5.3.*

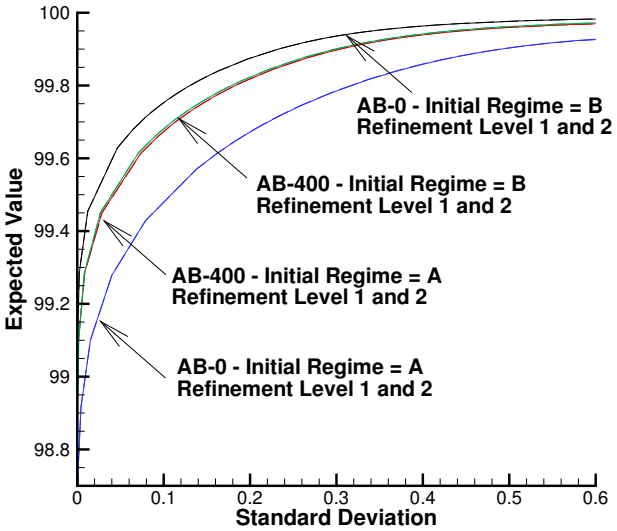

FIGURE 5.6: *Convergence of numerical solutions for Cases AB-0 and AB-400. Similar convergence results are observed for other cases in Table 5.7.*

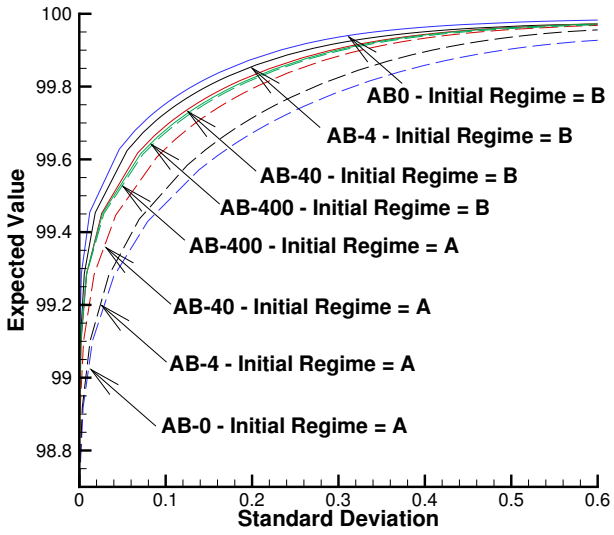

FIGURE 5.7: *Efficient frontiers for switching between Regime A and Regime B. Difference between "Initial Regime = A" and "Initial Regime = B" diminishes as switching intensity increases.*

5.3.3 Numerical Convergence

Figure 5.6 shows that the efficient frontiers computed[3] using Refinement Level 1 and Refinement Level 2 are essentially the same, for Cases AB-0 and AB-400 (similar results hold for other cases not shown here.). This means that the numerical solutions have essentially converged at Refinement Level 2. All subsequent numerical results reported are computed using Refinement Level 2.

5.3.4 Increasing Switching Intensities

In this subsection we compare Case AB-0, AB-4, AB-40 and AB-400 in Table 5.7 which differ only in the switching intensities between the two underlying regimes.

5.3.4.1 "Convergence" of Efficient Frontiers in Frequent Switching

Figure 5.7 plots the efficient frontiers for the regime switching cases, when initial regime (at $t = 0$) is Regime A or Regime B. Recall that the temporary impact is larger in Regime A. The following observations can be drawn from Figure 5.7:

[3]All efficient frontiers in this section are computed using the Hybrid method. We have shown previously in Section 5.2.4 that frontiers computed by the Hybrid method converge faster than those computed by the PDE Method.

- The frontiers "AB-0 - Initial Regime = A" and "AB-0 - Initial Regime = B" represent the efficient frontiers for the underlying regimes (i.e. Regime A and Regime B), since there is no switching in Case AB-0. The frontier "AB-0 - Initial Regime = A" is worse because of larger impact in Regime A.

- As switching intensities increase, the frontiers associated with "Initial Regime = A" become better. This is because switching to Regime B, which has a lower price impact, results in larger expected value. For similar reasons, as switching intensities increase, the frontiers associated with "Initial Regime = B" become worse.

- Consider the differences in the following pairs: AB-0 v.s. AB-4, AB-4 v.s. AB-40, and AB-40 v.s. AB-400. We note that the difference between AB-4 and AB-40 is particularly large.

- The frontiers "AB-400 - Initial Regime = A" and "AB-400 - Initial Regime = B" are very close to each other. As switching becomes extremely frequent, the initial regime has little effect on the end result.

- By extrapolating the results in Figure 5.7, we can see that as switching intensities go to infinity, the efficient frontiers will converge to a limiting efficient frontier between "AB-400 - Initial Regime = A" and "AB-400 - Initial Regime = B". It is interesting to know whether the limiting efficient frontier corresponds to that of a single regime, and what parameters that regime would have. The next section will shed some light on this problem.

5.3.4.2 Sell More Slowly when Price Impact is Larger

Figure 5.8 compares the optimal trading velocities between Case AB-0 and Case AB-400. The following observations can be drawn from Figure 5.8:

- The difference between "Initial Regime = A" and "Initial Regime = B" is smaller in Case AB-0 when there is no switching.

- The difference between "Initial Regime = A" and "Initial Regime = B" becomes larger when switching intensity is increased. As temporary price impact switches between Regime A and Regime B, an optimal strategy would try to sell more in Regime B (which has lower price impact) and less in Regime A. Such "selective selling" behavior becomes more pronounced as switching intensity becomes larger. Note that this is in contrast to Figure 5.7, in which the difference between the frontiers labeled "Initial Regime = A" and "Initial Regime = B" becomes smaller as switching intensity is increased.

- Despite the above, selling velocity does not drop to zero in "AB-400 Initial Regime = A". Therefore the straightforward strategy that simply sells in only the regime with lower price impact is sub-optimal. We will study such a strategy in detail in Section 5.3.5.

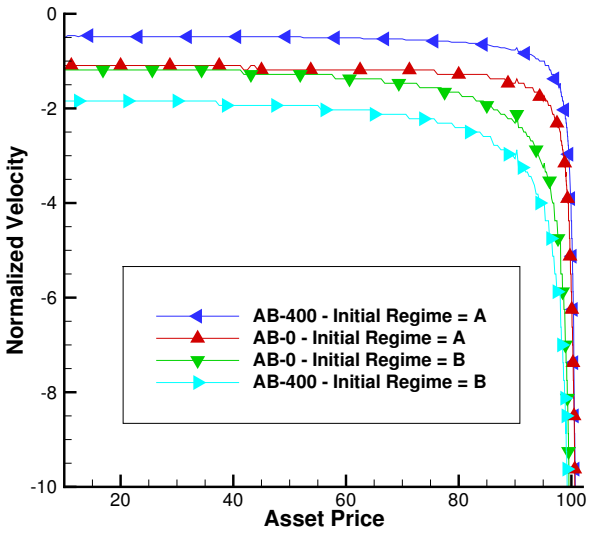

FIGURE 5.8: *Optimal selling velocities in Case AB-0 and Case AB-400. A normalized velocity of* -1 *corresponds to the liquidation rate* $-\alpha_{init}/T = -1/T$.

- A careful look would reveal that the selling velocity in "AB-400 Initial Regime = B" is four times that in "AB-400 Initial Regime = A" in Figure 5.7. Recall that κ_t in Regime B is one-fourth of that in Regime A. This relation can be explained by observing that the optimum of the objective function in the HJB PDE is approximately linear in $1/\kappa_t$ (holding everything else constant in the HJB PDE), and noting that the value functions at Regime A or B are approximately the same for rapid switching.

- The above analysis (regarding optimum of the objective function) is valid for all risk-aversion levels, and in particular at the risk-neutral limit where expected value is maximized regardless of standard deviation. By interpreting t as volume time (rather than clock time), a strategy that sells at a constant rate tracks the volume weighted averaged price (VWAP). Our results show that even if the objective is to solely maximize expected value, it is still beneficial to adapt selling speed to the (constantly changing) level of temporary price impact in the market.

5.3.5 A Look at Greedy Strategies

As discussed in Section 5.3.4.2, when regime switching is frequent, a liquidation strategy that sells in only the lower-impact regime (henceforth referred to as a greedy strategy) is suboptimal. We now study in detail the sub-optimality of such greedy strategies.

We can forbid any selling in Regime A (which has a larger price impact) by changing the set of admissible selling velocities to $\{0\}$ in our numerical algorithm. Our algorithm

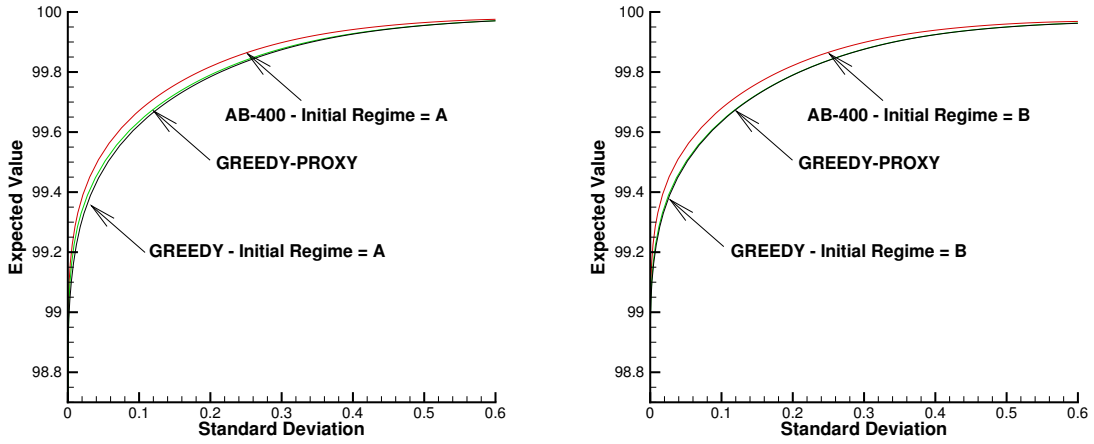

FIGURE 5.9: *The best greedy strategy is noticeable suboptimal. The efficient frontier of Regime C (GREEDY-PROXY) is close to that of GREEDY.*

will then solve for the best greedy strategy, which we denote by Case GREEDY in Table 5.7.

Figure 5.9(a) (respectively Figure 5.9(b)) shows that even the best greedy strategy is still noticeably suboptimal compared with the truly optimal strategy, when the initial regime is Regime A (respectively Regime B).

It is interesting to note in Figure 5.9(a) and Figure 5.9(b) that the efficient frontier of Case C, which has roughly[4] double the temporary impact of the lower-impact regime (Regime B), is very close to that of Case GREEDY. Intuitively, approximately half of the time is spent in the lower-impact regime when switching is frequent, thus the optimal strategy in Case GREEDY needs to "double the selling speed" to finish liquidation in time. Consequently, "doubling the selling speed" for $\kappa_t = 6 \times 10^{-7}$ (Regime B) gives an effective κ_t of $2 \times 6 \times 10^{-7} = 1.2 \times 10^{-6}$, which is the price impact in Regime C. This reasoning is supported by numerical results in Figure 5.10 which shows that the optimal selling velocity in Case GREEDY is very close to double of that in Case C.

5.3.6 Sub-optimality from Mis-specification

Note that for a strategy that sells at a constant rate, its expected trading impacts under the following two market dynamics are the same.[5]

1. Rapid switching between regime A with $\kappa_t = \kappa_t^A$ and regime B with $\kappa_t = \kappa_t^B$ (with equal switching intensities)

[4]We say roughly because $\exp\{\kappa_t v\} \approx 1 + \kappa_t v$.

[5]In fact they are just approximately the same since $\exp\{\kappa_t v\}$ is a slightly nonlinear function of κ_t for typical values of v. However, the difference is negligible for all practical purposes.

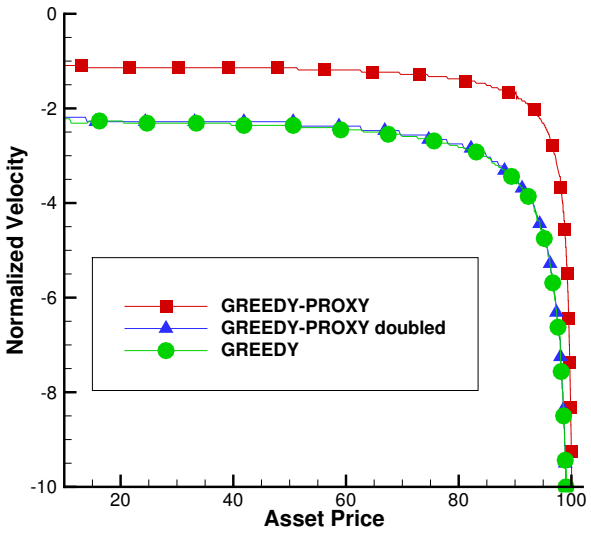

FIGURE 5.10: *The optimal selling velocity in Case GREEDY is approximately double of that in Case C.*

2. Single regime with $\kappa_t = (\kappa_t^A + \kappa_t^B)/2$

Consequently, if the true dynamics follow rapid switching, but no switching is assumed in measuring κ_t, one would obtain the "averaged" value of κ_t from the measurement. Since the stochastic nature of κ_t is typically ignored and assumed to be constant in practice [7, 64], it is important to understand the consequences of such mis-specification.

Recall that κ_t in Regime D is the average of that of Regimes A and B. In Figure 5.11(a) and Figure 5.11(b), the sub-optimality of MISSPEC-AVERAGE (optimal strategy for Regime D) is seen to be quite large. Moreover, sub-optimality is clear even at the risk-neutral limit. Although this is not very surprising given the large difference between Regime A and B, it is still worth noting that MISSPEC-AVERAGE is clearly more suboptimal than GREEDY (plotted in Figures 5.9). This means that it is better to take advantage of stochastic changes in temporary price impacts, even in a sub-optimal way as in GREEDY, than simply assuming constant price impact.

5.4 Summary

The main results in this chapter are the followings.

- MV-optimal strategies sell much faster as the stock price increases.
- It is important to adapt MV-optimal strategies to random changes in temporary price impact. When the real dynamics is rapid switching between two regimes of

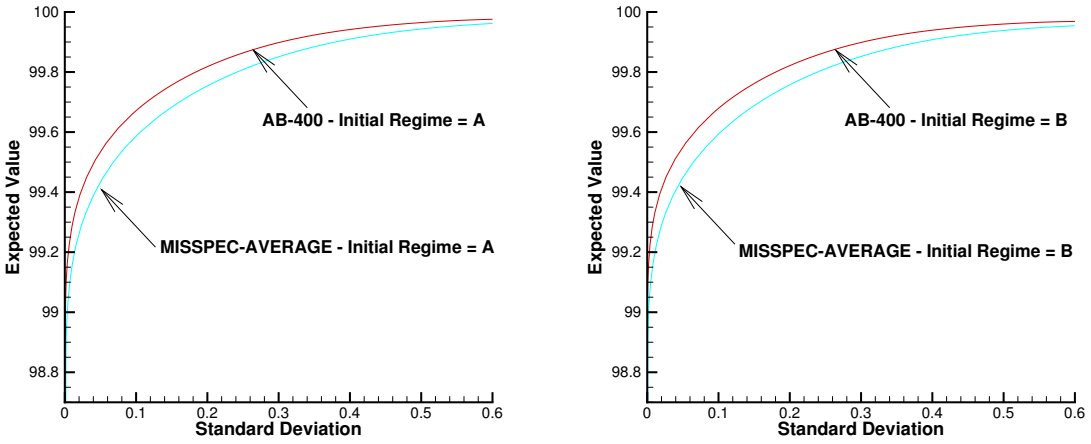

FIGURE 5.11: *The optimal strategy for Regime D is significantly suboptimal when the real dynamics is that of Case AB-400, even at the risk-neutral limit. Note that MISSPEC-AVERAGE is more sub-optimal than GREEDY; see Figure 5.9.*

differing price impacts, mis-specifying the dynamics as the non-switching mixture results in significant sub-optimality.

Chapter 6

Optimal Trade Execution: Mean Quadratic Variation Approach

This chapter discusses optimal trade execution using the Mean Quadratic Variation (MQV) optimization approach, as opposed to the Mean Variance (MV) optimization approach studied in earlier chapters. A main result in this chapter is the proof in Section 6.5 that the classic strategies in [9] are MQV-optimal, in contrast to the common belief that they are MV-optimal. This chapter also develops computational methods for determining MQV-optimal strategies, which will allow us to show in Chapter 7 that MQV-optimal strategies are poor approximations to MV-optimal strategies in many aspects.

The computational methods for determining MQV-optimal strategies are quite similar to those for determining MV-optimal strategies. Therefore, our discussion on computational methods in this chapter will be relatively brief compared to earlier chapters.

6.1 Mean Quadratic Variation Optimization

In this chapter we restrict attention to the single regime case and study MQV-optimal strategies primarily[1] under the Geometric Brownian Motion trade execution model introduced in Section 2.1.1.

6.1.1 Quadratic Variation as a Risk Measure

Formally, the quadratic variation risk measure is defined as

$$E\left[\int_0^T \big(A(t')dS(t')\big)^2\right]. \tag{6.1.1}$$

[1]The notable exception is Section 6.5, where we consider the Arithmetic Brownian Motion model to compare with results in the literature.

Informally, the risk measure definition (6.1.1) can be interpreted as the (expected) quadratic variation of the portfolio value process as follows: by expanding the square of $dP(t') = dB(t') + d(A(t')S(t'))$, we have

$$\int_0^T \big(A(t')dS(t')\big)^2 = \int_0^T \big(dP(t')\big)^2, \tag{6.1.2}$$

when the trading velocity process $v(t)$ is bounded.

From the interpretation (6.1.2), minimizing quadratic variation clearly corresponds to minimizing the volatility of the portfolio value process. The definition (6.1.1) shows that quadratic variation takes into account the trading trajectory $A(t')$ over the whole trading horizon. This is in contrast with using variance ($Var[B(T)]$) as a risk measure, which is independent of the trading trajectory $A(t')$ given the end result $B(T)$. We note that the idea of using quadratic variation as a risk measure was first suggested in [24].

6.1.2 Mean Quadratic Variation Optimality in the Pareto Sense

To simplify notations, we use $X(t) = (S(t), A(t))$ to denote the multi-dimensional space-state process and $x = (s, \alpha)$ to denote a space-state[2]. We also let $E^{x,t}_{v(\cdot)}[\cdot]$ denote expectation conditional on the initial state (x, t) and the control $v(\cdot) : (x, t) \mapsto v = v(x, t)$, as defined in Section 2.2.1.

Definition 6.1. Define the objective functionals $J_1^{x,t}\Big(v(\cdot)\Big)$ and $J_2^{x,t}\Big(v(\cdot)\Big)$ by

$$\begin{aligned}
J_1^{x,t}\Big(v(\cdot)\Big) &= E^{x,t}_{v(\cdot)}\left[\int_t^T \big(A(t')dS(t')\big)^2\right], \\
J_2^{x,t}\Big(v(\cdot)\Big) &= E^{x,t}_{v(\cdot)}\left[\int_t^{T^-} e^{r(T-t')}\big(-vS_{exec}(v,t')\big)\,dt' + \lim_{v\to-\infty} A(T^-)S_{exec}(v,T^-)\right].
\end{aligned}$$

Definition 6.2. An admissible strategy $v^*(\cdot)$ is defined to be Mean Quadratic Variation optimal in the Pareto sense if there exists no admissible strategy $v(\cdot)$ such that

1. $J_1^{x,t}\Big(v(\cdot)\Big) \le J_1^{x,t}\Big(v^*(\cdot)\Big)$, $J_2^{x,t}\Big(v(\cdot)\Big) \ge J_2^{x,t}\Big(v^*(\cdot)\Big)$.
2. At least one inequality in the above is strict.

Remark 6.3. *We note that Definition 6.2 does not require the definition of the state process $B(t)$, i.e. MQV-optimality is still well-defined even if we did not define the state process $B(t)$ in (2.1.3). For notational simplicity, we define $\tilde{B}(T)$ as a formal[3] shorthand*

[2]The notations $X(t)$ and x have slightly different meanings from that in previous chapters. The underlying meaning should be clear from the context and no confusion should arise.

[3]There is no state process $\tilde{B}(t)$ defined for $t \in [0, T]$.

as follows

$$\tilde{B}(T) = \int_t^{T^-} e^{r(T-t')}\big(-vS_{exec}(v,t')\big)\,dt' + \lim_{v\to-\infty} A(T^-)S_{exec}(v,T^-). \tag{6.1.3}$$

6.1.3 Scalarization

As we discussed in Section 2.2.1, Pareto-optimality is economically intuitive but mathematically inconvenient because there are two conflicting criteria to optimize. A standard scalarization reformulation combines the two criteria into a single objective (the subtleties of the scalarization reformulation was discussed in Chapter 3). More specifically, consider the following family of objective functionals parametrized by $\phi > 0$

$$\mathcal{F}_\phi = \left\{ J_\phi^{x,t}\Big(v(\cdot)\Big) : v(\cdot) \mapsto E_{v(\cdot)}^{x,t}\Big[\tilde{B}(T) - \phi\int_t^T \big(A(t')dS(t')\big)^2\Big] \right\}. \tag{6.1.4}$$

In the notation of (6.1.4), the members (functionals) in the family $\mathcal{F}_\phi$ have different initial states (x,t) but the same ϕ. Given (x,t) and ϕ, we use $v^*_{x,t,\phi}(\cdot)$ to denote an optimal strategy that maximizes the corresponding functional, i.e. $J_\phi^{x,t}\Big(v(\cdot)\Big)$.

6.1.4 Time Consistency of Optimal Strategies

Optimal strategies in the above Mean Quadratic Variation formulation optimization framework are time-consistent [17] in the following sense. Let (x_1,t_1) be some state at time t_1 and $v^*_{x_1,t_1,\phi}(\cdot)$ be a corresponding optimal strategy. Let (x_2,t_2) be some other state at time $t_2 > t_1$ and $v^*_{x_2,t_2,\phi}(\cdot)$ be a corresponding optimal strategy. The optimal strategies are time-consistent in the sense that

$$v^*_{x_1,t_1,\phi}(x',t') \;\; = \;\; v^*_{x_2,t_2,\phi}(x',t') \;;\; t' \geq t_2 \;\; .$$

6.2 HJB PDE Formulation

In view of the formulation (6.1.4), define

$$\hat{V}(s,\alpha,t;\phi) = \sup_{v(\cdot)}\Big\{E_{v(\cdot)}^{s,\alpha,t}\Big[\tilde{B}(T) - \phi\int_t^T \big(A(t')dS(t')\big)^2\Big]\Big\} \tag{6.2.1}$$

for initial states $(x,t) = (s,\alpha,t)$ and risk aversion parameter $\phi > 0$.

For $t < T$, let $V = V(s,\alpha,\tau = T-t;\phi) = \hat{V}(s,\alpha,t;\phi)$. For notational simplicity, we drop the parameter ϕ from V henceforth, i.e. we simply write $V = V(s,\alpha,\tau)$.

The dynamic programming principle is directly applicable[4] to (6.2.1). Standard derivation of the HJB PDE (see Appendix B) gives

$$V_\tau = \eta s V_s + \frac{\sigma^2 s^2}{2} V_{ss} - \phi \sigma^2 \alpha^2 s^2 + \max_{v \in [v_{min}, 0]} \left\{ - e^{r\tau} v f(v) s + g(v) s V_s + v V_\alpha \right\} \tag{6.2.2}$$

for $\tau > 0$; with initial condition

$$V(s, \alpha, \tau = 0) = \lim_{v \to -\infty} \alpha s f(v) \tag{6.2.3}$$

in accordance with (6.1.3).

In order to plot expected value ($E^{x,t}_{v(\cdot)}[\tilde{B}(T)]$) against expected quadratic variation ($E^{x,t}_{v(\cdot)}[\int_t^T \left(A(t')dS(t')\right)^2]$), we will need to know the values of each term in (6.2.1). To compute only the expected value, let $\hat{U}(s, \alpha, t)$ be defined by

$$\hat{U}(s, \alpha, t) = E^{s,\alpha,t}_{v^*(\cdot)}[\tilde{B}(T)] \ ,$$

where $v^*(\cdot)$ is found by solving the HJB PDE (6.2.2).

Let $U(s, \alpha, \tau = T - t) = \hat{U}(s, \alpha, t)$. Following the same steps as used to derive equation (6.2.2), or simply setting $\phi = 0$, we obtain

$$U_\tau \ = \ \eta s U_s + \frac{\sigma^2 s^2}{2} U_{ss} - e^{r\tau} v^* f(v^*) s + g(v^*) s U_s + v^* U_\alpha \ . \tag{6.2.4}$$

We have the initial condition

$$U(s, \alpha, \tau = 0) = \lim_{v \to -\infty} \alpha s f(v). \tag{6.2.5}$$

in accordance with (6.1.3).

6.3 Localization and Boundary Conditions

For computational purposes, we localize the computational domain to $\Omega_L = \{s \in [0, s_{max}], \alpha \in [0, 1], \tau \in [0, T]\}$.

No boundary condition is required for V in (6.2.2) at $s = 0$ because the V_s and V_{ss} terms vanish and we simply need to solve

$$V_\tau \ = \ \max_{v \in [v_{\min}, 0]} \Big[v V_\alpha \Big]. \tag{6.3.1}$$

[4] In contrast, the dynamic programming principle cannot be directly applied to the objective functional (2.2.1) in the (pre-commitment) Mean Variance problem; see Section 3.1.

Notation	Descriptions
$x = (s, \alpha, \tau)$	a point in the localized domain
Ω_h	grid with spacing $O(h)$
$x_{i,k,n}$	grid node in Ω_h
V_h	**R**-valued discrete function defined on Ω_h
$V_{i,k,n}$	value of V_h at grid node
$\hat{x}_{i,k,n}(v) = (s_{\hat{i}}, \alpha_{\hat{k}}, \tau_n)$	foot of Lagrangian characteristics
$V_{interp}(\hat{x}_{i,k,n}(v))$	linear interpolated value of V_h

TABLE 6.1: *Summary of discretization notations for the MQV problem.*

No boundary condition is required at $\alpha = 1$ since $v \leq 0$ and thus the characteristic is outgoing there.

At $\alpha = 0$, we impose $v = 0$ so that (s, α, τ) stays in Ω_L. More specifically, this ensures that we do not allow α to become negative (i.e. a short position).

At $s = s_{\max}$, we make the assumption that $V \simeq C(\alpha, \tau)s^2$, which can be justified by noting that the term $\phi\sigma^2\alpha^2 s^2$ acts as a source term in equation (6.2.2). We also assume that the effect of any permanent price impact at $s = s_{\max}$ can be ignored i.e. $g(v) = 0$ at $s = s_{\max}$. This gives

$$V_\tau = (2\eta + \sigma^2)V - \phi\sigma^2\alpha^2 s^2 + \max_{v \in [v_{min}, 0]} \left[-e^{r\tau} v f(v) s + v V_\alpha \right]. \tag{6.3.2}$$

Equation (6.3.2) is clearly an approximation. We will carry out numerical tests with varying $s_{\max}$ to show that the error in this approximation can be made small in regions of interest.

Similar reasoning suggests that no boundary condition is needed for U in (6.2.4) at $\alpha = 0$, $\alpha = 1$ or $s = 0$. At $s = s_{\max}$, we assume $U \simeq D(\alpha, \tau)s$ (based on the initial condition (6.2.5)) and $g(v) = 0$. Consequently,

$$U_\tau = \eta U - e^{r\tau} v^* f(v^*) s + v^* U_\alpha \ ; \ s = s_{\max}. \tag{6.3.3}$$

Again, equation (6.3.3) is clearly an approximation. We will verify that the error of this approximation is small for sufficiently large $s_{\max}$.

6.4 Discretization

Since much of the discretization is similar to that in the MV problem (Section 3.5), the discussion will be relatively brief here. Adapting the discretization notations for the MV problem to the MQV problem, we summarize the discretization notations for the MQV problem in Table 6.1.

Define a set of nodes $\{s_i\}$, $\{\alpha_k\}$ and $\{\tau_n\}$, where $0 \le i \le i_{max}$, $0 \le k \le k_{max}$, and $0 \le n \le n_{max}$. We make $\tau_n = n\triangle\tau$, where $\triangle\tau = T/n_{max}$.

Define the differential operator $\mathcal{L}$ by

$$\mathcal{L}V = \eta s V_s + \frac{\sigma^2 s^2}{2} V_{ss}.$$

Define the Lagrangian differential operator $\frac{D}{D\tau}(v)$ by

$$\frac{DV}{D\tau}(v) = V_\tau - V_s g(v) s - V_\alpha v,$$

which is the rate of change of V along the characteristics $s = s(\tau)$, $\alpha = \alpha(\tau)$ defined by the trading velocity v through

$$\frac{ds}{d\tau} = -g(v)s, \quad \frac{d\alpha}{d\tau} = -v. \tag{6.4.1}$$

Equation (6.2.2) can be rewritten as

$$-\mathcal{L}V + \min_{v\in[v_{min},0]}\left[\frac{DV}{D\tau}(v) + e^{r\tau} v f(v) s\right] + \phi\alpha^2 s^2 \sigma^2 = 0.$$

We use standard finite difference methods to discretize $\mathcal{L}V$. Let $(\mathcal{L}_h V_h)_{i,k,n+1}$ denote the discretized version of $\mathcal{L}V$ at node $x_{i,k,n+1}$. $\mathcal{L}V$ is discretized using central, forward, or backward differencing in the s direction to give

$$(\mathcal{L}_h V_h)_{i,k,n+1} = a_i^l\big(V_{i-1,k,n+1}\big) - \big(a_i^l + b_i^l\big)\big(V_{i,k,n+1}\big) + b_i^l\big(V_{i+1,k,n+1}\big)$$
$$\text{for all } i \text{ except } i = 0, i_{max},$$

where the positive coefficient condition

$$a_i^l \ge 0 \text{ and } b_i^l \ge 0$$

is guaranteed by the algorithm [28].

Note that $\mathcal{L}V$ does not appear in the boundary conditions at $s = 0$ (6.3.1) and $s = s_{max}$ (6.3.2).

The discretized version of the Lagrangian derivative $\frac{DV}{D\tau}(v)$ at node $x_{i,k,n+1}$ is given by

$$\Big(\frac{DV}{D\tau}(v)\Big)_{i,k,n+1} = \frac{1}{\triangle\tau}\Big(V_{i,k,n+1} - V_{interp}(\hat{x}_{i,k,n}(v))\Big),$$

where $\hat{x}_{i,k,n}(v) = (s_{\hat{i}}, \alpha_{\hat{k}}, \tau_n)$ is the foot of the characteristics when we solve the ODEs (6.4.1) initially at $x_{i,k,n+1}$, from τ_{n+1} to τ_n; and $V_{interp}(\hat{x}_{i,k,n}(v))$ is a linear interpolated value.

Since the point $\hat{x}_{i,k,n}(v)$ may go out of Ω_L for some $v \in [v_{min}, 0]$, we need to restrict the set of admissible velocities for the localized discrete problem. Since the details are very similar to that in Section 3.5.4 for the MV problem; here we just state the discretization as

$$\min_{v\in[v_{min},0]} \Big\{ \Big(\frac{DV}{D\tau}(v) \Big)_{i,k,n+1} \Big\} \approx \min_{v\in\hat{\mathbf{V}}_{h,res}(x_{i,k,n+1})} \Big\{ \frac{1}{\triangle\tau} \Big(V_{i,k,n+1} - V_{interp}(\hat{x}_{i,k,n}(v)) \Big) \Big\},$$

where $\hat{\mathbf{V}}_{h,res}(x_{i,k,n+1})$ is a discrete set of restricted admissible velocities.

The final discretization is

$$\begin{aligned} 0 = & \min_{v\in\hat{\mathbf{V}}_{h,res}(x_{i,k,n+1})} \Big\{ \frac{1}{\triangle\tau} \Big(V_{i,k,n+1} - V_{interp}(\hat{x}_{i,k,n}(v)) \Big) + e^{r\tau_{n+1}} v f(v) s_i \Big\} \\ & - (\mathcal{L}_h V_h)_{i,k,n+1} + \phi \alpha_k^2 s_i^2 \sigma^2. \end{aligned} \tag{6.4.2}$$

We will use two methods to determine the minimum in (6.4.2). The first method uses a linear search, which guarantees convergence to the global minimum. The second method uses a one dimensional optimization algorithm [22] to determine the optimal control. This has the advantage of being less computationally expensive. The drawback, however, is that one dimensional optimization methods are not guaranteed to converge to the global minimum. We will carry out numerical tests using both methods.

Our discretization of the HJB PDE (6.2.2) is very similar to that of (3.2.7) in the Mean Variance problem. By following similar steps in Chapter 3 and 4, we can show that our discretization of (6.2.2) is monotone, consistent and stable. Assuming a strong comparison principle for (6.2.2), numerical solutions converge to the viscosity solution by the result in [16].

6.5 Arithmetic Brownian Motion Model

In the context of optimal trade execution, the trading horizon T is typically short (e.g. one day). Therefore, it is typical in the literature, see e.g. [9, 60], to approximate Geometric Brownian Motion (GBM) by Arithmetic Brownian Motion (ABM). In this section we use the ABM model in the Mean Quadratic Variation framework to compare with the analytic result in the seminal work [9]. We did not use the ABM model in the Mean Variance framework because there is no corresponding analytic result in that framework.

6.5.1 Trade Execution Model

Recall that the basic GBM model was introduced in Section 2.1.1. This section describes our ABM optimal execution model based on modifications to the GBM model.

The asset price dynamics (2.1.4) is modified to the ABM process

$$dS(t) \;=\; \big(\eta + g(v)\big) S(0)\; dt + \sigma S(0)\; d\mathbb{W}(t)\;. \tag{6.5.1}$$

In addition, we assume that temporary price impact is asset-price-independent, i.e.

$$S_{exec}(v,t) = S(t) + S(0)h(v), \tag{6.5.2}$$

where

$$h(v) = \kappa_s \operatorname{sgn}(v) + \kappa_t v, \tag{6.5.3}$$

to be in accordance with [9]. Note that $S_{exec}(v,t)$ may be negative for $v \to -\infty$, i.e. (6.5.3) is valid only for small trading rates.

Temporary impact in the ABM model (6.5.2) - (6.5.3) is related to that in the GBM model (2.1.5) - (2.1.6) as follows. Assuming $\beta = 1$, $\kappa_t|v| \ll 1$ and $\kappa_t\kappa_s \ll 1$, temporary impact of the form (2.1.6) is approximately

$$f(v) \approx 1 + \kappa_s \operatorname{sgn}(v) + \kappa_t v$$

by Taylor's expansion. By (2.1.5), the price impact (in dollar terms) is

$$S_{exec}(v,t) - S(t) = f(v)S(t) - S(t) = S(t)[\kappa_s \operatorname{sgn}(v) + \kappa_t v] \approx S(0)[\kappa_s \operatorname{sgn}(v) + \kappa_t v] \tag{6.5.4}$$

for $S(t) \approx S(0)$. Note that (6.5.4) now agrees with (6.5.2) - (6.5.3).

The permanent price impact function in the ABM model takes the same form (2.1.7) as that in the GBM model, i.e.

$$g(v) \;\; = \;\; \kappa_p v. \tag{6.5.5}$$

We also assume $r = 0$ in the ABM model, since trades are usually executed within one day.

6.5.2 HJB PDE Formulation

We define the value functions V and U for the ABM model as for the GBM model. A derivation similar to that in the GBM case gives the HJB PDE

$$V_\tau = \eta S(0) V_s + \frac{\sigma^2 S(0)^2}{2} V_{ss} - \phi\sigma^2\alpha^2 S(0)^2 + \max_{v \in [v_{min}, 0]} \Big[v(V_\alpha - s) - v h(v) S(0) + g(v) S(0) V_s \Big], \tag{6.5.6}$$

where $h(v)$ and $g(v)$ were defined in (6.5.3) and (6.5.5).

Note that the explicit s dependence in (6.5.6) appears only in the term $v(V_\alpha - s)$. Let

$$\tilde{V}(s,\alpha,\tau) = V(s,\alpha,\tau) - \alpha s. \tag{6.5.7}$$

Substituting (6.5.7) into (6.5.6) gives

$$\tilde{V}_\tau = \eta S(0)(\tilde{V}_s + \alpha) + \frac{\sigma^2 S(0)^2}{2}\tilde{V}_{ss} - \phi\sigma^2\alpha^2 S(0)^2 + \max_{v\in[v_{min},0]}\Big[v\tilde{V}_\alpha - vh(v)S(0) + g(v)S(0)\big(\tilde{V}_s + \alpha\big)\Big]. \tag{6.5.8}$$

From (6.5.3) and (6.1.3), the initial condition for V is

$$V(s,\alpha,\tau=0) \;=\; \lim_{v\to-\infty}\alpha(s + S(0)h(v)). \tag{6.5.9}$$

Therefore, from (6.5.7) we obtain

$$\tilde{V}(s,\alpha,\tau=0) \;=\; \lim_{v\to-\infty}\alpha(s + S(0)h(v)) - \alpha s = \lim_{v\to-\infty}\alpha S(0)h(v). \tag{6.5.10}$$

Now, note that (6.5.8) has no explicit s dependence, and that the initial condition (6.5.10) has no s dependence. It therefore follows that (6.5.8) with initial condition (6.5.10) can be satisfied by a function

$$\bar{V}(\alpha,\tau) = \tilde{V}(s,\alpha,\tau), \tag{6.5.11}$$

where $\bar{V}(\alpha,\tau)$ satisfies the PDE

$$\bar{V}_\tau = \eta S(0)\alpha - \phi\sigma^2\alpha^2 S(0)^2 + \max_{v\in[v_{min},0]}\Big[v\bar{V}_\alpha - vh(v)S(0) + g(v)S(0)\alpha\Big], \tag{6.5.12}$$

with initial condition

$$\bar{V}(\alpha,\tau=0) \;=\; \lim_{v\to-\infty}\alpha S(0)h(v). \tag{6.5.13}$$

6.5.3 Analytic Results

Proposition 6.4. *Assuming Arithmetic Brownian Motion (6.5.1), asset-price-independent temporary price impact (6.5.2), zero interest rate, and initial condition (6.5.9), an optimal control for equation (6.5.6) is static, even when optimization is over the class of dynamic strategies.*

Proof. An optimal control for equation (6.5.6) is also an optimal control for equation (6.5.12), which is independent of s, i.e. $v^*(\cdot) : (\alpha,\tau) \mapsto v^*$, hence an optimal control for problem (6.5.6) is also independent of s, i.e. static. □

In general, the PDE (6.5.12) has no known analytical solution. This section gives a special case analytical solution under the additional assumptions of zero drift, unconstrained control and linear price impact functions. More formally, we make the following

set of common assumptions[5] which gives the result in Proposition 6.6.

Assumption 6.5.

$$\begin{aligned} dS(t) &= g(v)S(0)dt + \sigma S(0)d\mathbb{W}(t), \\ r &= 0, \\ h(v) &= \kappa_s \operatorname{sgn}(v) + \kappa_t v, \\ g(v) &= \kappa_p v, \\ v &\in (-\infty, \infty) \end{aligned}$$

Proposition 6.6. *Under Assumption 6.5, an optimal control for (6.5.12) is identical with the (continuous equivalent of the) static strategy in [9, 5], i.e.*

$$v^*(\alpha, \tau) = -\frac{\alpha K \cosh(K\tau)}{\sinh(K\tau)} \tag{6.5.14}$$

where $K = \sqrt{\phi\, \sigma^2 S(0)/\kappa_t}$.

In addition, the value function $\bar{V}(\alpha, \tau)$ *is*

$$\bar{V} = E + \phi F \ , \tag{6.5.15}$$

where

$$\begin{aligned} E &= \frac{S(0)\,\alpha\ (2\,\kappa_s f_1(\tau)^2 + \alpha\,\kappa_p f_1(\tau)^2 + \alpha\,\phi\,\sigma^2 S(0)\,\tau + \alpha\,\kappa_t K f_1(\tau) f_2(\tau))}{-2 f_1(\tau)^2}, \\ F &= \frac{\sigma^2 S(0)^2 \alpha^2 \left(-f_3(\tau)^2 f_1(\tau) - f_1(\tau) + 2\,\tau\, K f_3(\tau)\right)}{4K f_1(\tau)^2 f_3(\tau)} \ , \\ f_1(\tau) &= \sinh(K\tau) \ , \\ f_2(\tau) &= \cosh(K\tau) \ , \\ f_3(\tau) &= \exp(K\tau) \ . \end{aligned} \tag{6.5.16}$$

Note that if $\kappa_s = 0$*, then both* E *and* F*, and hence* $\bar{V}$ *are proportional to* α^2.

Proof. Under Assumption 6.5, the PDE (6.5.12) has the form

$$\bar{V}_\tau = -\phi\sigma^2\alpha^2 S(0)^2 + \max_{v\in(-\infty,\infty)} \left[v\bar{V}_\alpha - \left(\kappa_s v \operatorname{sgn}(v) + \kappa_t v^2\right) S(0) + \kappa_p v S(0) \alpha \right]. \tag{6.5.17}$$

Using an initial condition that is consistent with (6.5.13) for $\bar{V}(\alpha, \tau)$ gives

$$\bar{V}(\alpha, 0) = \begin{cases} 0 & \alpha = 0 \\ -\infty & \text{otherwise} \end{cases} \tag{6.5.18}$$

[5]Note that the assumption of unconstrained control may not be desirable as it allows buying shares during stock liquidation.

by using the definitions (6.5.7) and (6.5.11). It can be verified by straightforward calculations that the value function (6.5.15) and the control (6.5.14) solves the HJB PDE (6.5.17) with initial condition (6.5.18). □

In general, we would like to restrict v from taking all real values. For example, in the case of selling, a natural constraint is $v \in [v_{min}, 0]$, as in this thesis. This constraint may take effect if $\eta \neq 0$, in which case the analytical solution will no longer be valid.

6.6 Computing Results of Practical Interest

In this section we briefly discuss using the PDE method and the Hybrid (PDE-Monte Carlo) method to compute results of practical interest about Mean Quadratic Variation-optimal strategies. The PDE method and the Hybrid method are introduced in Section 3.6 in the context of Mean Variance optimization.

The PDE method can be used to obtain the mean quadratic variation efficient frontier by straightforward evaluations of value functions. The PDE method requires solving the linear PDE (6.2.4) in addition to solving the nonlinear HJB PDE (6.2.2). For each value of risk aversion level ϕ, the corresponding point on the frontier is given by the formula

$$\begin{aligned} E^{s,\alpha,t=0}_{v^*(\cdot)}[\tilde{B}(T)] &= U(s,\alpha,\tau=T;\phi) \\ E^{s,\alpha,t=0}_{v^*(\cdot)}\Big[\int_0^T \big(A(t')dS(t')\big)^2\Big] &= \frac{U(s,\alpha,\tau=T;\phi) - V(s,\alpha,\tau=T;\phi)}{\phi}, \end{aligned}$$

where the optimal control $v^*(\cdot)$ found by solving V is used in solving U.

In the Hybrid method, the optimal control $v^*(\cdot)$ is first obtained by solving the HJB PDE (6.2.2). Monte Carlo simulations are then carried out to estimate quantities of interest, using the optimal control $v^*(\cdot)$ (see Appendix E for details). An advantage of the Hybrid method is that we can estimate interest statistics that are difficult to obtain directly from the value functions.

To plot expected value against risk in the same unit, we define $QVRisk$ as the square root of (expected) quadratic variation, i.e.

$$QVRisk = \sqrt{E^{s,\alpha,t=0}_{v^*(\cdot)}\Big[\int_0^T \big(A(t')dS(t')\big)^2\Big]},$$

which has the same unit (dollar) as $E^{s,\alpha,t=0}_{v^*(\cdot)}[\tilde{B}(T)]$.

6.7 Numerical Results

In this section we report numerical results for the Mean Quadratic Variation optimal trade execution problem under the basic Geometric Brownian Motion model of Section 2.1.1.

Refinement Level	Timesteps	s nodes	α nodes	v nodes
0	800	67	41	30
1	1600	133	81	59
2	3200	265	161	107
3	6400	529	321	213

TABLE 6.2: *Computational grid for Mean Quadratic Variation optimization. The same grid is used for solving the PDEs (6.2.2) and (6.2.4), and for the Hybrid method.*

Refinement Level	V	U (Mean)	Quadratic Variation	$QVRisk$
0	98.4268	99.2824	0.8556	0.9250
1	98.4403	99.2876	0.8473	0.9205
2	98.4472	99.2902	0.8431	0.9182
3	98.4506	99.2916	0.8410	0.9170

TABLE 6.3: *Convergence table for solving the PDEs (6.2.2) and (6.2.4) for the value functions V and U, respectively. The one-dimensional optimization method is used in local optimization. Quadratic variation and $QVRisk$ are calculated from the value functions as discussed in Section 6.6. Results are reported for Case 1 at the risk aversion level $\phi = 1$. First order convergence rate is observed for this case (and other cases not reported), as expected.*

The computational cases we consider have the same parameters as those listed in Table 5.2. In this section we will present results for only Case 1 in Table 5.2. Results for other cases will be reported in Chapter 7 when we compare MV-optimal and MQV-optimal strategies.

Table 6.2 shows the computational grid for solving the PDEs (6.2.2) and (6.2.4), and for the Hybrid method (for interpolating optimal selling velocities v^* during Monte Carlo simulations).

We note that the v nodes are used only in the linear search method; they are not needed in the one-dimensional optimization method (see the end of Section 6.4). We will use the one-dimensional optimization method since it is faster. It will be shown that the two methods have similar accuracy.

Table 6.3 reports convergence information in solving the PDEs (6.2.2) and (6.2.4) for Case 1 in Table 5.2. We note that first order convergence rate is observed.

Table 6.4 shows that s_{max} is sufficiently large so that the boundary conditions at $s = s_{max}$ introduce negligible errors.

The mean quadratic variation efficient frontier can be computed using either the PDE method or the Hybrid method discussed in Section 6.6. Figure 6.1 plots the efficient frontiers computed using the two methods for Case 1 in Table 5.2. We make the following comments on Figure 6.1 from a computational point of view.

Refinement Level	s_{max}	V	U (Mean)	Quadratic Variation	$QV Risk$
1	5,000	98.4403	99.2876	0.8473	0.9205
1	10,000	98.4403	99.2876	0.8473	0.9205

TABLE 6.4: *Convergence test to confirm s_{max} is sufficient large for the Mean Quadratic Variation problem. Result for $s_{max} = 5,000$ is the same as that reported in Table 6.3. Result for $s_{max} = 10,000$ shows that increasing s_{max} makes negligible difference.*

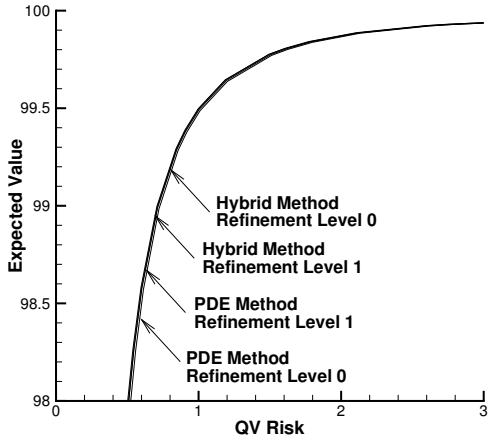

FIGURE 6.1: *Efficient frontier of Mean Quadratic Variation optimal strategies for Case 1. The frontiers labeled with PDE are obtained from the PDE value functions. The frontiers labeled with Hybrid are obtained from Monte Carlo simulations which use the optimal controls determined by solving the HJB PDE (6.2.2).*

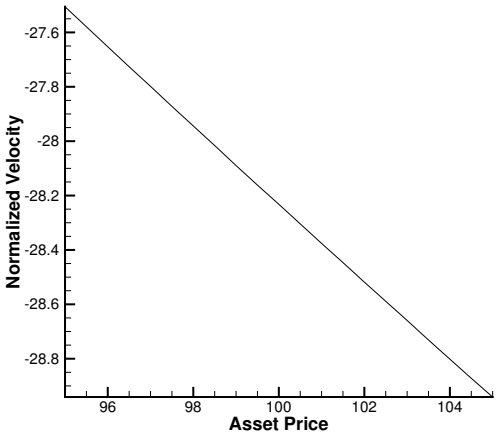

FIGURE 6.2: *An optimal mean quadratic variation strategy for Case 1 in Table 5.2, plotted at* $t = 0$ *and* $s = s_{init} = 100$*. This strategy has mean* 99.29*, QVRisk 0.93, and corresponds to the risk aversion level* $\phi = 1$*. A normalized velocity of* -1.0 *corresponds to the constant liquidation rate* $-\alpha_{init}/T$*. Refinement level 1 is used to compute the results.*

- Numerical convergence has essentially been reached at Refinement Level 1. There is little change between the frontiers at Level 0 and those at Level 1, especially for the Hybrid method.
- The comments we made in Section 5.2.4 on Figure 5.1 for the Mean Variance problem are all applicable here.

Figure 6.2 plots the MQV-optimal strategies in Case 1 for the risk aversion level $\phi = 1$. We note that the strategy sells slightly faster as the stock price increases (becomes more favorable for selling). MQV-optimal strategies for the other cases (and other risk aversion levels) have similar properties.

Figure 6.3 shows that the one-dimensional method has similar accuracy as the linear search method.

6.8 Summary

The main results in this chapter are the followings.

- The classic strategies in [9] are MQV-optimal, in contrary to the common belief that they are MV-optimal.
- MQV-optimal strategies sell slightly faster as the stock price increases.

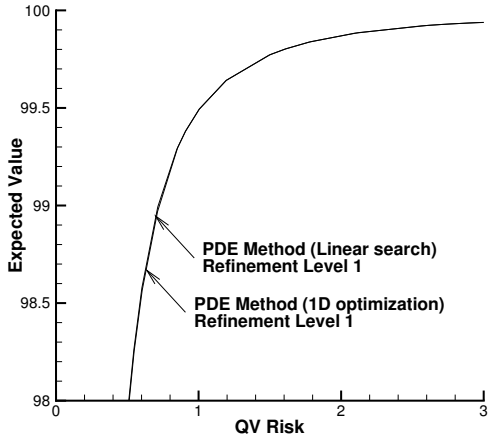

FIGURE 6.3: *The efficient frontier computed using the one-dimensional method is essentially the same as that computed using the linear search method.*

Chapter 7

Comparing Mean Variance and Mean Quadratic Variation

In this chapter we compare Mean Variance (MV) optimal strategies with Mean Quadratic Variation (MQV) optimal strategies. We demonstrate that MV-optimal strategies are quite different from MQV-optimal strategies in many aspects. These differences are in stark contrast to the common belief that MQV-optimal strategies are similar to, or even the same as, MV-optimal strategies. This is important in the practice of trade execution since performance is measured in terms of MV-optimality (see Section 2.2), whereas the classic strategy in [9], which is the industry standard [44, 42, 40], is actually MQV-optimal (see Section 6.5).

7.1 MQV as an Approximation to MV

So far we have considered Mean Variance optimization and Mean Quadratic Variation optimization as two separate approaches and on equal footing. In this section we will see that the two approaches are closely related, and that it is natural to consider the MQV approach as an approximation to the MV approach.

The key connection between MV and MQV is that variance is the same as expected quadratic variation for static (asset price independent) strategies, i.e.

$$Var^{x,t=0}_{v(\cdot)\text{ static}}\Big[B(T)\Big] = E^{x,t=0}_{v(\cdot)\text{ static}}\Big[\int_0^T (A(t')dS(t'))^2\Big], \tag{7.1.1}$$

under some additional mild assumptions; see Appendix D for details.

From a practical point of view, there is no reason to restrict admissible strategies to static strategies. For dynamic strategies, variance is (of course) not the same as expected quadratic variation. However, in view of the equality (7.1.1) in the above special case, it is natural to consider using expected quadratic variation as an approximation to variance,

i.e.

$$Var_{v(\cdot)}^{x,t=0}\Big[B(T)\Big] \approx E_{v(\cdot)}^{x,t=0}\Big[\int_0^T \big(A(t')dS(t')\big)^2\Big]. \tag{7.1.2}$$

The approximation (7.1.2) is mathematically convenient, since we have seen that the MQV problem is easier to solve than the MV problem. In particular, the dynamic programming principle can be directly applied to the MQV problem but not to the MV problem (see Section 3.1). Nevertheless, the approximation (7.1.2) can be quite poor for practical parametric cases; see the numerical results in this chapter.

7.2 Optimality of the Classic Strategy

This section explains in what sense the classic strategy (6.5.14) in [9] is optimal or not optimal. Before we explain the subtleties, let us first summarize the key points. For ease of exposition, we denote by **S** the classic strategy (6.5.14) in [9].

1. MV-optimal strategies are dynamic (s-dependent) under (a) the GBM model; and (b) the ABM model.
2. **S** is static (s-independent).
3. By the above, **S** is not MV-optimal. We remark that **S** is used as the industry standard, however, even though performance is measured in terms of MV-optimality.
4. No other *static* strategy has better MV-performance than **S** (in the sense of Definition 2.3).
5. **S** is MQV-optimal under the ABM model. No other strategy, including dynamic strategies, has better MQV-performance better than **S** (in the sense of Definition 6.2).
6. MQV-optimal strategies are dynamic under the GBM model. Thus **S** is not MQV-optimal under the GBM model.

In fact we have shown points 1(a), 2, 3, 5 and 6 in previous chapters. Point 1(a) is illustrated in the numerical results in Chapter 5. Point 2 is clear from the formula (6.5.14). Point 5 is proved in Section 6.5. Point 6 is illustrated in the numerical results in Chapter 6. Point 1(b) is the result in [12, 50].

Point 4 is in fact the main result in [9], which optimizes MV-performance over the class of static strategies. Interestingly, through the equality (7.1.1), the paper [9] is actually adopting the MQV objective function! However, we emphasize that the paper [9] does not show that the strategy **S** is MQV-optimal over the class of dynamic strategies; we prove the MQV-optimality of **S** as a consequence of the result in Section 6.5.

Remark 7.1 (Static as a restriction or as a property)**.** *It should be clear at this point that it is important to distinguish between whether the use of the concepts static or dynamic refer to the class of admissible strategies, or to a property of an optimal strategy. In particular, even if optimization is over the class of dynamic strategies, an optimal control may turn out to be static. As explained above, the classic strategy in [9] is a case in point. Another example can be found in [60].*

7.3 Numerical Results

In this section we compare MV-optimal strategies and MQV-optimal strategies.

We consider all five computational cases listed in Table 5.2. In computing MV-optimal strategies and MQV-optimal strategies, we use the computational grids specified in Table 5.3 and Table 6.2, respectively.

We will compare MV-optimal strategies and MQV-optimal strategies using 800 and 1600 timesteps[1]. We have previously shown that the numerical solutions have essentially converged at 1600 timesteps for both MV and MQV.

We will compare the two strategies using the Hybrid (PDE-Monte Carlo) method. Monte Carlo simulations allow us to estimate the $QVRisk$ of MV-optimal strategies and standard deviation of MQV-optimal strategies; these estimates cannot be obtained directly from the value functions. Note also that the frontiers computed by the Hybrid method converge faster to the limit solution than those computed by the PDE method, as shown earlier in Chapter 5 and Chapter 6.

7.3.1 Comparing the Two Risk Measures

The left subplots in Figures 7.1 to 7.5 compare MV-optimal and MQV-optimal strategies using standard deviation as the risk measure. The right subplots in Figures 7.1 to 7.5 compare MV-optimal and MQV-optimal strategies using $QVRisk$ as the risk measure.

Several conclusions can be drawn from the comparisons.

- As one would expect, in using standard deviation as the risk measure, MV-optimal strategies dominate MQV-optimal strategies.
- Conversely, in using $QVRisk$ as the risk measure, MQV-optimal strategies dominate MV-optimal strategies.
- It appears that the MV-optimal strategies perform reasonably well using either risk measure. The difference between the MV-optimal strategies and MQV-optimal strategies is most pronounced at lower risk levels.

[1]These correspond to Refinement Level 2 and 3 in Table 5.3 for MV, and to Refinement Level 0 and 1 in Table 6.2.

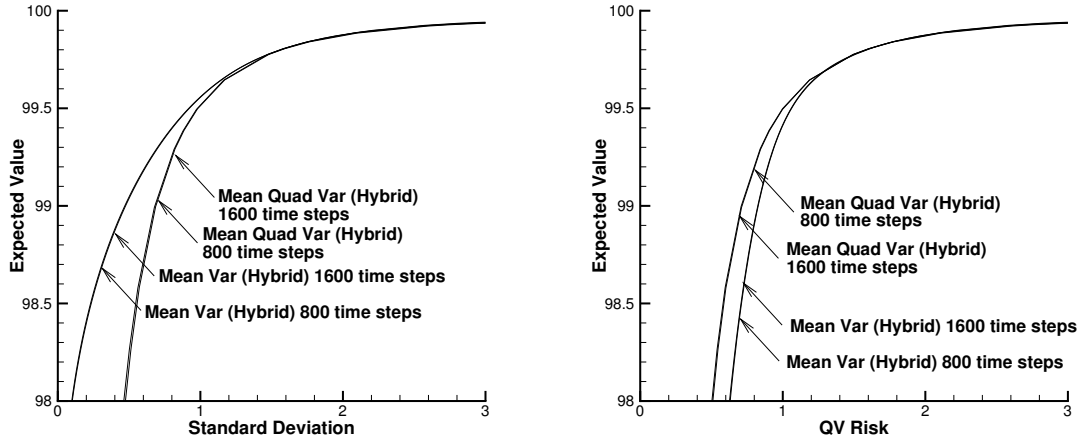

FIGURE 7.1: *Comparison between MV-optimal strategies and MQV-optimal strategies for the case σ=1.0, $\kappa_t = 2 \times 10^{-6}$.*

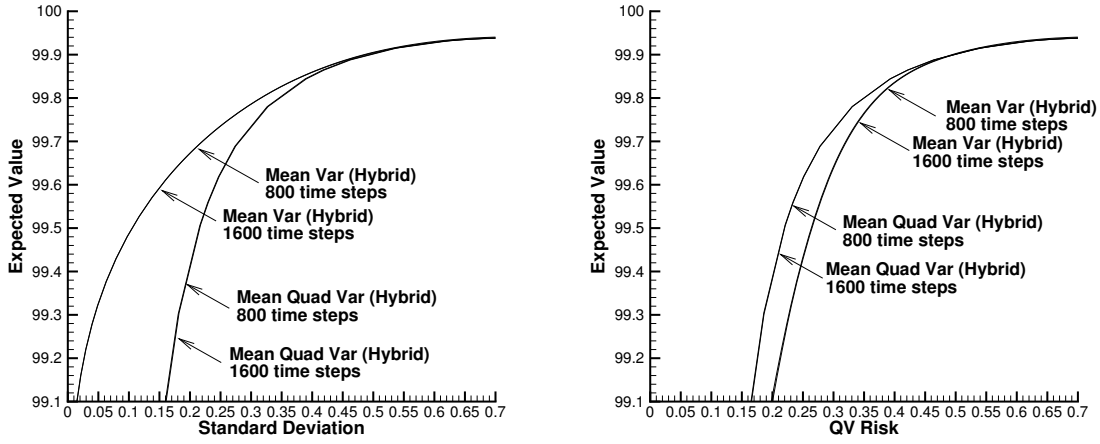

FIGURE 7.2: *Comparison between MV-optimal strategies and MQV-optimal strategies for the case σ=0.2, $\kappa_t = 2.4 \times 10^{-6}$.*

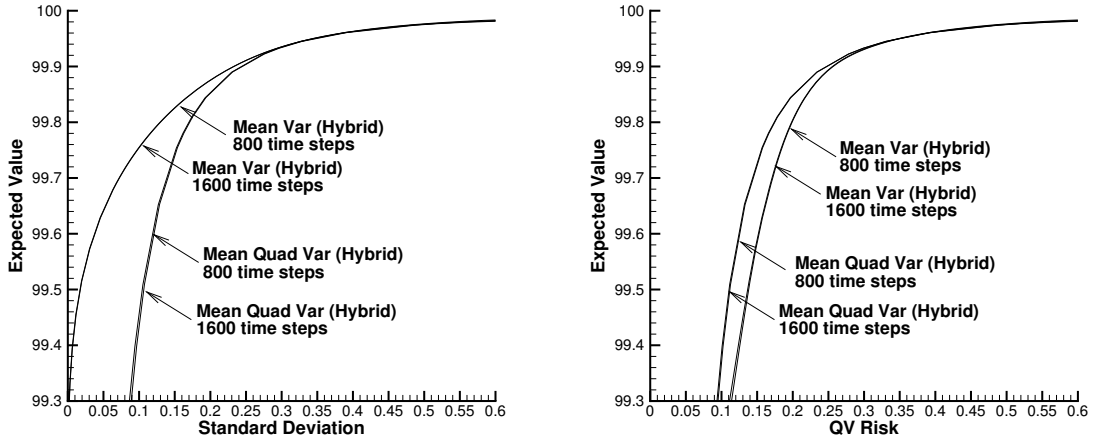

FIGURE 7.3: *Comparison between MV-optimal strategies and MQV-optimal strategies for the case σ=0.2, $\kappa_t = 6 \times 10^{-7}$.*

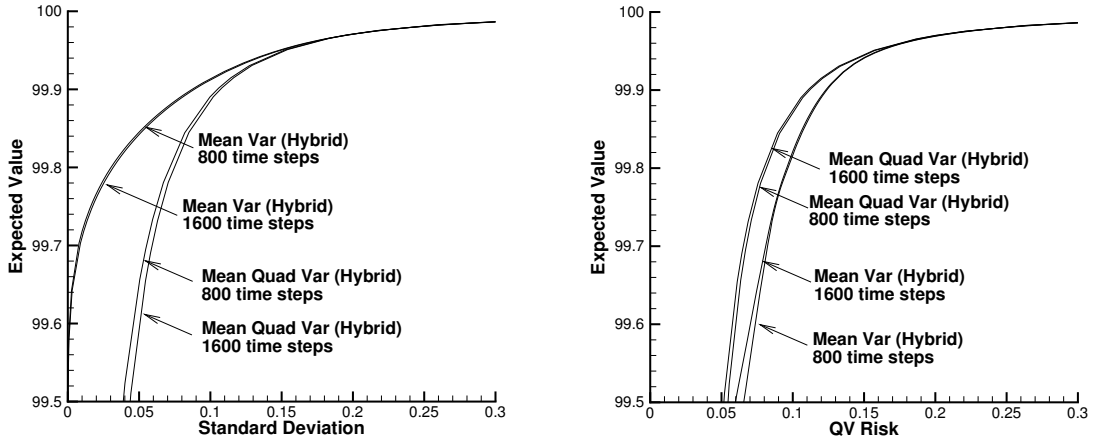

FIGURE 7.4: *Comparison between MV-optimal strategies and MQV-optimal strategies for the case σ=0.2, $\kappa_t = 1.2 \times 10^{-7}$.*

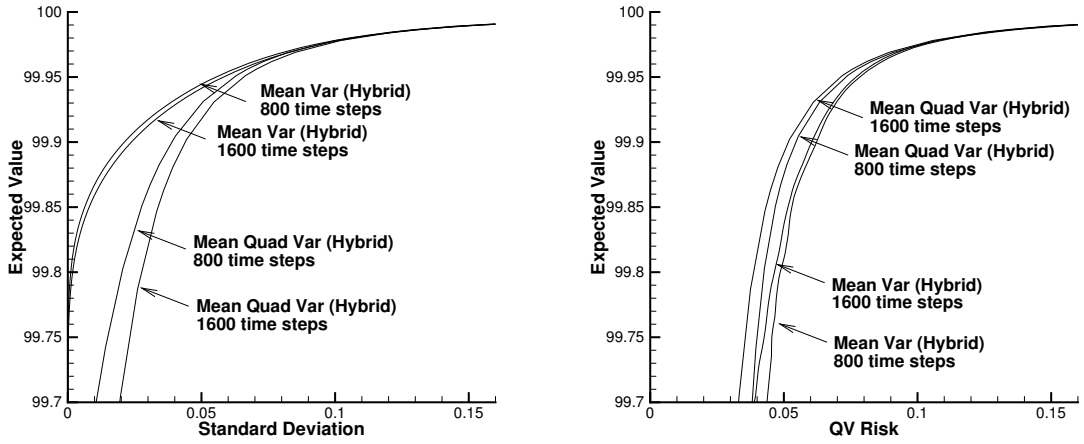

FIGURE 7.5: *Comparison between MV-optimal strategies and MQV-optimal strategies for the case σ=0.2, $\kappa_t = 2.4 \times 10^{-8}$.*

Market practitioners may consider expected implementation shortfall (the relative difference between expected value and initial stock price) of 10 basis points to be significant. To achieve small implementation shortfall, liquidation must be done slowly to reduce trading impact, at the expense of increasing timing risk. Striking a good balance is important here, as it might not be wise to aim at an expected shortfall of 10 bps if the risk (as measured by either standard deviation or $QVRisk$) is several times larger. Our plots show that risk can be several times of a 10 bps expected shortfall in the parametric cases (a) $\sigma = 1.0$, 16.7% daily volume; (b) $\sigma = 0.2$, 20% daily volume; and (c) $\sigma = 0.2$, 5% daily volume.

The analysis above suggests that one way to choose a risk aversion level on an efficient frontier is to choose a ratio between the implementation shortfall and risk. Alternatively, a common practice among market practitioners is to pick the "corner of the frontier". Our plots show that picking the corner can result in expected implementation shortfall much larger than 10 bps.

7.3.2 Comparison of Strategies for Similar Expected Values

In this section we compare MV-optimal strategies with MQV-optimal strategies that give similar expected values. In particular, we focus on the parametric case $\sigma = 1$, $\kappa_t = 2\times10^{-6}$ since the differences are more apparent when volatility and pricing impacts are larger.

Figures 7.6 to 7.9 correspond to comparisons across four horizontal lines in Figure 7.1, with four different expected values chosen to represent the more interesting part of the frontiers. For example, in Figure 7.6 both strategies give an expected value of around 99.29. For the MV-optimal strategy, this corresponds to $\gamma = 199.82$; for the MQV-optimal strategy, this corresponds to $\phi = 1$.

7.3.2.1 Common Observations for Each Level of Expected Value

In each of Figures 7.6 to 7.9, the subplots labeled (a) and (b) compare the optimal trading velocities at $t = 0$, where we normalized the trading velocities so that a normalized velocity of -1.0 corresponds to the constant liquidation rate $-\alpha_{init}/T$. It is clear that while both strategies sell faster as price becomes more favorable[2], the sensitivity in the MV-optimal strategy is much more non-linear. More specifically, around the initial asset price $s_{init} = 100$, the optimal control for the MV-optimal is a curve with rapidly changing slope whereas that for the MQV-optimal strategy is more or less a straight line.

In each of Figures 7.6 to 7.9, the subplots labeled (c) and (d) compare the mean ($E[A(t)]$) and standard deviation ($Std[A(t)]$), respectively, of the liquidation profiles $A(t)$ of the MV-optimal strategies and the MQV-optimal strategies over the trading horizon. It is interesting to note that while the mean profiles are very similar, the standard deviation profile of the MV-optimal strategy is much larger than that of the MQV-optimal strategy. This reflects the fact that the MV-optimal strategy is much more sensitive to change in asset price during the liquidation, which is also suggested by the strategy subplots. We also note that the mean profiles are convex, i.e. the mean liquidation rate is always decreasing over time, as expected.

7.3.2.2 Differences among Different Levels of Expected Values

As we move from Figure 7.6 to 7.9, the expected value is increasing, and so as the standard deviation and QV Risk. By comparing subplots (a) and (b), we see that the optimal selling rates become slower as expected value increases. Recall that the mean profiles are convex, so that the mean liquidation rate is always decreasing over time. By comparing subplots (c), we observe that the convexities of the mean liquidation profiles diminish as expected value increases, and the mean liquidation profiles approach a straight line. By comparing subplots (d), we observe that the mean-variance strategy becomes less variable as expected value increases.

7.4 Summary

The main result in this chapter is the following.

- MQV-optimal strategies are poor approximations to MV-optimal strategies in many aspects. In particular, for the same variance, an MQV-optimal strategy can have significantly smaller expected revenue compared to an MV-optimal strategy.

[2]For the buying case, mean-variance optimal strategies would buy faster as price becomes more favorable (drops). For both selling and buying, mean-variance optimal strategies trade faster as price becomes more favorable; this property is called aggressive in the money [45]. Mean variance-optimal strategies are aggressive in the money because this introduces an anti-correlation between trading revenue and trading impacts [51]. Mean-quadratic-variation optimal strategies are different: for the buying case, mean-quadratic-variation optimal strategies would buy faster as price increases (unfavorable), to reduce quadratic variation of the remaining position; we have verified this numerically.

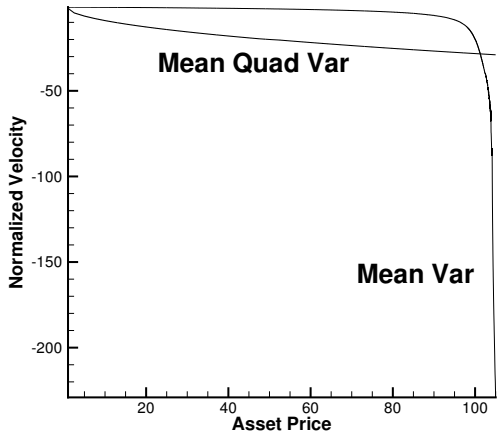

(a) strategy - complete view

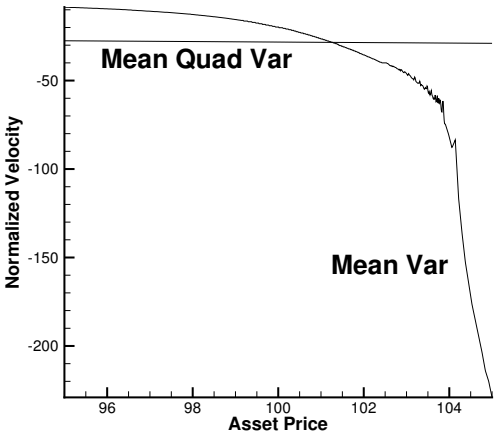

(b) strategy - zoom in

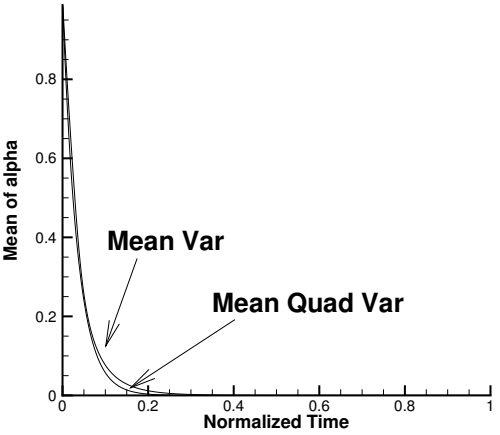

(c) mean of liquidation profile

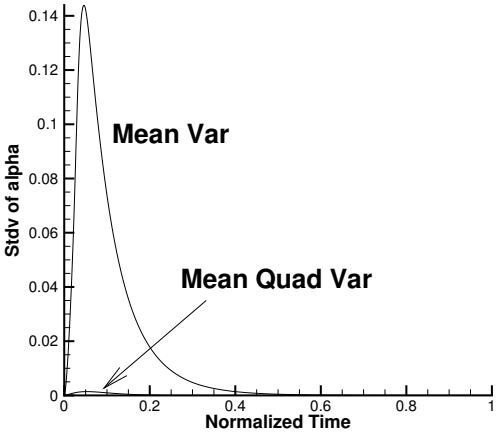

(d) standard deviation of liquidation profile

FIGURE 7.6: *Comparison between MV-optimal strategy and MQV-optimal strategy for the case σ=1.0, $\kappa_t = 2 \times 10^{-6}$. The MV-optimal strategy plotted has mean 99.29, standard deviation 0.68, QVRisk 0.93, and corresponds to γ=199.82. The MQV-optimal strategy plotted has mean 99.29, standard deviation 0.82, QVRisk 0.84, and corresponds to ϕ=1. 1600 time steps are used to compute the results.*

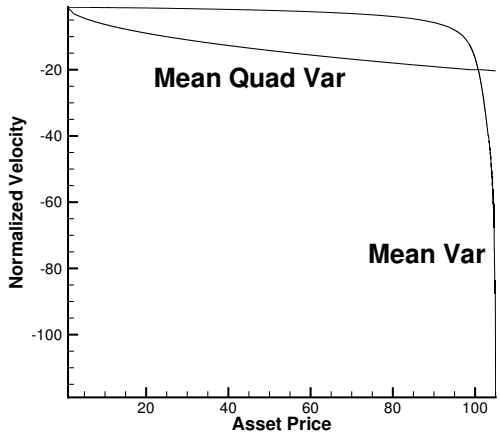

(a) strategy - complete view

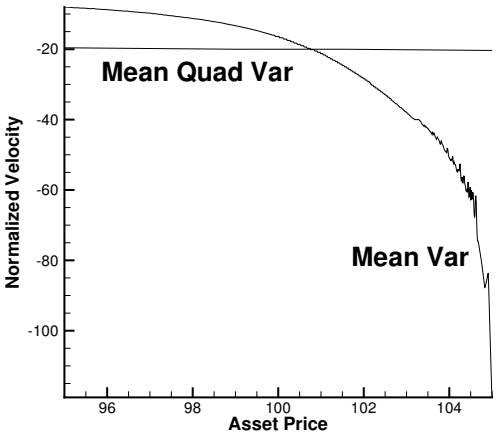

(b) strategy - zoom in

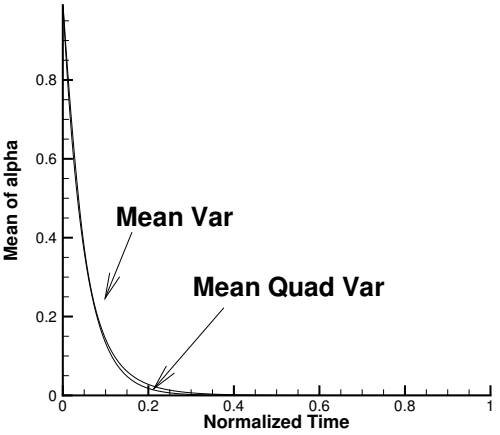

(c) mean of liquidation profile

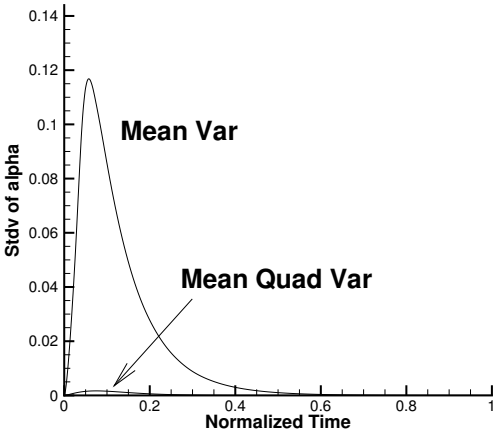

(d) standard deviation of liquidation profile

FIGURE 7.7: *Comparison between MV-optimal strategy and MQV-optimal strategy for the case σ=1.0, $\kappa_t = 2 \times 10^{-6}$. The MV-optimal strategy plotted has mean 99.50, standard deviation 0.90, QVRisk 1.05, and corresponds to γ=201.30. The MQV-optimal strategy plotted has mean 99.50, standard deviation 0.98, QVRisk 1.00, and corresponds to ϕ=0.5. 1600 time steps are used to compute the results.*

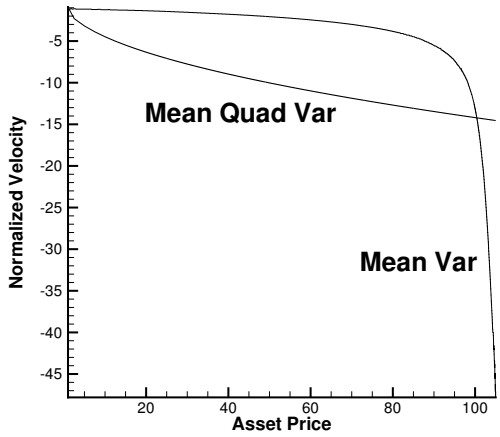

(a) strategy - complete view

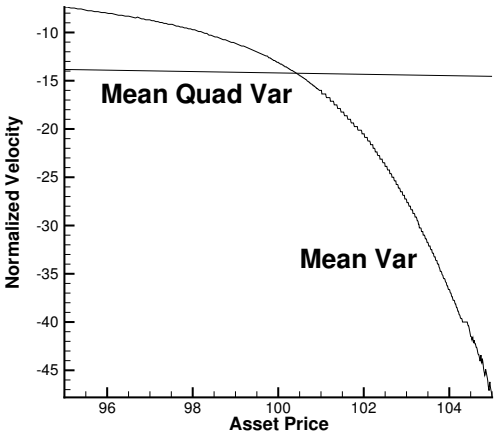

(b) strategy - zoom in

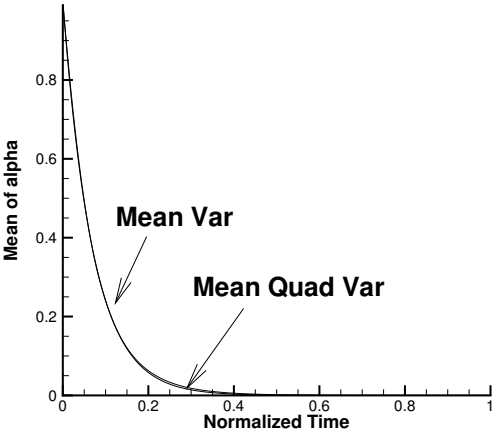

(c) mean of liquidation profile

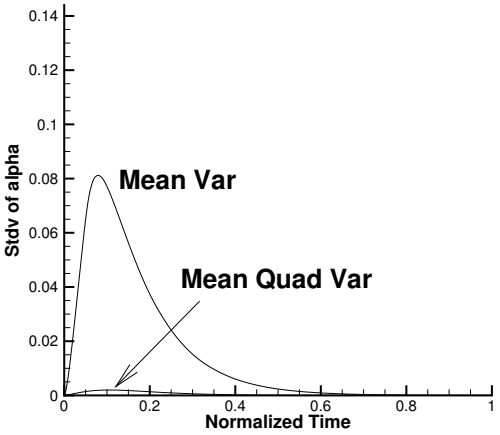

(d) standard deviation of liquidation profile

FIGURE 7.8: *Comparison between MV-optimal strategy and MQV-optimal strategy for the case σ=1.0, $\kappa_t = 2 \times 10^{-6}$. The MV-optimal strategy plotted has mean 99.65, standard deviation 1.13, QVRisk 1.21, and corresponds to γ=203.50. The MQV-optimal strategy plotted has mean 99.65, standard deviation 1.17, QVRisk 1.19, and corresponds to ϕ=0.25. 1600 time steps are used to compute the results.*

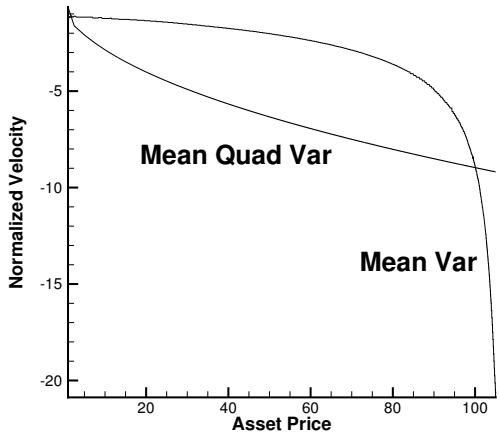

(a) strategy - complete view

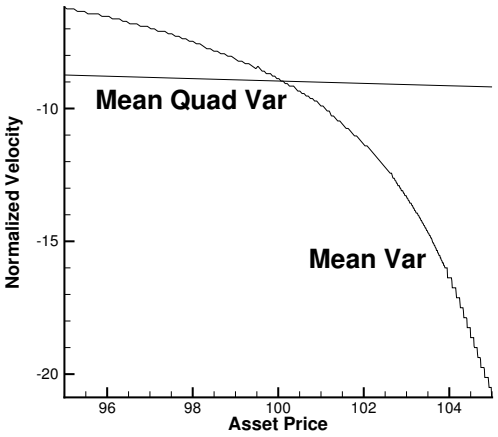

(b) strategy - zoom in

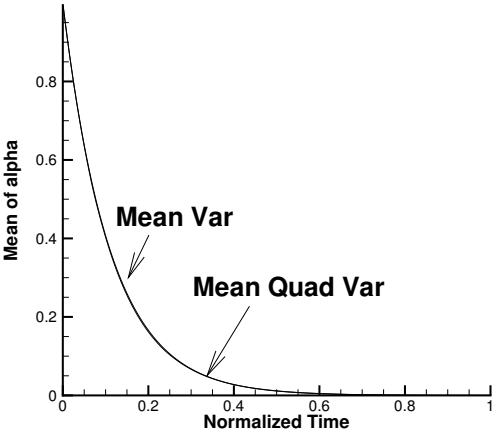

(c) mean of liquidation profile

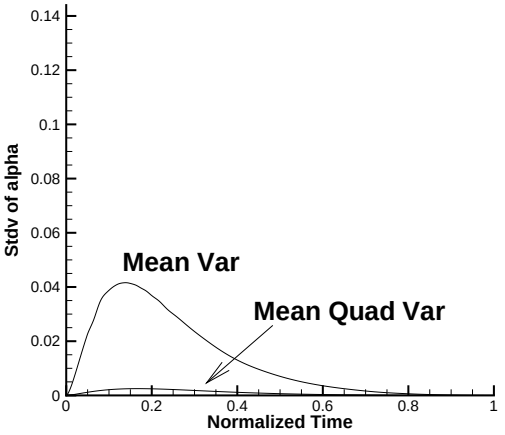

(d) standard deviation of liquidation profile

FIGURE 7.9: *Comparison between MV-optimal strategy and MQV-optimal strategy for the case σ=1.0, $\kappa_t = 2 \times 10^{-6}$. The MV-optimal strategy plotted has mean 99.78, standard deviation 1.46, QVRisk 1.49, and corresponds to γ=209.42. The MQV-optimal strategy plotted has mean 99.78, standard deviation 1.48, QVRisk 1.49, and corresponds to ϕ=0.1. 1600 time steps are used to compute the results.*

Chapter 8

Conclusions and Future Work

From the computational point of view, we developed efficient methods to solve for optimal trade execution strategies based on discretization of nonlinear HJB PDEs. We took particular care in rigorously proving that the numerically computed efficient frontier is indeed the complete Pareto-efficient frontier by (i) extending the result in [47] on the embedding technique to non-convex mean variance optimization problem, and in particular proving a simple post-processing algorithm guarantees Pareto-optimality of the computed frontier; and (ii) extending the result in [16] to prove convergence of numerical solutions to viscosity solution of a system of nonlinear HJB PDEs.

From the optimal trade execution point of view, we illustrated in detail many interesting properties of Mean Variance-optimal strategies (which align with performance measurement) and their unexpected differences from Mean Quadratic Variation-optimal strategies. These differences should interest practitioners since MQV-optimal strategies are used widely in practice to approximate MV-optimal strategies, but with little understanding of such differences.

8.1 Future Work

We suggest the following directions for future work.

- Stochastic trading impact was restricted to switching between two temporary price impact factors in the thesis. It would be interesting to adopt a more realistic model of stochastic trading impact based on high frequency analysis of trading data.
- The effect of temporary trading impact is assumed to be instantaneous in the current work. Empirical analysis of limit order books suggest that trading impact is transient, i.e. the impact decays over time.
- It would be interesting to consider the simultaneous liquidation of multiple assets that have correlated price movements.

Appendix A

Deriving the System of HJB PDEs for the Mean Variance Problem

In this section, we derive the system of HJB PDEs (3.2.7) from a dynamic programming principle.

By a slight abuse of notation, let us denote by V

$$V = V(s, \mathscr{b}, \alpha, l, t) = \inf_{v(\cdot)} E_{v(\cdot)}^{s,\mathscr{b},\alpha,l,t}\Big[\mathcal{B}(T)^2\Big]. \tag{A.0.1}$$

Note also that the original definition (3.2.3) uses the backward time τ as the last variable.

For notational simplicity, we define $X(t) = (S(t), \mathcal{B}(t), A(t), L(t))$ and $x = (s, \mathscr{b}, \alpha, l)$. We also use $X(t) = x$ to denote $(S(t) = s, \mathcal{B}(t) = \mathscr{b}, A(t) = \alpha, L(t) = l)$. We also write $x + \triangle x = X(t + \triangle t)$. Using these notations, we can rewrite (A.0.1) as

$$V = \inf_{v(\cdot)} E_{v(\cdot)}^{x,t}\Big[\mathcal{B}(T)^2\Big],$$

By using the law of iterated expectation, i.e.

$$E_{v(\cdot)}^{x,t}\Big[E_{v(\cdot)}^{x+\triangle x,t+\triangle t}\Big[\cdot\Big]\Big] = E_{v(\cdot)}^{x,t}\Big[\cdot\Big],$$

we have

$$\begin{aligned} V(s, \mathscr{b}, \alpha, l, t) &= \inf_{v(\cdot)} E_{v(\cdot)}^{x,t}\Big[\mathcal{B}(T)^2\Big] \\ &= \inf_{v(\cdot)} E_{v(\cdot)}^{x,t}\Big[E_{v(\cdot)}^{x+\triangle x,t+\triangle t}\Big[\mathcal{B}(T)^2\Big]\Big] \\ &= \inf_{v(\cdot)} E_{v(\cdot)}^{x,t}\Big[V(s + \triangle s, \mathscr{b} + \triangle \mathscr{b}, \alpha + \triangle\alpha, L(t + \triangle t), t + \triangle t)\Big], \end{aligned} \tag{A.0.2}$$

where the last equality follows by the optimality of the control.

Let $\triangle V = V(s+\triangle s, \text{ɓ}+\triangle \text{ɓ}, \alpha+\triangle\alpha, L(t+\triangle t), t+\triangle t) - V(s, \text{ɓ}, \alpha, l, t)$, we can rewrite (A.0.2) as

$$0 = \inf_{v(\cdot)} E^{x,t}_{v(\cdot)}\Big[\triangle V\Big] \tag{A.0.3}$$

By Ito's Lemma,

$$\begin{aligned}
&E^{x,t}_{v(\cdot)}\Big[\triangle V\Big] \\
=&E^{x,t}_{v(\cdot)}\Big[V_t\triangle t + V_s\triangle s + \frac{1}{2}V_{ss}(\triangle s)^2 + V_{\text{ɓ}}\triangle \text{ɓ} + V_\alpha\triangle\alpha + \sum_{\substack{m=1\\m\neq l}}^{M}\lambda^{lm}\triangle t\Big(V(\zeta^{lm}s, \text{ɓ}, \alpha, m, t) - V(s, \text{ɓ}, \alpha, l, t)\Big)\Big]
\end{aligned} \tag{A.0.4}$$

From (2.1.12), (2.1.14) and (3.2.2)

$$\begin{aligned}
E^{x,t}_{v(\cdot)}[\triangle s] &= \big(\eta^l + g^l(v) - \sum_{\substack{m=1\\m\neq l}}^{M}\lambda^{lm}(\zeta^{lm}-1)\big)s\ \triangle t \\
E^{x,t}_{v(\cdot)}[(\triangle s)^2] &= (\sigma^l s)^2\triangle t \\
E^{x,t}_{v(\cdot)}[\triangle \text{ɓ}] &= -e^{r(T-t)}vf^l(v)s\triangle t \\
E^{x,t}_{v(\cdot)}[\triangle\alpha] &= v\triangle t
\end{aligned} \tag{A.0.5}$$

Substituting (A.0.5) into (A.0.4), we have

$$\begin{aligned}
&E^{x,t}_{v(\cdot)}\Big[\triangle V\Big] \\
=&\triangle t\Bigg(V_t + \big(\eta^l + g^l(v) - \sum_{\substack{m=1\\m\neq l}}^{M}\lambda^{lm}(\zeta^{lm}-1)\big)sV_s + \frac{(\sigma^l s)^2}{2}V_{ss} + -e^{r(T-t)}vf^l(v)sV_{\text{ɓ}} + vV_\alpha \\
&+ \sum_{\substack{m=1\\m\neq l}}^{M}\lambda^{lm}\Big(V(\zeta^{lm}s, \text{ɓ}, \alpha, m, t) - V(s, \text{ɓ}, \alpha, l, t)\Big)\Bigg)
\end{aligned} \tag{A.0.6}$$

By substituting (A.0.6) into (A.0.3), dividing by $\triangle t$, and then changing back to the backward time variable τ, we will have derived the system of nonlinear HJB PDEs (3.2.7).

Appendix B

Deriving the HJB PDE for the Mean Quadratic Variation Problem

In this appendix, we derive the HJB PDE (6.2.2) from a dynamic programming principle.

For the asset-price dynamics (2.1.4) in our trade execution model,

$$\int_t^T \left(A(t')\ dS(t')\right)^2 = \int_t^T \sigma^2 A(t')^2 S(t')^2\ dt'\ . \tag{B.0.1}$$

Using the definitions (6.1.4), (6.2.1) and (6.1.3), as well as (B.0.1) we have

$$\begin{aligned}
&\hat{V}(s,\alpha,t;\phi) \\
&= \sup_{v(\cdot)} E^{s,\alpha,t}_{v(\cdot)}\left[\tilde{B}(T) - \phi\int_t^T \left(A(t')\ dS(t')\right)^2\right] \\
&= \sup_{v(\cdot)} E^{s,\alpha,t}_{v(\cdot)}\left[\int_t^T \Big(e^{r(T-t')}\big(-vS_{exec}(v,t')\big) - \phi\sigma^2 A(t')^2 S(t')^2\Big)\ dt' + \lim_{v\to-\infty} A(T^-)S_{exec}(v,T^-)\right]
\end{aligned} \tag{B.0.2}$$

Using the law of iterated expectation on (B.0.2), i.e.

$$E^{s,\alpha,t}_{v(\cdot)}\big[E^{s+\Delta s,\alpha+\Delta\alpha,t+\Delta t}_{v(\cdot)}[\cdot]\big] = E^{s,\alpha,t}_{v(\cdot)}[\cdot],$$

we have

$$\begin{aligned}
&\hat{V}(s,\alpha,t;\phi)\\
&= \sup_{v(\cdot)} E_{v(\cdot)}^{s,\alpha,t}\Bigg[\int_t^{t+\Delta t}\Big(e^{r(T-t')}\big(-vS_{exec}(v,t')\big)-\phi\sigma^2A(t')^2S(t')^2\Big)\,dt'\\
&\quad + E_{v(\cdot)}^{s+\Delta s,\alpha+\Delta\alpha,t+\Delta t}\int_{t+\Delta t}^{T}\Big(e^{r(T-t')}\big(-vS_{exec}(v,t')\big)-\phi\sigma^2A(t')^2S(t')^2\Big)\,dt'\\
&\quad + E_{v(\cdot)}^{s+\Delta s,\alpha+\Delta\alpha,t+\Delta t}\Big[\lim_{v\to-\infty}A(T^-)S_{exec}(v,T^-)\Big]\Bigg] \qquad \text{(B.0.3)}
\end{aligned}$$

Noting that for an optimal control $v^*(\cdot)$,

$$\begin{aligned}
&E_{v^*(\cdot)}^{s+\Delta s,\alpha+\Delta\alpha,t+\Delta t}\Bigg[\int_{t+\Delta t}^{T}\Big(e^{r(T-t')}\big(-vS_{exec}(v,t')\big)-\phi\sigma^2A(t')^2S(t')^2\Big)\,dt'+\lim_{v\to-\infty}A(T^-)S_{exec}(v,T^-)\Bigg]\\
&=\hat{V}(s+\Delta s,\alpha+\Delta\alpha,t+\Delta t;\phi). \qquad \text{(B.0.4)}
\end{aligned}$$

From equations (B.0.3-B.0.4) and the form of the price impact (2.1.5),

$$\begin{aligned}
&\hat{V}(s,\alpha,t;\phi)\\
&=\sup_{v(\cdot)} E_{v(\cdot)}^{s,\alpha,t}\Big[e^{r(T-t)}(-vf(v)s)\Delta t-\phi\sigma^2\alpha^2s^2\Delta t+\hat{V}(s+\Delta s,\alpha+\Delta\alpha,t+\Delta t;\phi)\Big]+O((\Delta t)^{3/2}).
\end{aligned} \qquad \text{(B.0.5)}$$

Define

$$\Delta\hat{V}=\hat{V}(s+\Delta s,\alpha+\Delta\alpha,t+\Delta t;\phi)-\hat{V}(s,\alpha,t;\phi).$$

Rearranging equation (B.0.5) gives

$$0=\sup_{v(\cdot)} E_{v(\cdot)}^{s,\alpha,t}\Big[e^{r(T-t)}(-vf(v)s)\Delta t-\phi\sigma^2\alpha^2s^2\Delta t+\Delta\hat{V}\Big]+O((\Delta t)^{3/2})\ . \qquad \text{(B.0.6)}$$

Using Ito's Lemma, and equations (2.1.2) and (2.1.4), we obtain

$$E_{v(\cdot)}^{s,\alpha,t}[\Delta\hat{V}]=\Delta t\Big[\hat{V}_t+(\eta+g(v)s\hat{V}_s+\frac{\sigma^2s^2}{2}\hat{V}_{ss}+v\hat{V}_\alpha\Big]+O((\Delta t)^{3/2})\ . \qquad \text{(B.0.7)}$$

Let $V=V(s,\alpha,\tau=T-t;\phi)=\hat{V}(s,\alpha,t;\phi)$. Substituting equation (B.0.7) into equation (B.0.6), dividing by Δt, and letting $\Delta t\to 0$, then we obtain the HJB PDE

$$V_\tau=\eta sV_s+\frac{\sigma^2s^2}{2}V_{ss}-\phi\sigma^2\alpha^2s^2+\sup_v\Big[e^{r\tau}(-vf(v))s+g(v)sV_s+vV_\alpha\Big]\ .$$

Appendix C

Proof of No Round-trip Price Manipulation

Since temporary impact always leads to trading losses, there is no restriction on the functional form of the temporary impact [38, 13]. In contrast, the form of the permanent price impact must be restricted to ensure non-positive expected gain from round-trip trades, as noted by [38]. In this appendix, we show that a linear permanent price impact function of the form (2.1.7) is consistent with the no round-trip price manipulation condition of [38], which basically states that the expected gain from a round trip trading strategy should be non-positive.

Note that while previous work considered only Arithmetic Brownian Motion, we handle both Geometric Brownian Motion (GBM) and Arithmetic Brownian Motion here.

In the following, we assume that there is no temporary price impact, since this is irrelevant in terms of no round-trip price manipulation.

We assume that the deterministic drift rate η is zero, so that the the asset price dynamics (2.1.4) is

$$dS(t) = \kappa_p v(X(t), t) S(t) dt + \sigma S(t) d\mathbb{W}(t) \ , \tag{C.0.1}$$

which has the solution

$$S(T) = S(0) \exp\left[\kappa_p \int_0^T v(X(t), t) \ dt\right] \exp\left[\sigma \mathbb{W}(T) - \sigma^2 T/2\right] \ . \tag{C.0.2}$$

Noting that

$$\int_0^T v(X(t), t) \ dt = \int_0^T \frac{dA(t)}{dt} dt = \int_0^T dA(t) = A(T) - A(0),$$

equation (C.0.2) becomes

$$S(T) \ = \ S(0) \exp\left[\kappa_p (A(T) - A(0))\right] \exp\left[\sigma \mathbb{W}(T) - \sigma^2 T/2\right] \ ,$$

and consequently

$$E[S(T)] \;=\; S(0)\exp\Big[\kappa_p(A(T)-A(0))\Big]\ .$$

For a round trip trade, $A(T)=A(0)$, hence

$$E[S(T)] \;=\; S(0)\ . \tag{C.0.3}$$

Let $R(t)$ be the revenue from a trading strategy $v(t)$, so that

$$dR(t) \;=\; -v(X(t),t)S(t)\ dt. \tag{C.0.4}$$

Rearranging equation (C.0.1), we obtain

$$v(X(t),t)S(t)\ dt \;=\; \frac{dS(t)}{\kappa_p}-\frac{\sigma S(t)}{\kappa_p}\ d\mathbb{W}(t)\ . \tag{C.0.5}$$

Substituting equation (C.0.5) into (C.0.4) gives

$$R(T)=-\int_0^T\left[\frac{dS(t)}{\kappa_p}-\frac{\sigma S(t)}{\kappa_p}\ d\mathbb{W}(t)\right]=-\frac{S(T)-S(0)}{\kappa_p}+\frac{\sigma}{\kappa_p}\int_0^T S(t)\ d\mathbb{W}(t)\ .$$

Noting that

$$E\big[\int_0^T S(t)\ d\mathbb{W}(t)\big]=0\ ,$$

then, for a round trip trade (from equation (C.0.3))

$$E[R(T)]=-\frac{E[S(T)]-S(0)}{\kappa_p}=0\ .$$

Consequently, the expected revenue for any round trip trade for a permanent price impact of the form (2.1.7) is zero, hence this precludes round-trip price manipulation.

Note that equation (C.0.3) also holds in the ABM case, and the rest of the proof is similar.

Appendix D

Equivalence between Variance and Expected Quadratic Variation

In this appendix, we give conditions under which the approximation

$$Var_{v(\cdot)}\Big[B(T)\Big] \approx E_{v(\cdot)}\Big[\int_0^T \left(A(t)dS(t)\right)^2\Big]. \tag{D.0.1}$$

becomes an equality.

We specialize[1] our trade execution model of Section 2.1.1 as follows

$$dA(t) = v\ dt, \tag{D.0.2}$$
$$dS(t) = \sigma(S(t),t)\ d\mathbb{W}(t), \tag{D.0.3}$$
$$dB(t) = -vS_{exec}(v,t)dt, \tag{D.0.4}$$
$$S_{exec}(v,t) = S(t) + S(0)h(v) \tag{D.0.5}$$

For generality, we will first[2] consider dynamic strategies $v(\cdot)$, i.e.

$$v(\cdot) : (S(t), A(t), t) \mapsto v = v(S(t), A(t), t).$$

We also assume $A(T^-) = A(T) = 0$, i.e. all shares are liquidated before T^-.

From the above model we have that

$$dB(t) = -vS(t)dt - S(0)vh(v)dt = -S(t)dA(t) - S(0)vh(v)dt,$$

Using the integration by part formula for stochastic integrals on the product $A(t)S(t)$, we

[1] We assume zero drift in (D.0.3), zero interest rate in (D.0.4) and asset-price independent price impact (6.5.2) in (D.0.4). Note also that (D.0.3) encompasses both our GBM model and ABM model as special cases.

[2] We will later impose the assumption of static $v(\cdot)$ for proving equality in (D.0.1).

have

$$-S(t)dA(t) = -d(S(t)A(t)) + A(t)dS(t)$$

since $dA(t)dS(t) = o(dt)$. Consequently,

$$dB(t) = -d(S(t)A(t)) + A(t)dS(t) - S(0)vh(v)dt. \tag{D.0.6}$$

Integrating (D.0.6) from 0 to T, and noting $A(T^-) = A(T) = 0$, gives

$$B(T) = S(0)A(0) + \int_0^T A(t)dS(t) - \int_0^T S(0)vh(v)dt \tag{D.0.7}$$

Note that the last term $B_{impact} \equiv \int_0^T S(0)vh(v)dt = \int_0^T S(0)v(S(t), A(t), t)h(v(S(t), A(t), t))dt$ corresponds to the cost from nonzero trading impact and is stochastic in general. Now we restrict $v(\cdot)$ to be static.

Assumption D.1. The control $v(\cdot)$ is of the form

$$v(\cdot) : (A(t), t) \mapsto v = v(A(t), t),$$

i.e. a static strategy that is independent of $S(t)$.

With Assumption D.1, the term $B_{impact} = \int_0^T S(0)v(A(t), t)h(v(A(t), t))dt$ becomes deterministic. As a result, equation (D.0.7) implies

$$Var\Big[B(T)\Big] = Var\Big[\int_0^T A(t)dS(t)\Big] = E\Big[\Big(\int_0^T A(t)dS(t)\Big)^2\Big] = E\Big[\Big(\int_0^T A(t)\sigma(S(t), t)d\mathbb{W}(t)\Big)^2\Big]$$

since the Ito integral has zero expectation. Now we have

$$E\Big[\Big(\int_0^T A(t)\sigma(S(t), t)\ d\mathbb{W}(t)\Big)^2\Big] = E\Big[\int_0^T \big(A(t)\sigma(S(t), t)\big)^2 dt\Big] = E\Big[\Big(\int_0^T A(t)dS(t)\Big)^2\Big],$$

where the first equality is a result of the Ito isometry.

In conclusion, we have shown that under the model (D.0.2 - D.0.5),

$$Var_{v(\cdot)\text{ static}}\Big[B(T)\Big] = E_{v(\cdot)\text{ static}}\Big[\int_0^T \big(A(t)dS(t)\big)^2\Big].$$

Appendix E

Details of Monte Carlo Simulations

In this appendix, we provide some details about how to perform Monte Carlo simulations in the Hybrid (PDE-Monte Carlo) method of Section 3.6. For ease of exposition, we will explain in the context of Mean Variance optimization using the basic Geometric Brownian Motion model, i.e no regime switching.

Numerically solving the HJB PDE (3.2.7) gives us the optimal strategy on the discrete computational mesh, i.e. $v_{MV}(s_i, \mathscr{b}_j, \alpha_k, t_n)$[1]. By using $v_{MV}(s_i, \mathscr{b}_j, \alpha_k, t_n)$ as input for Monte Carlo simulations, we can obtain information about the trading strategy that is not readily available from the value functions. For example, we can estimate the probability distribution of $B(T)$, and the mean and the standard deviation of the liquidation profile (plot of $A(t)$ against t). In particular, Monte Carlo simulations enable us to measure the MQV-performance of MV-optimal strategies, and conversely, the MV-performance of MQV-optimal strategies; see Chapter 7 for examples.

The Monte Carlo simulations also provide a verification of the solution from the PDE method (Section 3.6), in the sense that given an optimal control, we can obtain independent estimates of mean and variance.

E.1 Change of Variable

Suppose that the optimal strategy $v_{MV}(s_i, \mathscr{b}_j, \alpha_k, t_n)$ is obtained from solving the HJB PDE (3.2.7). For a fixed value of γ, each Monte Carlo simulation starts with the initial values $S(0), B(0), A(0)$ at time $t = 0$ and is updated at the discrete times t_n. In the following we give a full specification of the simulation procedure by detailing the simulation from time point t_{old} to the immediate next time point t_{new}.

At t_{old}, the state is $(S_{old}, B_{old}, A_{old})$. To look up the optimal trading velocity, we first need to change the variable from B to $\mathcal{B}$. For the fixed value of γ, we have $\mathcal{B}_{old} = e^{r(T-t_{old})}B_{old} - \gamma/2$ from equation (3.2.2). Now the optimal trading velocity $v(S_{old}, \mathcal{B}_{old}, A_{old}, t_{old})$ needs to be interpolated from the discrete $v_{MV}(s_i, \mathscr{b}_j, \alpha_k, t_n)$.

[1]Note the use of forward time notation.

E.2 Interpolation

Our numerical study (see Section 3.7.2) shows that it is more accurate to linearly interpolate $v_{MV}(s_i, \mathcal{b}_j, \alpha_k, t_n)$ along a constant line of wealth $\{\alpha s + \mathcal{b} = \text{constant}\}$ than along the coordinate axes. Therefore, we interpolate $v_{MV}(s_i, \mathcal{b}_j, \alpha_k, t_n)$ as in Figure 3.1(b) with L given by the constant line of wealth $\{\alpha s + \mathcal{b} = \text{constant}\}$. Note that the form of the line L as defined by equation (3.7.7) is not applicable in the current context because there is no candidate control v.

E.3 Updating State Variables

Let $\triangle t = t_{new} - t_{old}$, we update the state variable as follows:

$$\begin{aligned}
A_{opt} &= A_{old} + v(S_{old}, \mathcal{B}_{old}, A_{old}, t_{old})\triangle t, \\
A_{new} &= \max(A_{opt}, 0), \\
v_{opt} &= (A_{new} - A_{old})/\triangle t, \\
S_{new} &= S_{old} \exp\{(\eta + g(v_{opt}) - \frac{1}{2}\sigma^2)\triangle t + \sigma\sqrt{\triangle t}\mathcal{N}(0,1)\}, \\
B_{new} &= B_{old} - e^{r(T-t_{old})} v_{opt} f(v_{opt}) S_{old} \triangle t, \\
QV_{new} &= QV_{old} + (A_{old}(S_{new} - S_{old}))^2,
\end{aligned}$$

where $\mathcal{N}(0,1)$ is a standard normal variate and QV_{new} is an approximation of $\int_0^{t_{new}} (A(t')\ dS(t'))^2$.

Appendix F

Example Computation for the Temporary Price Impact Factor

In this appendix we discuss how to relate an execution program's participation (in terms of percentage of daily volume) and the temporary price impact factor κ_t in our model. We describe a simplified, yet realistic, scenario in which using a temporary price impact factor $\kappa_t = 1.2 \times 10^{-7}$ in our model corresponds to liquidating 1% of the daily volume of a stock.

Suppose that the initial stock price $s_{init} = 100$ dollars, buy rate = 1,000 shares/min, corresponding temporary price impact = 3 dollars/min, daily trading time = 420 minutes, and daily volume = 42,000,000 shares. For such a scenario, our trading corresponds to 1% of the daily volume, and the daily market turnover for the stock is 4.2 billion dollars, corresponding to that typical of a large-cap stock.

Assuming a constant trading rate over one day ($T = 1/250$), then the total price impact is 3×420 dollars. The impact ratio, i.e. ratio of total post-execution value to total initial value of stock, is then given by

$$\begin{aligned} R = \frac{\text{total post-execution value}}{\text{total initial value}} &= \frac{\text{total initial value} - \text{total price impact}}{\text{total initial value}} \\ &= 1 - \frac{3 \times 420}{420 \times 1000 \times 100} = 1 - 3 \times 10^{-5} \end{aligned}$$

Using our trading model[1] (2.1.3), (2.1.5) and (2.1.6), the impact ratio is $f(v) = \exp(\kappa_t v) \approx 1 + \kappa_t v$. Therefore, the ratio R is approximately $1 + \kappa_t v$.

Since $\alpha_{init} = 1$ in our model and $T = 1/250$, the constant trading rate is $v = -250$. Substituting $v = -250$ into

$$1 + \kappa_t v = 1 - 3 \times 10^{-5}$$

gives $\kappa_t = 1.2 \times 10^{-7}$.

[1] We also set $\kappa_s = 0$ and $\beta = 1$.

Appendix G

Proof of uniform boundedness of $E[S(t)]$

Proposition G.1. *In the regime switching model of Section 2.1.2, $E[S(t)]$ is uniformly bounded over $t \in [0,T]$, i.e. $\sup_{t\in[0,T]} E[S(t)]$ is bounded by a constant $C_S > 0$.*

Proof. Without loss of generality, we can change the drift rate in (2.1.14) to any constant C_1 and replace ζ^{lm} by a single constant $C_2 = \max_{l,m} \zeta^{lm}$. Hence we consider

$$dS(t) = C_1 S(t)\ dt + \sigma^l S(t)\ d\mathbb{W}(t) + \sum_{\substack{m=1 \\ m\neq l}}^{M} (C_2 - 1) S(t)\, dL(t). \tag{G.0.1}$$

The uniformly boundedness then follows from the first-moment exponential stability result in [25]; to see this, we now write (G.0.1) using the notation in [25] as follows:

$$\begin{aligned} dx(t) &= f_{r(t)}(x(t))dt + \sigma_{r(t)}(x(t))\ d\mathbb{W}(t), \quad t \neq \tilde{t}_k \\ x(t) &= \xi_k J_{r(t^-)}(x(t^-)), \quad t = \tilde{t}_k, \quad k \in \{1,2,3,\cdots\}, \end{aligned} \tag{G.0.2}$$

where

$$\begin{aligned} x(t) &= S(t), \\ r(t) &\in Q = \{1,\cdots,M\} \text{ denotes the mode/regime at time } t, \\ f_q(x) &= C_1 x \text{ for all } q \in Q, \\ \sigma_q(x) &= \sigma^q x \text{ for all } q \in Q, \\ \xi_k &\equiv 1 \text{ is deterministic}, \\ J_q(x) &= C_2 x, \\ \tilde{t}_k &\text{ denotes the regime switching time.} \end{aligned} \tag{G.0.3}$$

Note that the conditions $f_q(0) = 0$ and $\sigma_q(0) = 0$ in [25] are satisfied in our model.

To apply Theorem 3.1 in [25], we pick $V_q(x) = x$, $a_q^1 = b_q^1 = 1$, $\beta = 1$, $\zeta = C_1$, and $\mu(\cdot) = C_2$. For $p = 1$, condition (7) (in [25]) is clearly satisfied. Note that $LV_q(x) = f_q(x) = C_1 x$, thus condition (8) is satisfied by the choice of ζ. It is clear that condition (9) is satisfied. Since $V_q(\xi_k J_q(x)) = V_q(J_q(x)) = J_q(x) = C_2 x$, condition (10) is satisfied. Since $\bar{\mu}, \lambda_J$ and λ_S are finite, condition (11) is satisfied for C_1 negative enough, which we can assume without loss of generality.

Applying Theorem 3.1 in [25] shows that there exists constants C and α such that

$$E[|x(t)|] \leq C|x(0)|e^{-\alpha t}, \tag{G.0.4}$$

which clearly implies $E[x(t)]$ is uniformly bounded over $t \in [0, T]$.

□

Bibliography

[1] A. Alfonsi, A. Fruth, and A. Schied. Optimal execution strategies in limit order books with general shape functions. *Quantitative Finance*, 10(2):143–157, 2010. 2

[2] A. Alfonsi and A. Schied. Optimal trade execution and absence of price manipulations in limit order book models. *SIAM Journal on Financial Mathematics*, 1(1):490–522, 2010. 2

[3] A. Alfonsi, A. Schied, and A. Slynko. Order book resilience, price manipulation, and the positive portfolio problem. *Forthcoming in SIAM Journal on Financial Mathematics*, 2012. 2

[4] R. Almgren. Optimal execution with nonlinear impact functions and trading-enhanced risk. *Applied Mathematical Finance*, 10(1):1–18, 2003. 5

[5] R. Almgren. Optimal trading in a dynamic market. Technical report, New York University, 2009. 78

[6] R. Almgren. Execution costs. *Encyclopedia of Quantitative Finance*, pages 1–5, 2010. 5

[7] R. Almgren. Optimal trading with stochastic liquidity and volatility. *SIAM Journal on Financial Mathematics*, 3(1):163–181, 2012. 61, 67

[8] R. Almgren and N. Chriss. Value under liquidation. *Risk*, 12(12):61–63, 1999. 2, 3

[9] R. Almgren and N. Chriss. Optimal execution of portfolio transactions. *Journal of Risk*, 3(2):5–39, 2000. 2, 3, 69, 75, 76, 78, 82, 84, 85, 86

[10] R. Almgren and N. Chriss. Bidding principles. *Risk*, 16(6):97–102, 2003. 61

[11] R. Almgren and J. Lorenz. Bayesian adaptive trading with a daily cycle. *The Journal of Trading*, 1(4):38–46, 2006. 51

[12] R. Almgren and J. Lorenz. Adaptive arrival price. *Algorithmic Trading III: Precision, Control*, pages 1–24, 2007. 85

[13] R. Almgren, C. Thum, E. Hauptmann, and H. Li. Direct estimation of equity market impact. *Risk*, 18(7):58–62, 2005. 5, 6, 100

[14] A.M. Andrew. Another efficient algorithm for convex hulls in two dimensions. *Information Processing Letters*, 9(5):216–219, 1979. 21

[15] G. Barles. Solutions de viscosité et equations elliptiques du deuxieme ordre. *Lecture notes at Université de Tours*, 1997. 37, 38

[16] G. Barles and P.E. Souganidis. Convergence of approximation schemes for fully nonlinear second order equations. *Asymptotic Analysis*, 4(3):271–283, 1991. 3, 36, 37, 38, 50, 75, 95

[17] S. Basak and G. Chabakauri. Dynamic mean-variance asset allocation. *Review of Financial Studies*, 23(8):2970–3016, 2010. 7, 9, 71

[18] D. Bertsimas and A. Lo. Optimal control of execution costs. *Journal of Financial Markets*, 1(1):1–50, 1998. 2

[19] T.R. Bielecki, H. Jin, S.R. Pliska, and X.Y. Zhou. Continuous-time mean-variance portfolio selection with bankruptcy prohibition. *Mathematical Finance*, 15(2):213–244, 2005. 11

[20] T. Bjork and A. Murgoci. A general theory of markovian time inconsistent stochastic control problems. *SSRN eLibrary*, 2010. 9, 15

[21] S.P. Boyd and L. Vandenberghe. *Convex optimization*. Cambridge University Press, 2004. 17

[22] R.P. Brent. *Algorithms for minimization without derivatives*. Dover Publications, 2002. 75

[23] A. Briani, F. Camilli, H. Zidani, et al. Approximation schemes for monotone systems of nonlinear second order partial differential equations: convergence result and error estimate. *Differential Equations and Applications*, 4(2):297–317, 2012. 37, 38

[24] P. Brugiere. Optimal portfolio and optimal trading in a dynamic continuous time framework. *Proceedings of the 6th AFIR Colloquium, Nurenberg, Germany*, 12:89–99, 1996. 70

[25] A. Cetinkaya, K. Kashima, and T. Hayakawa. Stability and stabilization of switching stochastic differential equations subject to probabilistic state jumps. In *49th IEEE Conference on Decision and Control*, pages 2378 –2383, Dec 2010. 13, 107, 108

[26] Z. Chen and P.A. Forsyth. A semi-Lagrangian approach for natural gas storage valuation and optimal operation. *SIAM Journal on Scientific Computing*, 30(1):339–368, 2007. 41

[27] M.G. Crandall, H. Ishii, and P.L. Lions. User's guide to viscosity solutions of second order partial differential equations. *Bulletin of the American Mathematical Society*, 27(1):1–67, 1992. 47

[28] Y. d'Halluin, P.A. Forsyth, and G. Labahn. A semi-Lagrangian approach for American Asian options under jump diffusion. *SIAM Journal on Scientific Computing*, 27(1):315, 2005. 27, 74

[29] I. Domowitz and H. Yegerman. Algorithmic trading usage patterns and their costs. *The Journal of Trading*, 6(3):9–21, 2011. 1

[30] M. Ehrgott. *Multicriteria optimization*, volume 491 of *Lecture Notes in Economics and Mathematical Systems*. Springer Verlag, 2005. 8

[31] P.A. Forsyth. A Hamilton Jacobi Bellman approach to optimal trade execution. *Applied Numerical Mathematics*, 61(2):241–265, 2011. 32, 36

[32] P. Gassiat, F. Gozzi, and H. Pham. Investment/consumption problem in illiquid markets with regimes switching. *ArXiv e-prints 1107.4210*, 2011. 47

[33] J. Gatheral. No-dynamic-arbitrage and market impact. *Quantitative Finance*, 10(7):749–759, 2010. 2

[34] J. Gatheral and A. Schied. Optimal trade execution under geometric brownian motion in the Almgren and Chriss framework. *International Journal of Theoretical and Applied Finance*, 14(3):353–368, 2011. 2

[35] J. Gatheral, A. Schied, and A. Slynko. Transient linear price impact and fredholm integral equations. *Mathematical Finance*, 22(3):445–474, 2012. 2

[36] Y. Huang, P. Forsyth, and G. Labahn. Methods for pricing American options under regime switching. *SIAM Journal on Scientific Computing*, 33(5):2144–2168, 2011. 30

[37] Y. Huang, P. Forsyth, and G. Labahn. Combined fixed point and policy iteration for Hamilton Jacobi Bellman equations in finance. *SIAM Journal on Numerical Analysis*, 50(4):1861–1882, 2012. 30

[38] G. Huberman and W. Stanzl. Price manipulation and quasi-arbitrage. *Econometrica*, 72(4):1247–1275, 2004. 6, 100

[39] H. Ishii and S. Koike. Viscosity solutions for monotone systems of second–order elliptic PDEs. *Communications in partial differential equations*, 16(6-7):1095–1128, 1991. 36, 37, 38

[40] C. Jackson, B. Schwieger, M. Simmonds, and C. Tynan. *Consultation paper: transparency and Standards in the Provision of Transaction Cost Analysis*. Trading Screen, 2011. 2, 84

[41] E.R. Jakobsen. Monotone schemes. *Encyclopedia of Quantitative Finance*, pages 1253–1263, 2010. 47

[42] B. Johnson. *Algorithmic Trading & DMA: An introduction to direct access trading strategies*. 4Myeloma Press, 2010. 1, 2, 84

[43] I. Kharroubi and H. Pham. Optimal portfolio liquidation with execution cost and risk. *Arxiv preprint arXiv:0906.2565*, 2009. 2

[44] R. Kissell and R. Malamut. Algorithmic decision-making framework. *The Journal of Trading*, 1:82–91, 2006. 2, 84

[45] R. Kissell and Malamut R. Understanding the profit and loss of trading algorithm. *Institutional Investor*, (1):41–49, 2005. 90

[46] A.S. Kyle. Continuous auctions and insider trading. *Econometrica*, 53(6):1315–1335, 1985. 2

[47] D. Li and W.L. Ng. Optimal dynamic portfolio selection: Multiperiod mean-variance formulation. *Mathematical Finance*, 10(3):387–406, 2000. 2, 10, 11, 12, 13, 14, 35, 95

[48] X. Li, X.Y. Zhou, and A.E.B. Lim. Dynamic mean-variance portfolio selection with no-shorting constraints. *SIAM Journal on Control and Optimization*, 40(5):1540–1555, 2002. 11

[49] F. Lillo, J.D. Farmer, and R.N. Mantegna. Master curve for price-impact function. *Nature*, 421(6919):129–130, 2003. 5

[50] J. Lorenz. *Optimal trading algorithms*. PhD thesis, ETH Zurich, 2008. 85

[51] J. Lorenz and R. Almgren. Mean–variance optimal adaptive execution. *Applied Mathematical Finance*, 18(5):395–422, 2011. 58, 90

[52] V. Ly Vath, M. Mnif, and H. Pham. A model of optimal portfolio selection under liquidity risk and price impact. *Finance and Stochastics*, 11(1):51–90, 2007. 2

[53] A. Obizhaeva and J. Wang. Optimal trading strategy and supply/demand dynamics. Technical report, National Bureau of Economic Research, 2005. 2

[54] M. Pemy and Q. Zhang. Optimal stock liquidation in a regime switching model with finite time horizon. *Journal of Mathematical Analysis and Applications*, 321(2):537–552, 2006. 38

[55] A.F. Perold. The implementation shortfall: Paper versus reality. *Journal of portfolio management*, 14(3):4–9, 1988. 1

[56] M. Potters and J.P. Bouchaud. More statistical properties of order books and price impact. *Physica A: Statistical Mechanics and its Applications*, 324(1-2):133–140, 2003. 5

[57] S. Predoiu, G. Shaikhet, and S. Shreve. Optimal execution in a general one-sided limit-order book. *SIAM Journal on Financial Mathematics*, 2(1):183–212, 2011. 2

[58] W. Rudin. *Principles of mathematical analysis*. McGraw-Hill New York, 1976. 49

[59] A. Schied and T. Schoneborn. Risk aversion and the dynamics of optimal liquidation strategies in illiquid markets. *Finance and Stochastics*, 13(2):181–204, 2009. 2

[60] A. Schied, T. Schoneborn, and M. Tehranchi. Optimal basket liquidation for CARA investors is deterministic. *Applied Mathematical Finance*, 17(6):471–489, 2010. 2, 75, 86

[61] R.C. Seydel. *Impulse Control for Jump-Diffusions: Viscosity Solutions of Quasi-Variational Inequalities and Applications in Bank Risk Management*. PhD thesis, Leipzig Universität, 2009. 37, 38

[62] E. Vigna. On efficiency of mean-variance based portfolio selection in DC pension schemes. Technical report, Collegio Carlo Alberto, 2010. 12

[63] J. Wang and P.A. Forsyth. Continuous time mean variance asset allocation: A time-consistent strategy. *European Journal of Operational Research*, 209(2):184–201, 2011. 7

[64] H. Windcliff. Private communications. 61, 67

[65] X.Y. Zhou and D. Li. Continuous-time mean-variance portfolio selection: A stochastic LQ framework. *Applied Mathematics & Optimization*, 42(1):19–33, 2000. 10, 11, 12, 13, 14